EVALUATING TIME-DEPENDENT AND BOND CHARACTERISTICS OF A LIGHTWEIGHT CONCRETE MIX FOR KANSAS PRESTRESSED CONCRETE BRIDGES

by

JOSEPH ROBERT HOLSTE

B.S., Kansas State University, 2008

A THESIS

submitted in partial fulfillment of the requirements for the degree

Master of Science

Department of Civil Engineering
College of Engineering

KANSAS STATE UNIVERSITY
Manhattan, Kansas

2010

Approved by:

Major Professor
Robert J. Peterman

Copyright

Abstract

This thesis details findings from testing done to determine bond and time-dependent characteristics of two lightweight concrete mixes. The lightweight mixes were tested to possibly provide a more cost-effective solution to replacing some of Kansas' older bridges. Testing included use of a conventional lightweight mix and a self-consolidating lightweight mix. Sixteen Inverted T-beams were cast at a prestress plant to determine prestress losses that had occurred in the two lightweight mixes. These losses were compared to ACI, PCI, and AASHTO code equations. Creep and shrinkage prisms were also cast and measured to accurately determine creep and shrinkage variables for the two lightweight mixes. Twelve flexural beams were also cast at the prestress plant and tested at Kansas State University's Civil Engineering Structures Laboratory to experimentally test development lengths of the lightweight mixes and to compare results with ACI code equations.

This study found compressive strengths of the lightweight concrete mixes varied greatly from laboratory testing. Low concrete strengths caused the prestress losses to be greater than the predicted code values. Flexure beam testing showed several of the beams were subject to strand slip, causing a sudden violent failure.

Table of Contents

List of Figures

List of Tables

Acknowledgements

I would like to thank Dr. Robert J. Peterman for his help and guidance with this project. His expertise in the field of prestress concrete greatly advanced with its completion. I would also like express gratitude towards the other two members of my committee, Dr. Kyle Ridding and Dr. Asad Esmaeily. I would like to thank the Kansas Department of Transportation for funding this project.

I would like to thank Tom Bergquist and the employees of Prestressed Concrete Inc., Newton, Kan. They were always helpful in pouring the test specimens and were willing to work around my schedule.

I would also like to recognize my fellow graduate students that helped with the research project: Patrick Sheedy, Jake Perkins, Steven Hammerschmidt, Robert Murphy, Brandon Bortz, Doug Duncan, and Lisa Beck. I would especially like to thank Becca Greif for her help in measuring the data. I also want to thank Peggy Selvidge, Debi Wahl, Danita Deters, and David Suhling, as well as the undergraduate students that helped with the project: Ryan Benteman, Kurt Hershey, Jordan Dettmer, and Brady Hedstrom.

I would finally like to thank my family and friends who have supported me throughout this venture.

CHAPTER 1 - Introduction

1.1 Background

The majority of the bridges in Kansas are in rural areas. Many of these are becoming structurally deficient, and are in need of replacement. Due to the location of these bridges, cost of transporting prestressed girders to these areas often makes use of cast-in-place bridges more economical. Use of lightweight aggregate in these bridge girders would reduce the total weight and could allow multiple girders to be shipped on one semi-truck. This would reduce transportation costs and allow the more economical prestressed girders to be used in rural areas. Lightweight prestressed girders could be put in place using a lower capacity crane due to the lower self-weight of the beam. The construction process would be quicker without the need of form work associated with cast-in-place girders. The lighter self-weight would also increase allowable live loads the bridges would be able to carry.

The Kansas Department of Transportation first published a report on the availability and suggested usage of lightweight aggregates and their uses in lightweight concrete in the 1950s (Research Department 1953). Since then, several projects have been involved with use of lightweight concrete, but mass production of lightweight concrete bridge members has yet to take hold in the state of Kansas. Various tests have been done on lightweight concrete mixes in the Kansas State University structural testing laboratory. These tests included large block pullout tests, transfer length tests, and flexural beam tests to determine development lengths. Additional testing was also done to determine creep and shrinkage coefficients. Testing results showed lightweight concrete mixes were adequate for testing and were capable of reaching 5,000 psi compressive strength in only 16 hours with a 28-day compressive strength of 7,000 psi (Perkins 2008). Ten of the 12 flexural beams tested reached nominal-moment capacity and the two that failed below nominal failed in compression without strand end-slip (Perkins 2008). Testing on beams cast at a precast/prestress plant would be needed as the next step in development and use of lightweight concrete mixes.

Self-consolidating concrete has become a more widely used product. Self-consolidating concrete (SCC) is defined as a highly workable concrete that can flow through densely reinforced or complex structural elements under its own weight, and adequately fill voids

without segregation or excessive bleeding, without the need for vibration (Interim Guidelines 2003). Its properties decrease the need of vibration during casting and create a better surface finish without the presence of "bugholes."

Testing was done by Kansas State University to examine use of SCC normal-weight concrete. The process included creep and shrinkage testing along with transfer length tests. Prestress losses were calculated using beams cast at Prestressed Concrete Incorporated (PCI) in Newton, Kan. Testing showed prestress losses, creep coefficients and ultimate shrinkage strains were all in general accordance with ACI code equations (Larson 2006). Research showed SCC mixes could be accurately designed and would not require any special design considerations. The combination of lightweight aggregate and self-compacting concrete would allow for a lighter, more durable, and aesthetically pleasing product that could be used for bridges in Kansas.

1.2 Objectives

The lightweight mix developed by Perkins (2008) was used to cast creep and shrinkage prisms and beams at a precast plant. The beams cast had properties and dimensions based on research done by Larson (2006). The beams were tested and monitored to determine if the lightweight concrete mix could be mass produced and keep the same properties as the laboratory mix.

1.2.1 Inverted Tee Beams

Eight inverted tee (IT) beams were cast to analyze prestress losses and transfer lengths of the lightweight mixes used in this project. The beams were instrumented and monitored to determine prestress losses due to elastic shortening, creep, and shrinkage, and these results were compared to current ACI, PCI, and AASHTO code equations. Designs of the beams were chosen to be similar to the ones used by Larson (Larson 2006). Due to low concrete strengths during the initial casting, a second set of IT beams were fabricated, which resulted in a total of 16 IT beams being monitored.

1.2.2 Creep and Shrinkage

Creep and shrinkage prisms were cast to determine the time-dependent characteristics of the lightweight mixes used in this project. These prisms were cast at the same time as the IT

beams and used the same mix to accurately correlate results from the two tests. Two sets of prisms were cast, since two sets of IT beams were cast due to low concrete strengths. Results from these prisms were compared to ACI 209 code equations.

1.2.3 Development Length of Flexure Beams

Twelve flexure beams were cast and tested to examine development lengths of the lightweight mixes used in this project. The beams included four T-beams, four rectangular beams with 100% development lengths (L_d), and four rectangular beams with 80% L_d. Cross sections of the beams were based on research beams that Larson had tested in determining properties of normal-weight SCC concrete mixes (Larson 2006). Results from these beams were compared to ACI code equations.

1.3 Scope

Section 2.0 reviews research that has been done on lightweight concrete, as well as various testing methods used to determine transfer and development lengths of prestressed concrete members.

Section 3.0 describes design and fabrication of the inverted tee (IT) beams that were used to determine transfer length and prestress losses of the lightweight mixes involved in this study.

Section 4.0 reports findings from the IT beams that were cast. These results were the transfer length and prestress losses that were compared to code equations.

Section 5.0 discusses the theory and equations that have been developed for creep and shrinkage, along with the fabrication of creep and shrinkage prisms used in this project.

Section 6.0 reports findings from the creep and shrinkages prisms and compares them to ACI 209 code equations.

S**ection 7.0** describes design and fabrication of the lightweight flexure beams that were cast and tested to verify the transfer and development length equations for lightweight concrete mixes.

Section 8.0 reports findings from the flexure beam tests and methods of failure of the beams with relation to the mixes that were used. Experimental moment capacities of the beams were compared with the theoretical nominal moment capacities.

Section 9.0 discusses conclusions and recommendations developed from this project.

CHAPTER 2 - Literature Review

Shing et al. (2000) reviewed the ACI and AASHTO transfer and development length equations for high-strength concrete box girders. The authors constructed three test specimens to verify the ACI and AASHTO formulas for transfer and development lengths when using high-strength concrete. The experiment consisted of three, 15-inch-wide and 21.75-inch-tall girders with a span of 33.4 feet. Nine-grade 270 low-relaxation 0.6-inch-diameter, seven-wire prestressing strands were used for flexural reinforcement, and #3 rebar stirrups were used as shear reinforcement. The girders were fabricated at Rocky Mountain Prestress in Boulder, Colo., using a mix with a transfer strength of 6,500 psi and 56-day strength of 10,000 psi. The girders had embedded points at the level of the 0.6-inch-diameter strand and were measured with a Whittemore gauge before and after detensioning to accurately measure the transfer lengths. End-slip measurements were also used to verify the transfer lengths. The specimens were then tested to determine development lengths and were monitored for end-slip using linear voltage differential transducers (LVDT) attached to the strands at each end of the beam. The authors discovered the ACI and AASHTO formulas had overestimated the transfer and development lengths when using high-performance concrete. The transfer length equations were overestimated by 18% and the development lengths were overestimated by 53%. Bond characteristics of the prestress strand were also investigated in the project. The strand came from Insteel Wire Products and had a small amount of rust on it. It was tested for bond strength using the Moustafa pullout block method. Average strength of the pullout tests was 48.3 kips, which was greater than the 36 kips advised by Logan (1997) for 0.5-inch-diameter strand.

Buckner (1995) reviewed various equations that had been developed by other researchers in regard to transfer and development lengths for prestressed members. He explained that code equations needed to be changed due to the fact that most precasters use grade 270 instead of the earlier version grade 250 seven-wire strand. The older equations were developed based on the area of the grade 250 strand, with the grade 270 strand is six percent larger. Buckner recommended increasing transfer lengths by 20% due to the higher jacking force the grade 270 strand experiences and the variation in the perimeters of the two grades of strand. Development

length was also recommended to be increased by at least 1.7 times to allow for strength and ductility in the prestressed members.

Ouchi (2001) discussed the theory and use of self-compacting concrete in Japan. Self-compacting concrete (SCC) was developed to reduce the amount of skilled laborers needed to pour concrete for high-performance, durable structures. Ouchi explained how use of super-plasticizer could allow for a lower water-to-cement ratio and still allow the concrete mix to have a high workability. The super-plasticizer enables the mortar and the course aggregate to "flow" between the reinforcement bars but prevents segregation of the two. The SCC mixture requires little or no vibration due to its self compaction through use of gravity. The author describes a project in Japan using SCC that decreased the number of skilled workers by 67% and completed the construction in 80% of the time required to finish the same project using non SCC.

Weerasekera et al. (2008) summarized various methods used to measure bond and strains in concrete and steel due to prestressing. Various tests included beam tests, pullout tests, x-ray techniques, and the photo-elastic method. The authors developed an experiment to test the use of strain gages mounted to the prestressing strand vs. use of demountable mechanical strain (DEMEC) gage measurements to determine the strain in the concrete. The two methods varied largely throughout the transfer length due to strand slip, but overall results for the entire beam were comparable for the two methods. The strain gage method required skilled techniques to attach the strain gages to the strand, and the gages were subject to damage during the testing process. The strain gages also change the surface condition of the strand by being glued to it. The DEMEC gage required a longer amount of time to take the required measurements and could become misleading at the point of a developing crack. The authors concluded that either technique could be used to determine transfer length, and use of either technique would provide verification of the results from the testing.

Kamel and Tadros (1996) developed an improved cross section of prestressed girder that could be used for construction in rural areas. The authors explained that from 1950 to 1990, 95% of the bridges built in the United States were less than 100 feet in length. These bridges are becoming structurally deficient or need strengthing. The authors explained the majority of these bridges are in rural areas and have limitations on the clearance allowed for bridges. A prestressed inverted tee (IT) beam was chosen as the main cross section to be used to replace these bridges. The IT section that was chosen consisted of a 600-mm flange width and a varying

height from 300 mm to 900 mm, depending on clearance and span length required. The IT could be placed in its final location without use of false work and wouldn't require the center pier that current cast-in-place design does. The IT could be produced quickly and the construction process would only require a small crane to place the ITs into their final position. The authors concluded the IT cross section would be an economical design to be used for repair and replacement of structurally deficient bridges in the rural United States.

Grace (2000) investigated the transfer length of strands made out of carbon fiber-reinforced polymers (CFRP) and carbon fiber composite cable (CFCC). The carbon fiber strand had a tensile strength of 328 ksi as opposed to steel strand, which had a tensile strength of 270 ksi. Along with having a higher tensile strength, carbon fiber is noncorrosive, making it a possible replacement for steel strand. Double-T girders were cast and used to measure transfer length. Sudden and gradual methods were used for releasing prestress force, and transfer lengths of the carbon fiber were compared to steel strand. The CFRPs transfer lengths were 66 to 73 times the diameter of the strand for a gradual release and varied from 47 to 59 times the diameter of the strand for a sudden release. The CFCC showed the same types of results by having a transfer length of 33 to 47 times the diameter of the strand for gradual release and 27 to 38 times the diameter of the strand for sudden release. The author concluded the results conflicted with the steel strand's transfer length, which had been found to be six to 30 percent higher for sudden release vs. gradual release.

Kahn and Lopez (2005) tested time-dependent characteristics of high-performance lightweight concrete (HPLC), and the prestress losses in prestressed bridge girders made for HPLC. The authors developed two different high-performance mixes to test; both used ½-inch expanded-slate lightweight aggregate and had design strengths of 8,000 and 10,000 psi, respectively, and unit weights below 120 lb/ft^3. The two mixes were used to cast three AASHTO Type II girders, with two having a length of 39 feet, and one at 43 feet, for each of the mixes. Laboratory tests were used to cast creep, shrinkage, and compressive strength specimens along with the coefficient of thermal expansion specimens. The girders' reinforcement consisted of eight 0.6-inch-diameter low-relaxation strands in the bottom flange, two 0.6-inch-diameter low-relaxation strands in the top flange and no. 4 rebar stirrups. Vibrating wire strain gages were imbedded in the girders to measure prestress losses. The authors compared the prestress losses using four different models: the PCI method, ACI method, and AASHTO lump sum and refined

methods. The authors concluded all four methods were conservative when estimating prestress losses for both of the HPLC mixes and recommended future research to develop improved prestress loss equations for HPLC.

Steinberg et al. (2001) monitored concrete strains that had developed from the cutting of the prestressing strand in pretensioned concrete beams. The study consisted of three rectangular prestressed concrete beams,32 feet long and a cross section of 5 ½ x 23 inches. The reinforcement of the beams consisted of four ½-inch-diameter, seven-wire, grade 270, prestressed strand and #3 stirrups. Two of the prestressing strands were located 6 1/8 inches from the bottom of the beam and the other two were located two inches above that. The stirrups were spaced at 16-inch centers to provide the required shear capacity. The authors instrumented the beams with internal and external strain gages, external DEMEC points mounted to the beam, and linear variable differential transformers were mounted to the ends of the strands so that end-slip measurements could also be taken. The authors found that transfer lengths were all longer than the recommended amount of 25 inches. Internal strain gages were used to monitor the strain during release of the strands. Data acquisition used to monitor the internal strain gages used a sample rate of 7,500 readings per second to insure accurate readings from the gages. The authors found that longitudinal tensile strains had developed during the cutting of the prestressing strand. These strains were found to range from 50 to 150 microstrain, which could cause cracking in the member near its ends. The authors concluded that DEMEC points and end-slip measurements were comparable methods of measuring the transfer length and that the strain gage results supported these two methods. The authors recommended future research should be done to verify the tensile strain results and to develop a more accurate transfer-length formula.

Logan (1997) reviewed the testing procedure for determining the bond quality of various ½-inch-diameter prestressing strand samples from precast manufacturers across North America. The author tested the samples in four separate bond characteristic tests: the pullout test (Moustafa) method, end-slip measurements at release and 21 days, and development-length tests. The pullout test consisted of embedding 18 inches of each of the 34-inch strand samples vertically and placing concrete around the strand. The concrete was then heat-cured overnight to a compressive strength of 4,350 psi. The strands were then pulled out of the concrete at a rate of 20 kips per minute until the strand load could not be kept constant. All but two of the groups of strand reached a maximum load of 36 kips. The two groups of strand that failed to reach 36 kips

pulled out at 12 kips. The end-slip and development-length tests were done using prestressed rectangular beams. The beams had a cross section of 6 ½ inches x 12 inches, with the reinforcement consisting of one ½-inch-diameter low-relaxation grade 270 strand. The beams were cast using each of the samples of strand from the manufacturers, and were released using flame cutting and saw cutting. The beams were cast as 90-foot specimens and were then saw-cut to various lengths. Lengths of the beams varied based on the desired embedment length that was going to be tested. Overnight end-slip measurements were taken at the ends of the beam that were flame-cut and also at the saw-cut ends of the beams. These lengths varied, but all but one group of strand exceeded the ACI predicted length. End-slip measurements were also taken at 7, 14, and 21 days after detensioning. The two groups of strand that failed the pullout test experienced a continually increasing transfer length by an average of 15 inches. These increased lengths were both longer than the predicted 29 inches by the ACI equation. The beams were then tested in flexure to determine the development lengths and to compare them with the end-slip and pullout results. The author discovered that higher pullout loads were in direct relationship to lower transfer and development lengths. Beams from the groups of strand with a lower pullout load failed suddenly and without any warning at a lower-than-calculated load. The author concluded that the pullout test developed by Moustafa (1974) was an acceptable method for determining bond characteristics of ½-inch-diameter prestressing strand. Beams from the strands that reached 36 kips on the pullout test, mainly failed from strand failure instead of strand slip. The author also concluded that immediate end-slip measurements failed to determine the final transfer- and development-length qualities on the strands and that 21-day, end-slip measurements more accurately predicted these qualities. The author recommended that future research should be done on the pullout method using high-range water reducers and pretensioned strand to test the effect that HRWR have on pullout capacity.

Cousins et al. (1992) developed a more realistic test method for determining bond parameters of various-sized prestressing strand. The test consisted of a concrete block with a single prestressing strand in the middle. The concrete block was pushed off of the strand after the concrete had cured. This method was developed to be a more realistic representation of the actual behavior of the strand than the direct pullout method. Strands that were tested included 3/8-, ½-, and 0.6-inch-diameter grade 270 low-relaxation strand. The ½-inch strand included lightly rusted, clean, and epoxy-coated strand with impregnated grit, whereas the 3/8- and 0.6-

inch-diameter strands only included clean and epoxy-coated with impregnated grit. The authors tested various concrete dimensions and chose an 8-inch x 8-inch block with an embedment length along the strand of 12 inches. The concrete was cast so that the prestressed strand was in the center of the block and was allowed to moist-cure for three days to reach an average compressive strength of about 4,000 psi. The authors discovered the newly developed method produced results similar to the direct pullout tests. The authors also concluded the varying standard deviation of the results could be attributed to grit density and rust variations of the strand. The authors finished by stating the bond stresses found by the new test method were higher and more practical than the direct-tension pullout method.

Martin and Scott (1976) developed a proposed new code equation for prestressing members whose span length is shorter than the calculated development length. The authors used previous research done by other researchers to develop a bi-linear curve to model the behavior of undeveloped members. The bi-linear curve allowed for an accurate method of predicting the design capacity of the shorter span members that would be more accurate than the current code equations. The authors concluded that the bi-linear curve was dependent on the diameter of the strand and embedment lengths, so the model could be used in all applications.

Khayat et al. (2004) analyzed various test methods available to test the performance of self-consolidating concrete (SCC). SCC has been increasing in popularity due to its flowable nature and reduced need for vibratory compaction. The authors tested various methods used to rate SCC mixes and compared the results. The test consisted of 16 SCC mixes whose water-to-cement ratios ranged from 0.32 to 0.47. The ratio of sand to course aggregate was kept the same for all mixes. High-range water-reducing admixture was used in all of the mixes and its amount was varied to produce the targeted slump. A set-retarding agent was used to maintain the targeted slump during testing. Each mix was tested with and without a viscosity-modifying admixture to test the changes in the mix. Each mixture was tested using the slump-cone, concrete rheometer, V-funnel, J-ring, L-box, U-box, and pressure-bleed tests, and all were given a visual stability index (VSI) rating. After comparing results from the tests, the authors had several conclusions. They found the slump and L-box or the slump and J-ring tests were both adequate to test the passing nature and deformability of the SCC mixes. The authors also concluded the VSI rating could be used along with the other tests to greatly improve the evaluation of the SCC mixtures.

Peterman (2007) tested the relationship of strand depth in relation to strand bond, and the effect of strand bond with relation to fluidity of the concrete. Three main tests were performed to determine these characteristics. The first consisted of casting beams at six different precast plants across the United States. Two different rectangular cross sections were cast, including 10 inches x 15 inches, 8 inches x 6 inches. The 8-inch x 6-inch beam had a strand at a depth of 4 ½ inches from the top of the beam. The 10-inch x 15-inch beams consisted of half with a strand two inches from the top of the beam and the other half with the strand 13 inches from the top of the beam. The strand used for all the beams was ½-inch in diameter, unweathered strand, from the same roll of strand. The strand was delivered to each plant prior to testing. Mixes from each plant varied, but the author recorded the rheological properties for each mix and found no correlation between them and the measured transfer lengths. Transfer lengths were measured on all of the beams using end-slip measurements after release by flame-cutting. The author discovered from the first test that transfer length decreased as distance from the top of the beam increased. The second test consisted of improved cross sections to reduce confinement of the strand. The cross sections were four-inch-wide rectangular beams, two with a height of 16 inches and two with a height of 28 inches. The strand location consisted of a bottom strand two inches from the bottom of the beam and a strand every six inches above that. This caused the 16-inch beam to have three strands and the 28-inch beam to have five strands, enabling a relationship between the strand location to the top and bottom of each beam. The author found the relationship between the transfer lengths and distance of the strand from the top surface had a coefficient of determination of 0.83. The author also found no relation between the column segregation test results and transfer length values. The third test consisted of casting four-inch panels and testing them while monitoring the end-slip measurement of the panels. The panels had a width of 24 inches and two 1/2-inch-diameter strands 2 ½ inches from the top and six inches in from each side of the beam. Lengths of the panels were varied to test embedment lengths of 30, 45, and 60 inches. The panels were cast using conventional and SCC mixes. The compressive strengths at 28 days were 6,850 psi and 6,985 psi for the SCC and conventional mixes, respectively. They were loaded to failure using a point load, and the SCC panels averaged a 30% lower nominal moment capacity than the conventional mix. Transfer lengths were also measured using end-slip measurements, and the SCC panels averaged a 30% longer transfer length than the conventional panels. The author concluded that location of the strand

with regard to the top of the beam was more influential than the amount of concrete below the strand. The author also concluded that as fluidity of the concrete increases, transfer length also increases.

Mitchell et al. (1993) tested the relationship concrete strength and strand diameter on transfer and development lengths of the prestressing strand. The test program consisted of 22 pretensioned concrete beams made using varying strand diameters and concrete mixes with different compressive strengths. The strand diameters tested were 3/8, ½, and 0.62 inches strand, and concrete compressive strengths ranged from 4,500 to 12,900 at 28 days. Tests showed the higher compressive strength concrete beams had lower transfer lengths. The increased strength provided a higher modulus and better bond characteristics, which decreased losses due to elastic shortening. Testing also confirmed previous research showing smaller strand diameters result in smaller transfer lengths. Testing showed that development length decreased in relation to the increase in concrete compressive strength. The authors concluded compressive strength of the concrete at release and long term has a large effect on embedment length and greatly changes the capacity of the beam.

Peterman et al. (2000) investigated transfer and development lengths of semi-lightweight concrete beams. Semi-lightweight concrete averaged a density on 130 lb/ft^3 and was achieved by replacing part of the course aggregate with expanded shale, which has a lower density. The investigation consisted of casting and testing 14 concrete beams that had rectangular and T-shaped cross sections. All of the prestressing strand used in this study was ½-inch-diameter special strand from two different manufacturers. The mix used for all tests in this investigation was designed to have a compressive strength of 7000 psi. Rectangular sections used for transfer-length equations were 4 inches x 6 inches and had two prestressing strands evenly placed in the beam. Two transfer-length beams were cast to test the transfer lengths of the two different manufacturers. The beams were mounted with stainless steel points to measure the transfer lengths with a Whittemore gage. Testing showed that all but one of the transfer lengths were found to be lower than the 50 times the strand diameter advised to be used by AASHTO and ACI. The transfer length 70 times the strand diameter was on the end of the beam that had experienced some cracking in the concrete. Rectangular beams used for development tests consisted of an 8-inch x 12-inch cross section, with one strand centered in the beam 10 inches from the top of the beam. Six 8-inch x 12-inch beams were fabricated to be used for 12 different

tests by making the length of the beams longer so that each end could be tested separately. Three of the beams used strand from manufacturer "A" and the other three used strand from manufacturer "B." The beams were loaded with a point load at the critical section of the member, which was the distance of the embedment length from the end to be tested. Flexure tests from the development lengths showed all the beams reached nominal moment capacity. Results showed the prescribed AASHTO and ACI equations were adequate to be used on semi-lightweight concrete prestressed beams. The final part of the investigation consisted of testing multiple-strand T-beam sections. The T-beam section used had a total height of 21 inches and a flange height of six inches. The flange had a width of 36 inches and the web had a width of 16 inches. Five prestressing strand were located two inches from the bottom and were centered and spaced two inches on center. Two of the beams had strand from manufacturer "A" and the other beam had strand from manufacturer "B." No. 4 stirrups were placed every six inches, which was more than twice the 15 inches recommended by AASHTO and ACI. The beams' lengths were twice the calculated embedment length plus six inches to account for the spreader beam that was to be used during testing. The T-beams were loaded to failure using a hydraulic actuator while load and deflection readings were taken. The two beams using strand from manufacturer "A" failed in a ductile mode after reaching the calculated nominal moment. The third beam, using strand from manufacture "B," failed suddenly by strand slip but it also reached the calculated nominal moment. Three additional beams were made using strand from manufacturer "B" to test the effect of shear reinforcement on the failure mode of the beams. Spacing at the center of the beams was varied to be three inches, six inches, and 15 inches for each of the three beams, respectively, with ends of all the beams having spacing of six inches. The beam with three-inch spacing failed in strand rupture and the other two failed by bond failure. The authors concluded that flexure-shear cracks developed prior to the bond failure of the three "B" beams. The flexure-shear crack caused the amount of tension force required to increase at the point of the crack and to cause the strand to slip, even though the T-beams reached nominal capacity and an increase in transverse reinforcement would increase the ductile nature of the failure. The authors also concluded code equations for transverse reinforcement should be multiplied by 2.5 to 5 times to effectively cause the beam to fail in flexure and not bond failure.

Mitchell and Marzouk (2007) tested high-strength lightweight concrete's bonding properties. The testing procedure was used to determine if the 30% increase in development

length for the ACI code equation was justified. The program consisted of 72 pullout and push-in specimens being fabricated using high-strength lightweight concrete. Each of the specimens had a #8 or #11 bar cast in its center. The concrete mix had a water-to-cement ratio of 0.30, and a high-range water-reducing agent was used to increase the fluidity of the mix. A ¾iinch max-sized lightweight aggregate was used and average compressive strength achieved by the different mixes was 12,049 psi. The authors discovered that the relationship of bond strength of the concrete was closer in comparison to the European-used cubic root of the concrete strength, than the square root used by ACI. The authors also concluded that bond strength of the lightweight concrete was only 6 to 10% below the code equations for normal weight, instead of the 30% recommended by ACI for lightweight aggregates.

Russell and Burns (1996) investigated the transfer lengths that are present in 0.5-and-0.6 inch-diameter prestressing strand. The authors tested the transfer lengths of specimens while changing several variables: strand size and number per specimen, shape of the specimen, amount of mild steel reinforcement causing confinement, spacing of the strand, and presence of debonding strand. The test was used to compare results with the equations given by ACI and AASHTO. Transfer lengths were measured using end-slip readings and DEMEC points. The authors used a smoothed-line technique to create the strain profile along the beam, using DEMEC measurements. The authors explained that transfer length was 95% of the average max strain value on the strain profile. The research showed the amount of confinement on the strands did not increase the transfer lengths. The 0.6-inch-diameter strand was found to produce reliable and repeatable transfer lengths; however, these lengths were on average 36% longer than the 0.5-inch-diameter strand. The authors concluded the code equations should be amended for 0.6-inch-diameter strand to enable it to be used with at least a spacing of two inches. The amended code equation could also be used for the 0.5-inch-diameter strand to be a more conservative estimate of the transfer length.

Barnes et al. (2003) tested factors that cause transfer length to vary, including concrete strength, strand surface condition, method of prestress release, and time at which the transfer length is recorded. The authors tested the transfer length of 36 AASHTO Type I girders during this investigation. Testing showed that rusted strand experienced a shorter transfer length then brighter strand. Transfer lengths were also found to increase over time, with the average increase being between 10 to 20 percent. This increase was found to happen within the first 28

days after transfer of the prestress force. The authors concluded that sudden release of prestress force increased transfer lengths of rusted prestressing strand by as much as 50% but had little effect on concrete with strengths higher than 7,000 psi.

Girgis and Tuan (2005) researched bond characteristics of self-consolidating concrete. Testing included measuring transfer length of three girders, each poured using a specially designed mix. Two of the girders were cast using two specially designed SCC mixtures. The third girder, to be used as a control, was cast using a regular conventional mixture. The mixtures were tested for bond strength using a 0.6-inch-diameter strand with the Moustafa (1974) pullout test. Testing showed all three mixes had pullout strengths greater than the 36 kips recommended by Moustafa (1974). The girders were mounted with DEMEC points to measure transfer lengths of the three mixtures. The two SCC mixtures had transfer lengths, at 36 and 43 inches, that averaged longer than the ACI-recommended 30 inches. The control mix girder had an average transfer length of 20 inches. Compressive strength of the control mix was higher than the SCC mixes, which could account for shorter transfer lengths. The authors concluded that SCC mixes may have longer transfer lengths than conventional mixes and that future research is needed to verify these results.

Larson et al. (2007) tested bond properties of self-consolidating concrete. Transfer and development-length equations were tested by casting SCC beams that had been monitored for transfer and development length. Various cross sections were used to test the development length, and one cross section tested the effect of a top strand and its bonding characteristics. The strand used for these beams was tested using the pullout method recommended by Moustafa (1974) to verify the bonding quality of the SCC mixture. Pullout tests showed the recommended values by Moustafa (1974) should only be used for conventional mixes, and a higher value should be expected for SCC mixtures. Transfer-length results showed that equations proposed by AASHTO and ACI were acceptable for determining the transfer lengths of SCC mixtures. Transfer lengths were found to increase over the first 21 days after detensioning. This increase was more pronounced in the top strand, which increased on average, 40% to 45%. Bottom strand transfer lengths were found to increase 10% to 20%. Flexural testing on the SCC beams showed that equations for 100% and 80% embedment lengths were conservative in predicting the nominal moment capacity of the SCC flexure beams. The 100% embedment lengths held 10% to 20% more than predicted, and the 80% beams held 25% to 35% more load than

predicted. The authors concluded that the SCC mixture performed adequately well and the AASHTO and ACI equations, while conservative, can be used dependably to predict behavior of SCC mixes and beams.

CHAPTER 3 - IT Design and Fabrication

This section discusses design and fabrication of inverted tee beams (ITs). ITs were cast to determine the transfer length and prestress losses of lightweight **s**elf-**c**onsolidating **c**oncrete (SCC) and **con**ventional concrete (CON) mixes. Two sets of ITs were cast due to low concrete strengths on the first set. Both sets of ITs were cast in Newton, Kan., at Prestressed Concrete Incorporated (PCI). The first set of beams were cast on December 3, 2008, and the second set on September 29, 2009.

3.1 IT Design

The IT 600s selected were eight feet in length and the cross-sectional dimensions are shown in Figure 3.1. The beams were chosen to be able to provide enough length to fully transfer the prestress force into the concrete. Design assumptions of the IT 600 can be seen in Table 3.1. There were eight beams in each set poured—four conventional mix beams, along with four SCC beams. Two of the beams were prestressed, and the other two included the same amount and location of prestressing steel but were not stressed.

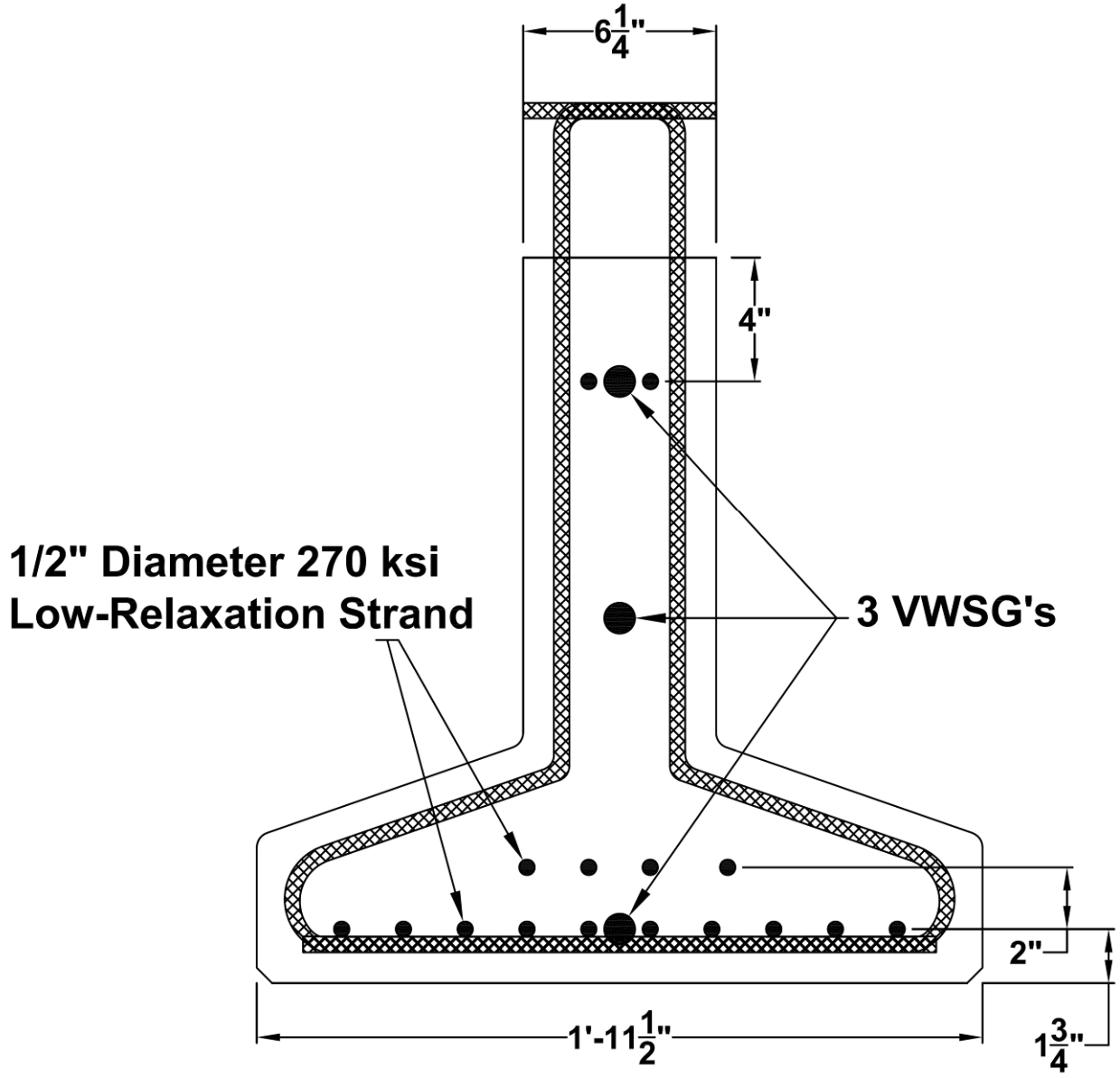

Figure 3.1 Cross section of IT 600

Table 3.1 Design assumptions of IT 600

f_{ci}=	3,500	psi	L=	96	in
E_{ci}=	2,250	ksi	V/S=	2.87	in
A=	256	in^2	f_{pj}=	198	ksi
I=	12,822	in^4	E_{ps}=	28,500	ksi
Y_{bot}=	8.45	in	RH=	65	%
e=	3.86	in	A_{ps}=	2.448	in^2
H=	23.5	in	f'_c=	5,000	psi

3.2 IT Fabrication

SCC IT specimens were poured in two different batches (SCC #1 and SCC #2) based on the capacity of the pan mixer at PCI. One tensioned beam was poured along with one untensioned beam for each batch to ensure the specimens would be companion specimens. All four CON IT specimens were poured using the same mix. Figures 3.2 and 3.3 show the forms for the tensioned and untensioned beams, respectively. Figure 3.4 shows one of the SCC IT beams being cast.

Figure 3.2 Tensioned beams' forms

Figure 3.3 Untensioned beams' forms

Figure 3.4 SCC beam being poured

Whittemore points were cast on each side of the tensioned ITs at the same height as the centroid of the prestressed strand. These points were used to measure the transfer length of the ITs. The points were brass inserts mounted to a steel bar that was attached to the forms prior to pouring the specimens, as can be seen in Figure 3.5.

Figure 3.5 Whittemore points attached to IT forms

When the beams were ready to be removed from the forms, the steel bars were unbolted from the forms. Once the forms were removed, screws attaching the brass inserts to the steel bar were removed and the steel bar was pulled away from the side of the specimens. Figure 3.6 shows the steel bar attached to the IT after the forms were removed, and Figure 3.7 shows the brass inserts left after the steel bar was removed from the side of the specimen.

Figure 3.6 Steel bar attached to Whittemore points

Figure 3.7 Whittemore points cast into ITs

The untensioned beams were cast to measure shrinkage in the beams and subtract it from the tensioned beams to isolate creep in the ITs. All the beams were instrumented with vibrating wire strain gages (VWSGs) to measure internal strains in the beams. The VWSGs were Model VCE-4200's manufactured by Geokon Inc., Lebanon, New Hampshire. Three VWSGs were cast at the mid-span of each beam; the location of each can be seen in Figure 3.1. The VWSGs were mounted prior to pouring the specimens and were attached to the strand or stirrups, depending on their location, using foam and zip ties. This was done to insure the VWSGs stayed in place during the pour and to ensure they were not damaged. Figure 3.8 shows a VWSG mounted to one of the bottom strands, and Figure 3.9 shows all three VWSGs mounted prior to casting of the specimens.

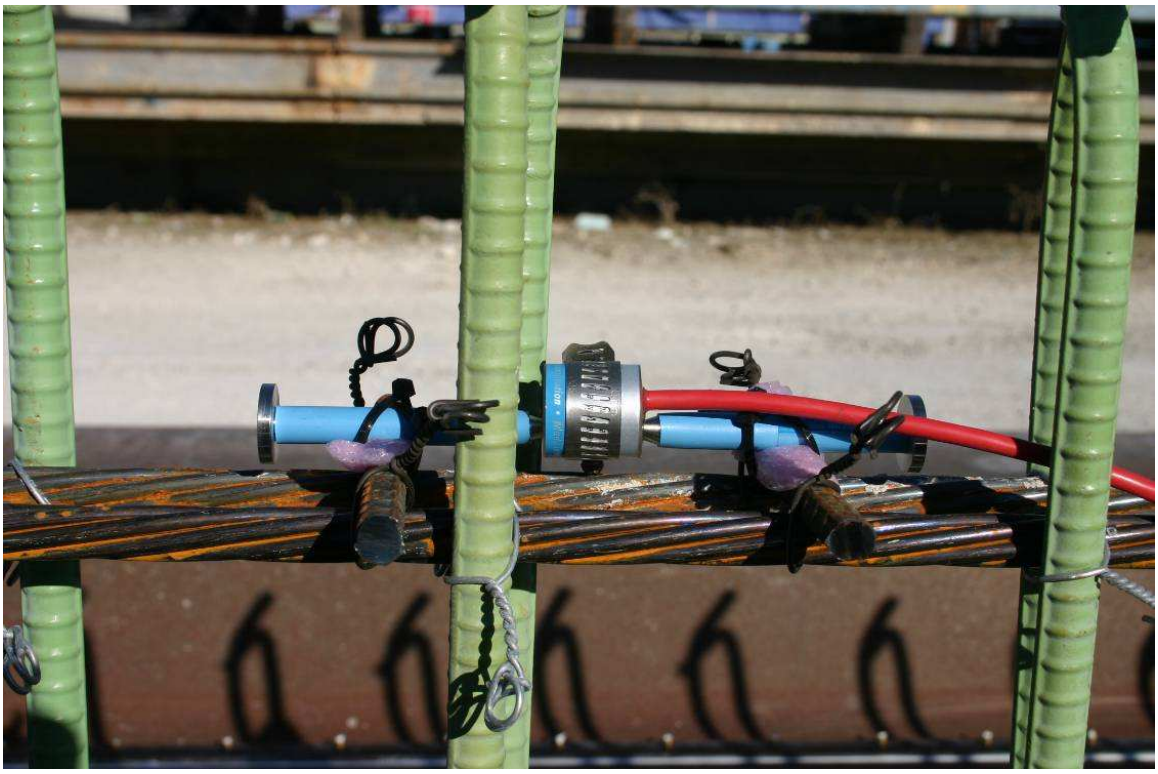

Figure 3.8 VWSG mounted to top strands

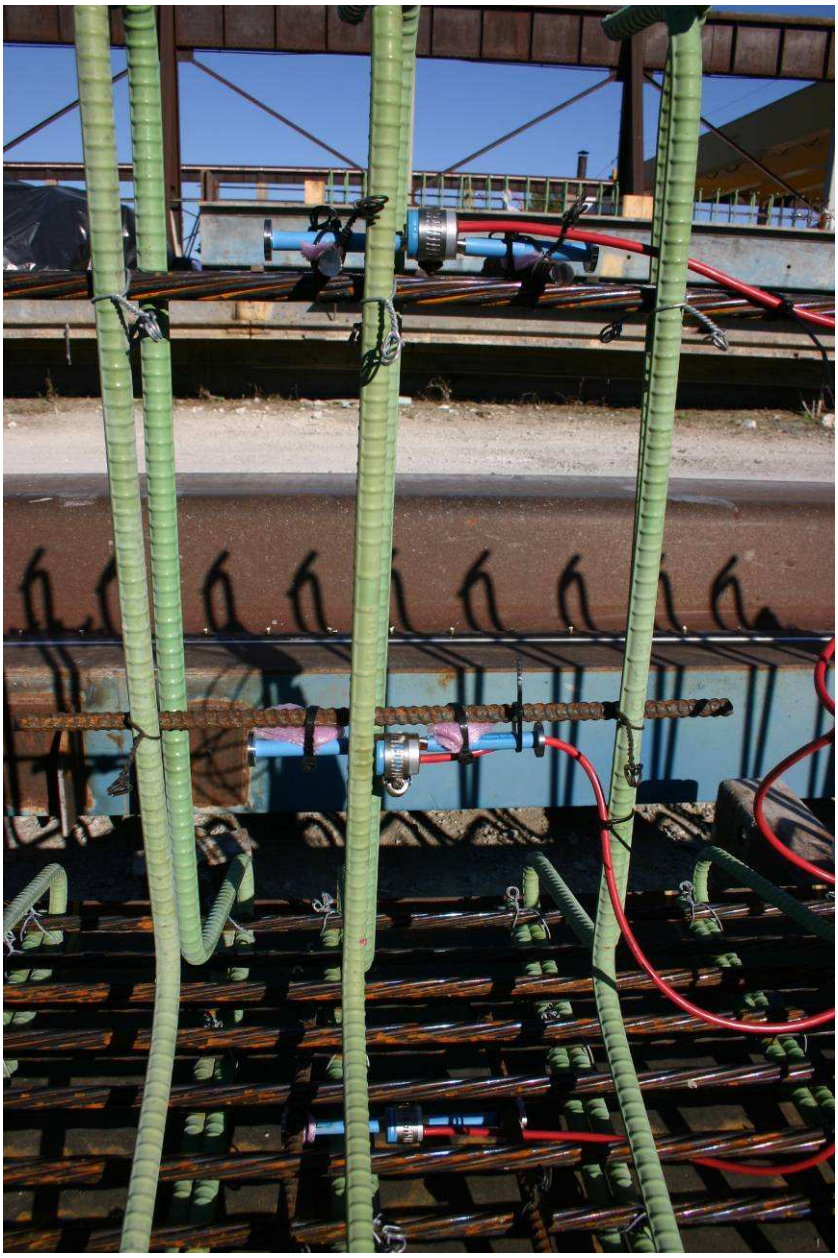

Figure 3.9 Location of VWSGs in beam

3.3 Mix Properties

Test cylinders were made for each set of beams to be able to determine the concrete strength at release following ASTM C31 and C192 (2009). The compressive and splitting tensile strength testing followed ASTM C39 and C496 (2009). Along with test cylinders, creep and shrinkages specimens were also cast with each set of beams. All testing of the lightweight mixes

was done according to ASTM C330 (2009). Slump, air, and unit weight of each conventional mix was measured according to ATSM C143, C173, and C138 (2009), respectively. For the SCC mixes, spread, air, unit weight, J-ring, L-box, and VSI were measured. The spread and J-ring were measured according to ASTM C1611 and C1621 (2009). J-ring testing showed minimal blocking of the aggregate. No visible bleeding was seen by the author during testing of any of the SCC mixes. Figure 3.10 shows the J-ring and L-box being tested for one of the SCC mixes. The lightweight aggregate was from Buildex in Marquette, Kan. The properties of the lightweight aggregate can be seen in Table 3.2. The sand that was used in this study had a specific gravity of 2.62. The sand and lightweight aggregate batch weights were adjusted for tested surface moisture.

Figure 3.10 Performing J-ring and L-box tests

Table 3.2 Buildex aggregate properties

Buildex Marquette Aggregate	
Blend Used	3/8" x No. 8
Dry Specific Gravity	1.3
Absorbtion after 24 hours	20%
S.G. with 15% moisture absorbed	1.45*

***value used in mix design**

Mix designs for the two sets of beams can be seen in Table 3.3. The pour properties can be seen in Table 3.4 along with compressive and splitting tensile strengths of the IT beams. The beams were detensioned by flame-cutting the strand. Each strand was cut at the same time on each side of the beams. Figure 3.11 shows workers flame-cutting the strands simultaneously.

Table 3.3 Mix designs of ITs

Batch (per yd^3)		Dry Sand (lbs)	Surface Dry Marquette (lbs)	Type III Cement (lbs)	Water (lbs)	Adva Cast 530 (oz)	Adva Flow 555 (oz)	Air Entrainer (oz)	Theoretical unit weight (pcf)	Theoretical water to cement ratio
First ITs Cast on December 3, 2008	SCC #1	1350	807	697	231	125	0	5.8	117.9	0.331
	SCC #2	1358	800	702	231	116	0	5.8	117.7	0.329
	CON #1	1667	693	656	217	0	91	6	121.9	0.331
Second ITs Cast on September 29, 2009	SCC #1	1396	827	661	214	109	0	5.5	118.8	0.323
	SCC #2	1398	828	662	212	110	0	6.4	118.4	0.32
	CON #1	1667	693	656	217	0	91	6	121.9	0.331

Table 3.4 Pour properties of both sets of ITs

Batch		Spread/ Slump (in)	Air (%)	Unit Weight (pcf)	1-Day Compressive Strength (psi)	4-Day Release Strength (psi)	28-Day Compressive Strength (psi)	28-Day Split-Tensile Strength (psi)
First ITs Cast on December 3, 2008	SCC #1	26	4.5	116.5	1765	2315	3275	318
	SCC #2	25.5	5	115.2	1845	2438	3365	310
	CON	6.5	4.5	114.5	3524	3994	5124	424
Second ITs Cast on September 29, 2009	SCC #1	17	7	108.07	3382	3541	4294	350
	SCC #2	20.5	8	104.6	2505	2881	3418	312
	CON	7	9	109.5	2984	3661	5190	435

Figure 3.11 Workers simultaneously flame-cutting the prestress strand

The ITs were transported to Kansas State University (KSU) after being removed from the forms. There they were monitored outside to measure time-dependent losses, creep, and shrinkage of the specimens. Figure 3.12 shows the specimens blocked off the ground at each end to be able to take measurements at KSU. Readings were taken everyday until a week after transfer; then the readings were taken every week until a month after transfer. The remaining readings were taken monthy.

Figure 3.12 SCC IT beams at KSU

3.4 Additional Mix Testing

After low concrete strengths on both sets of IT beams, addition SCC mixes were batched at PCI. The mixes had the same design as the mixes used in the IT specimens. Table 3.5 shows the results from these trial batches. The trial mixes showed consistency in the one day compressive strengths.

Table 3.5 Additional trial mix results

Date	Spread (in)	Air (%)	Unit Weight (pcf)	1 Day Compressive Strength (psi)
7/23/2009	26	3	122.6	5371
8/6/2009	22	4	121.7	5491
8/19/2009	23	4.5	116.6	5239

CHAPTER 4 - IT Results

This section discusses results from the ITs instrumented with Whittemore points and VWSGs. Measurements were taken before and after detensioning. The readings were also taken at KSU to determine long-term results.

4.1 Transfer Length Results

The ITs were monitored using Whittemore points cast into the sides of the beams. These reading were taken before and after detensioning. They were also taken for several months at KSU. These readings were used to calculate the amount of surface strain each IT developed and at what location of the beam these strains became constant. As the prestress force is transferred to the beam, the concrete will develop strain. The prestress force is transferred over a certain length dependent on the strand and the concrete mix, which is called the transfer length. When the surface strains become constant, the strand force is considered to be transferred. Distance between the Whittemore points was measured using a Whittemore strain gage shown in Figure 4.1.

Figure 4.1 Whittemore strain gage

These measurements were converted into strain based on Equation 4.1. Strain measurements for each location on the beam were used to graph the strain with relation to its horizontal location on the beam.

$$\varepsilon = \frac{\Delta L}{L} \tag{4.1}$$

where:

ε = strain reading

ΔL = change in length

L = original gauge length

The values were smoothed using Equation 4.2 (Russell and Burns 1996).

$$(Strain)_x = \frac{(Strain)_{x-1} + (Strain)_x + (Strain)_{x+1}}{3} \tag{4.2}$$

Both sets of ITs were monitored to find the transfer lengths of the SCC and CON mixes. The nomenclature used for these specimens was **S**CC **t**ensioned (ST) and **C**ON **t**ensioned (CT). Transfer lengths were measured at various times to account for any increase in length found by Barnes et al. (2003). Data from several of these times were plotted. The "95% average maximum strain" method was used to find the transfer length of each side of the IT beams (Russell and Burns 1996). Values from each side of the beams were averaged to find the mean strain value for each location along the beam. Figures 4.2 and 4.3 show transfer length graphs for the first set of CT #1 and ST #1 IT beams. Transfer length graphs for the second set of CT #1 and ST #1 specimens can be seen in Figures 4.4 and 4.5, respectively. Graphs for both sets of CT #2 and ST #2 beam specimens can be seen in Appendix A-1.

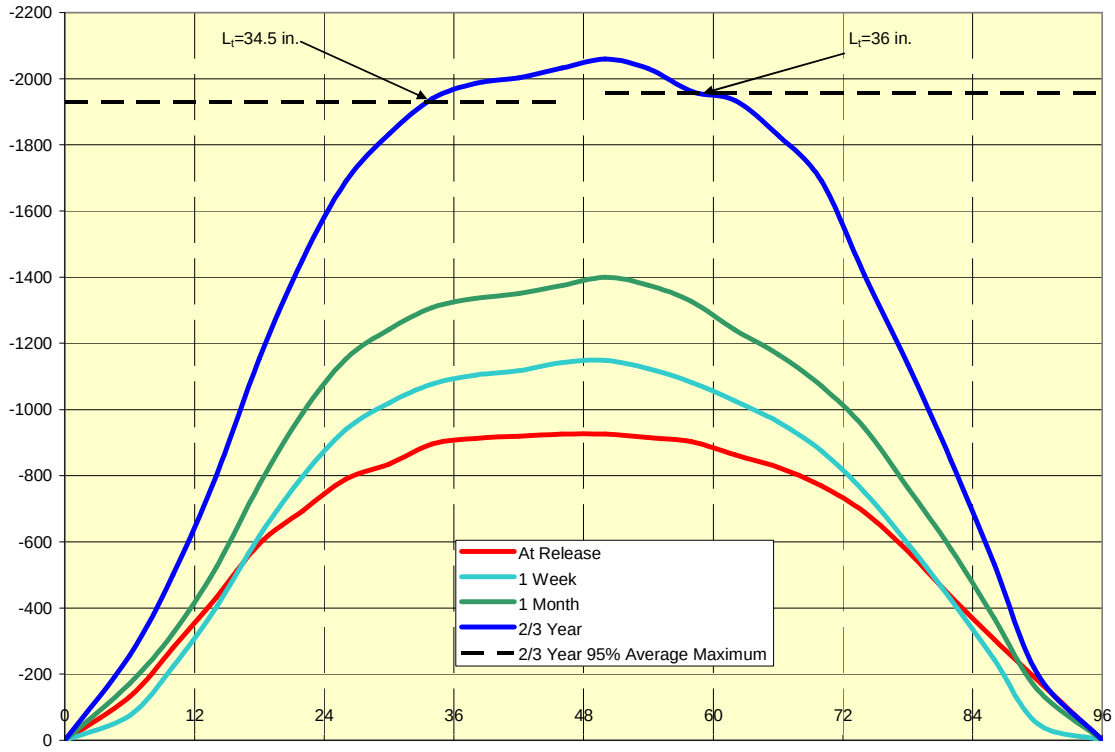

Figure 4.2 First set CT #1 transfer length

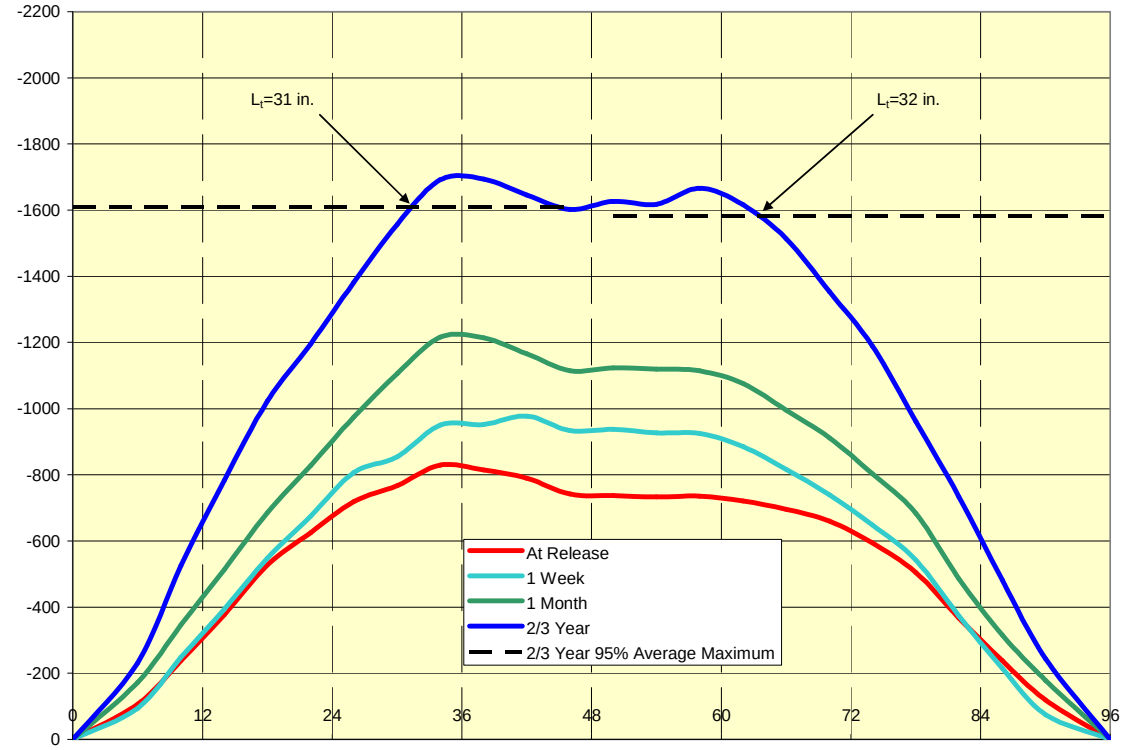

Figure 4.3 First set ST #1 transfer length

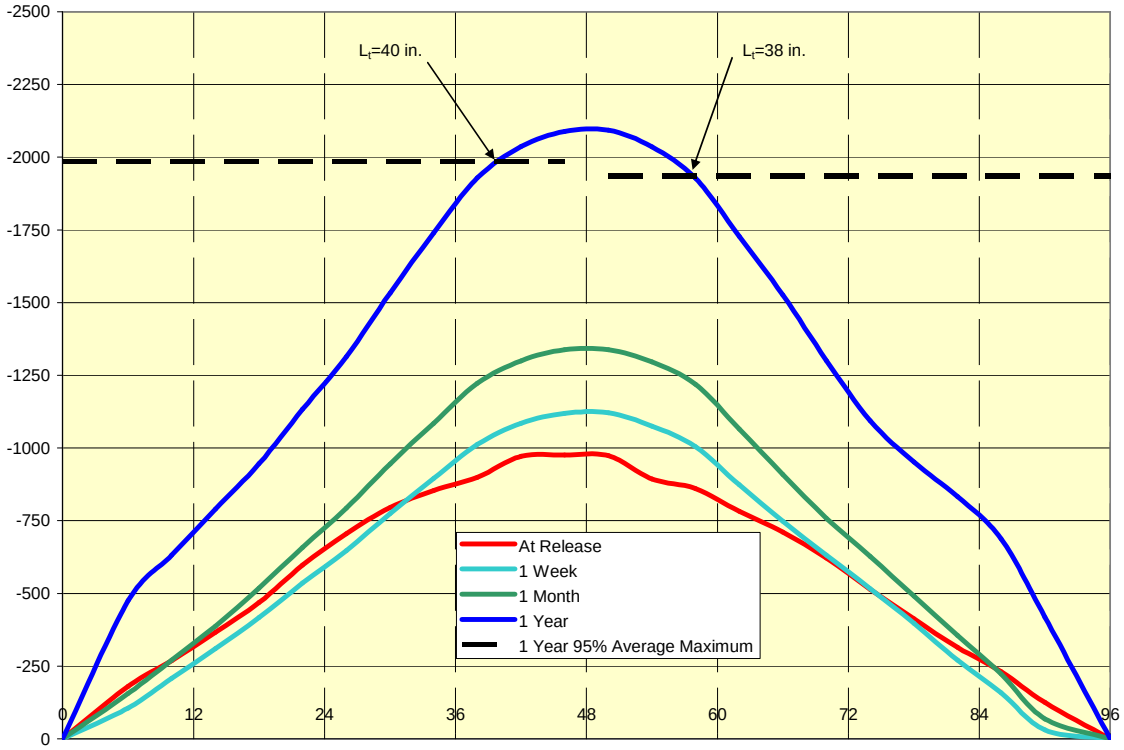

Figure 4.4 Second set CT #1 transfer length

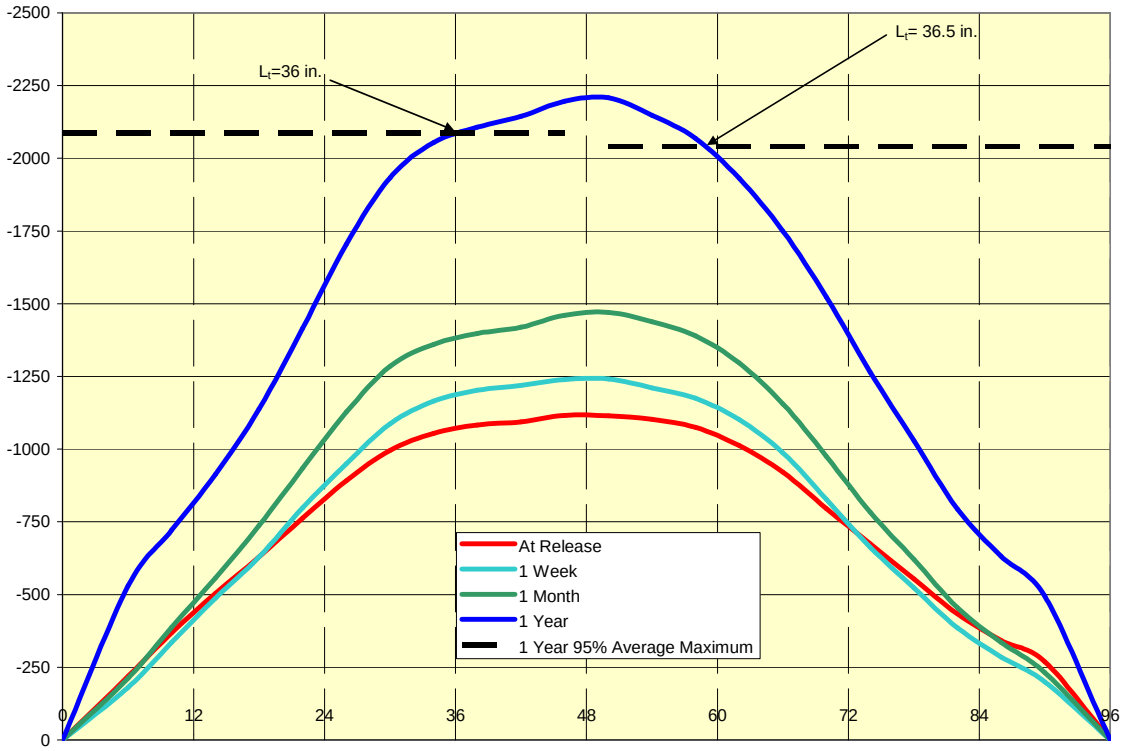

Figure 4.5 Second set ST #1 transfer length

A summary of transfer lengths from both sets of the IT beams can be seen in Table 4.1. All of the IT beams failed to have transfer lengths below the AASHTO recommended 60 times the strand diameter or 30 inches (2004). The transfer lengths were all found to be greater than 35 inches at one year for all of the beams tested. The low concrete strengths at transfer could cause the increase in transfer lengths. The long term transfer lengths were found to be 19 to 30 percent higher than the recommended AASHTO value. Use of longer IT specimens could produce better plateau in transfer length graphs instead of a peaked graph.

Table 4.1 Summary of IT transfer lengths

	Transfer Lengths									
	At Release		1 Week		1 Month		2/3 or 1 Year		2/3 or 1 Year	Exp. L_t/
Beam	Left	Right	Left	Right	Left	Right	Left	Right	Average	AASHTO L_t
1st Set										
CT #1	34	36	34	39	28.5	34	34.5	36	35.25	1.18
CT #2	30	33	30	36	27	31	31.5	33	32.25	1.08
ST #1	31	30	33	34.5	29.5	25	31	32	31.5	1.05
ST #2	30	29	31	29	24	27.5	33	32	32.5	1.08
2nd Set										
CT #1	40	37	40	39	40	38	40	38	39	1.30
CT #2	34	36	35	38.5	33	38	33.5	38	35.75	1.19
ST #1	34	36	35	36	36	36	36	36.5	36.25	1.21
ST #2	36	34	41	38	41	38	41	36.5	38.75	1.29

4.2 Prestress Loss Results

All 16 IT beams were internally instrumented with VWSGs. These gages were installed to monitor time-dependent losses of prestress force. Strains recorded by the VWSGs were plotted, along with the location in the beam at which each gage was mounted. Figures 4.6 and 4.7 show the graphs for the first set of CT #1 and ST #1 specimens. The second set of tensioned beams can be seen in Figures 4.8 and 4.9. The untensioned specimen results were used to subtract shrinkage strains from creep strains. The nomenclature used for these beams was **C**ON **u**n**t**ensioned (CUT) and **S**CC **u**n**t**ensioned (SUT). Figures 4.10 and 4.11 show the VWSG strains for the first set of untensioned IT beams, CUT #1 and SUT #1, respectively. The second set of control beams are shown in Figures 4.12 and 4.13. Graphs for the remaining eight beams can be seen in Appendix A.2.

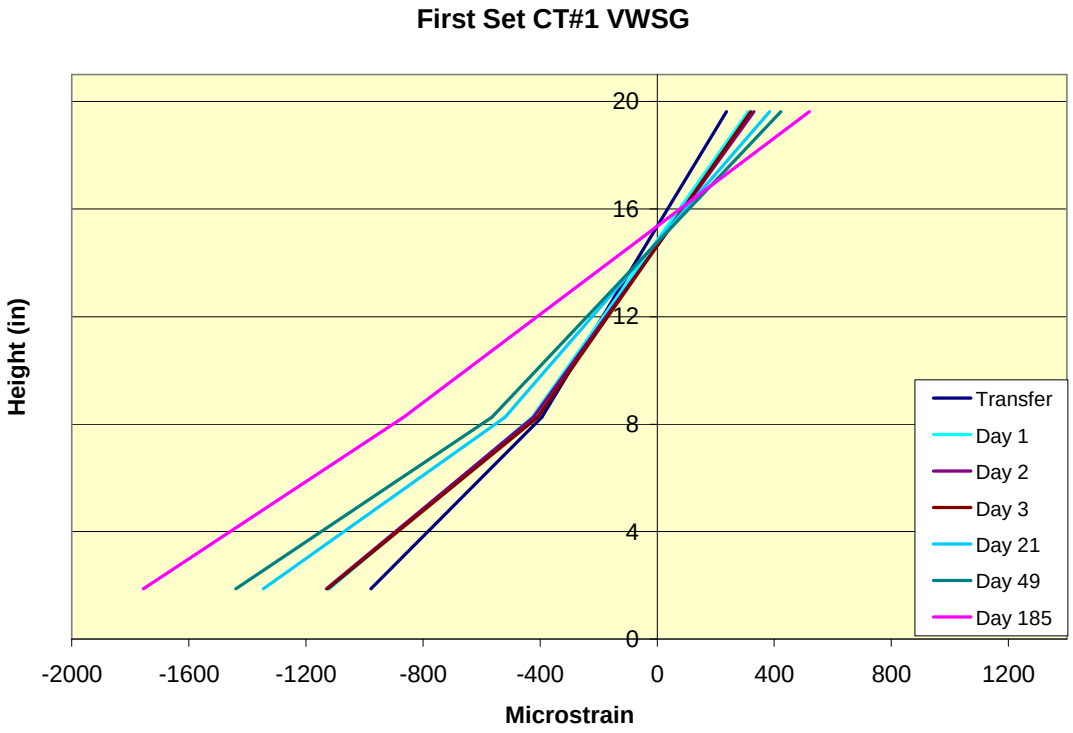

Figure 4.6 First set CT #1 strains (due to creep, shrinkage, and elastic shortening losses)

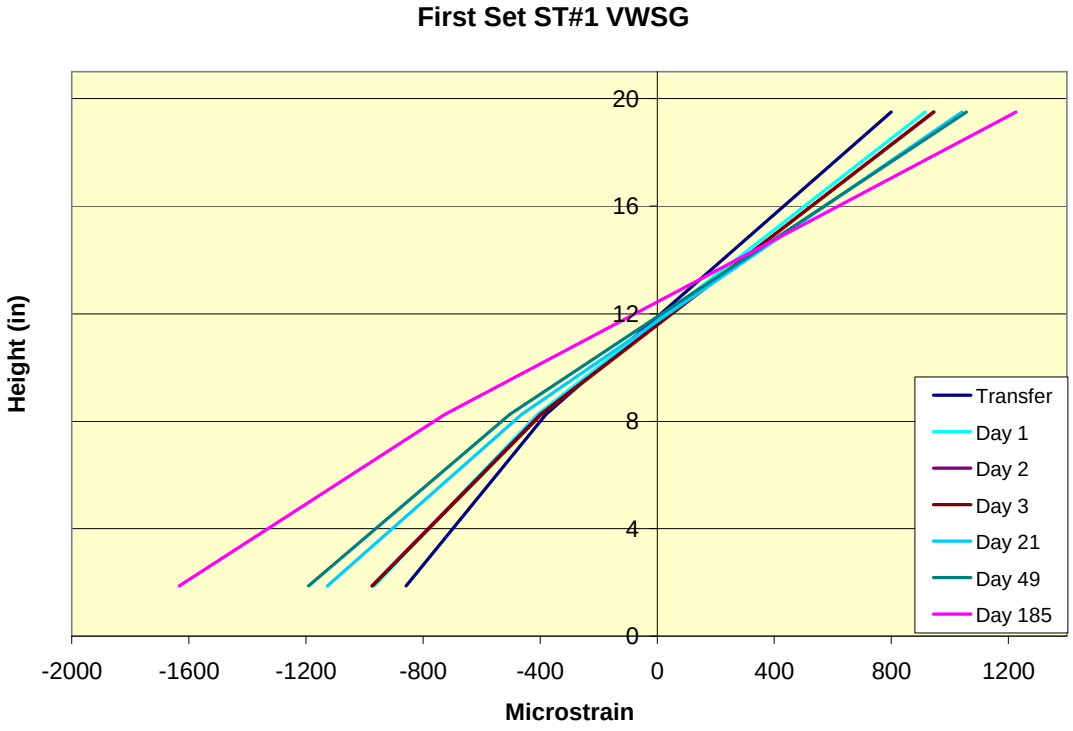

Figure 4.7 First set ST#1 strains (due to creep, shrinkage, and elastic shortening losses)

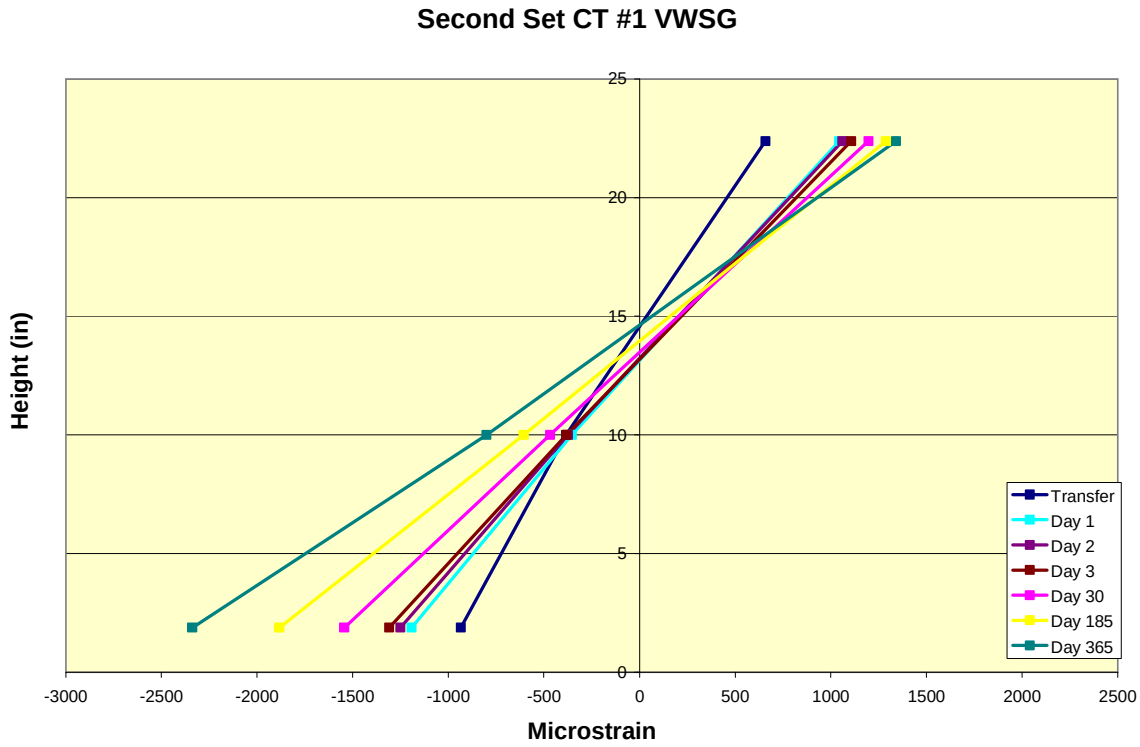

Figure 4.8 Second set CT #1 strains (due to creep, shrinkage, and elastic shortening losses)

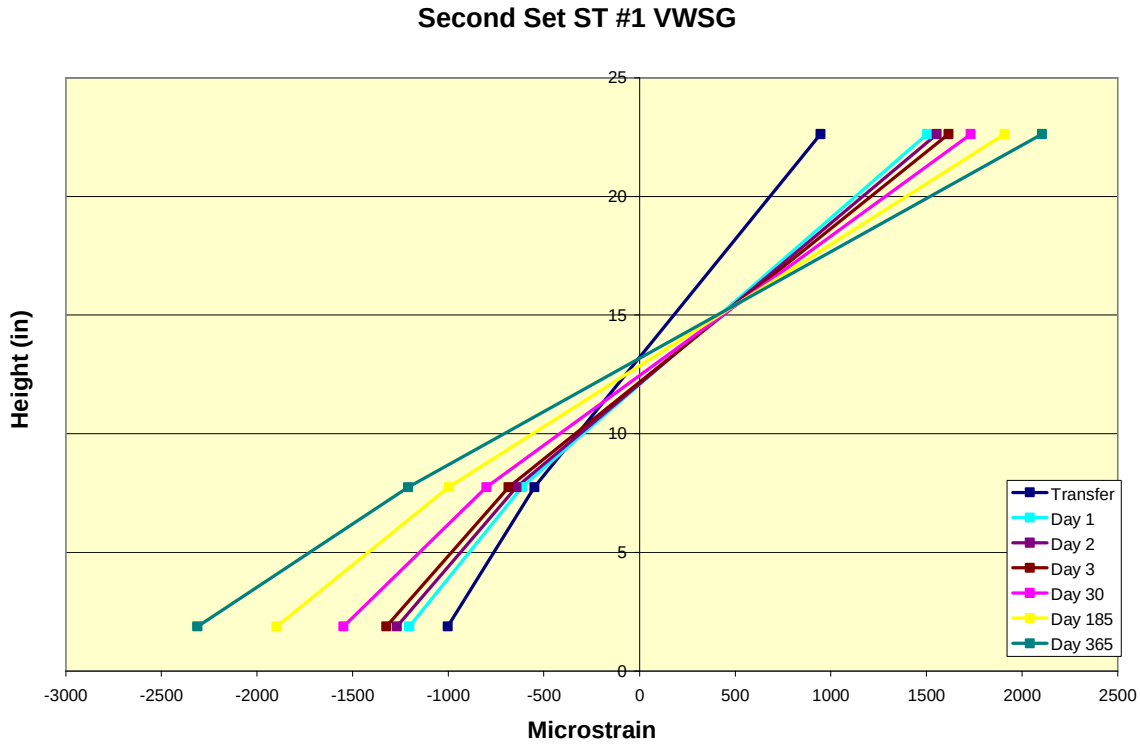

Figure 4.9 Second set ST #1 strains (due to creep, shrinkage, and elastic shortening losses)

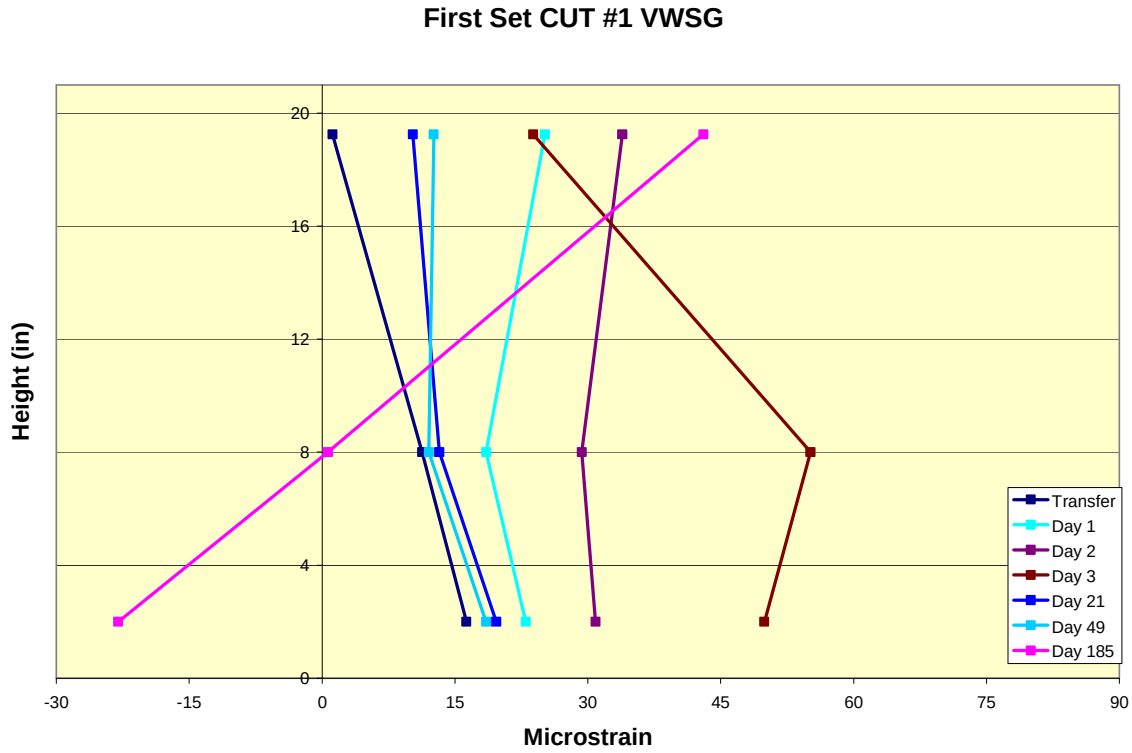

Figure 4.10 First set CUT #1 concrete strains (change due to shrinkage losses)

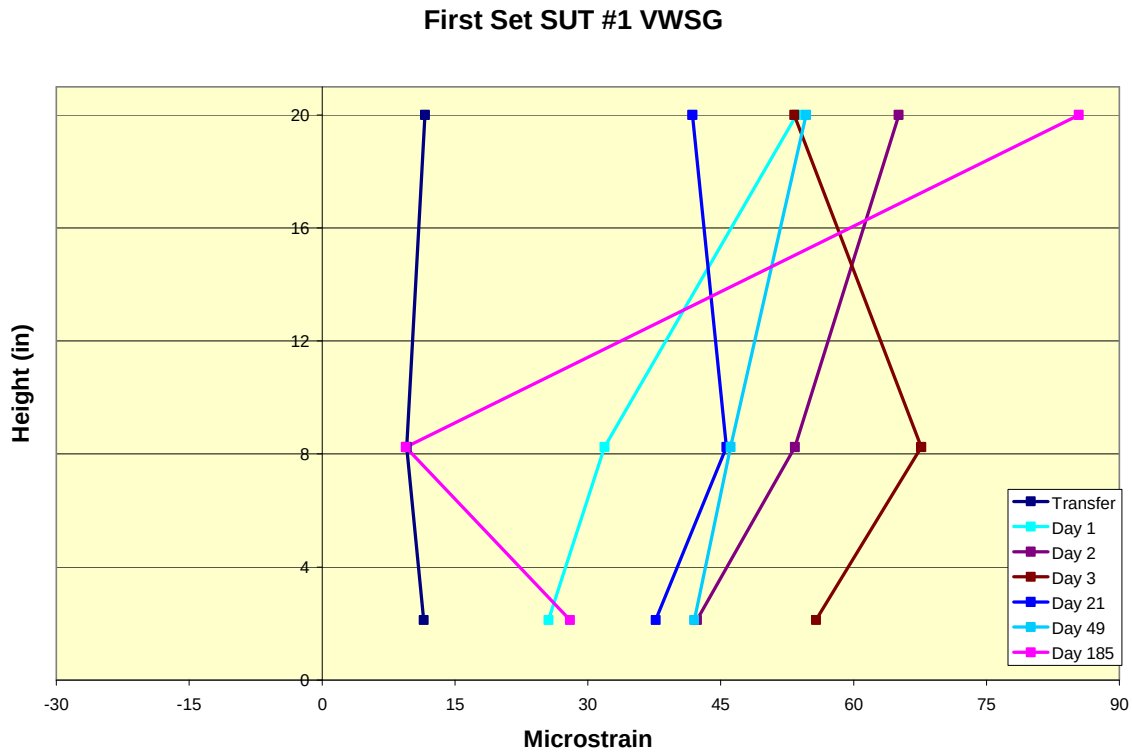

Figure 4.11 First set SUT #1 concrete strains (change due to shrinkage losses)

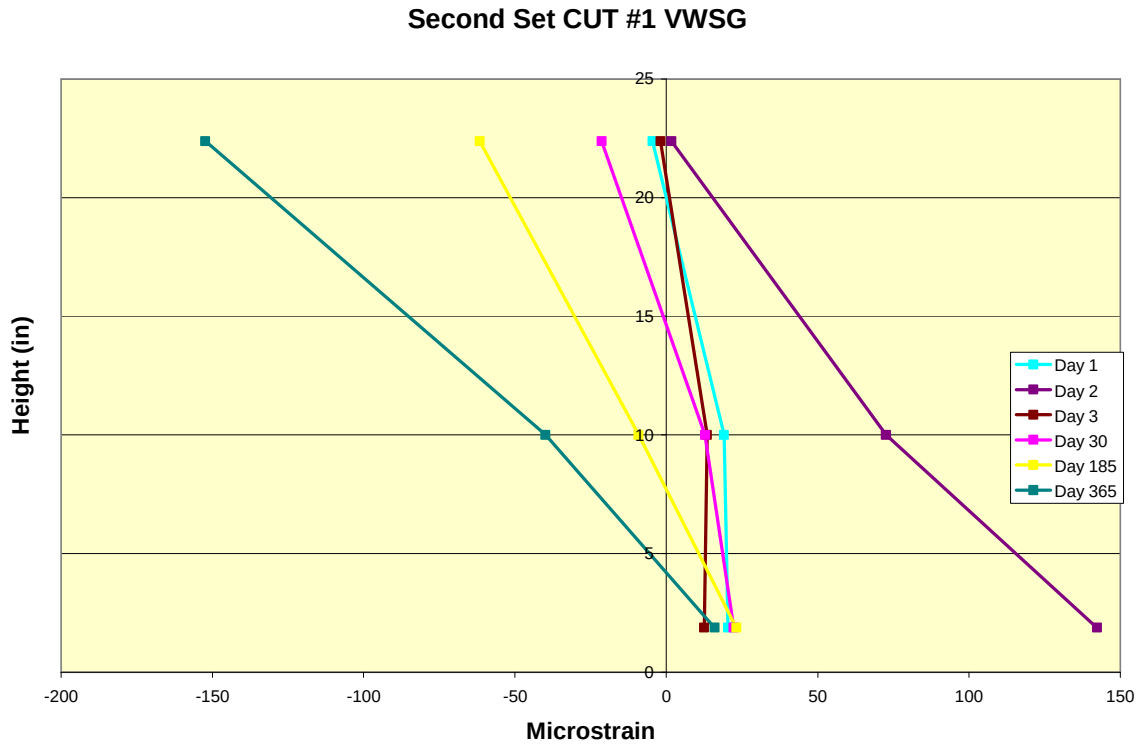

Figure 4.8 Second set CUT #1 concrete strains (change due to shrinkage losses)

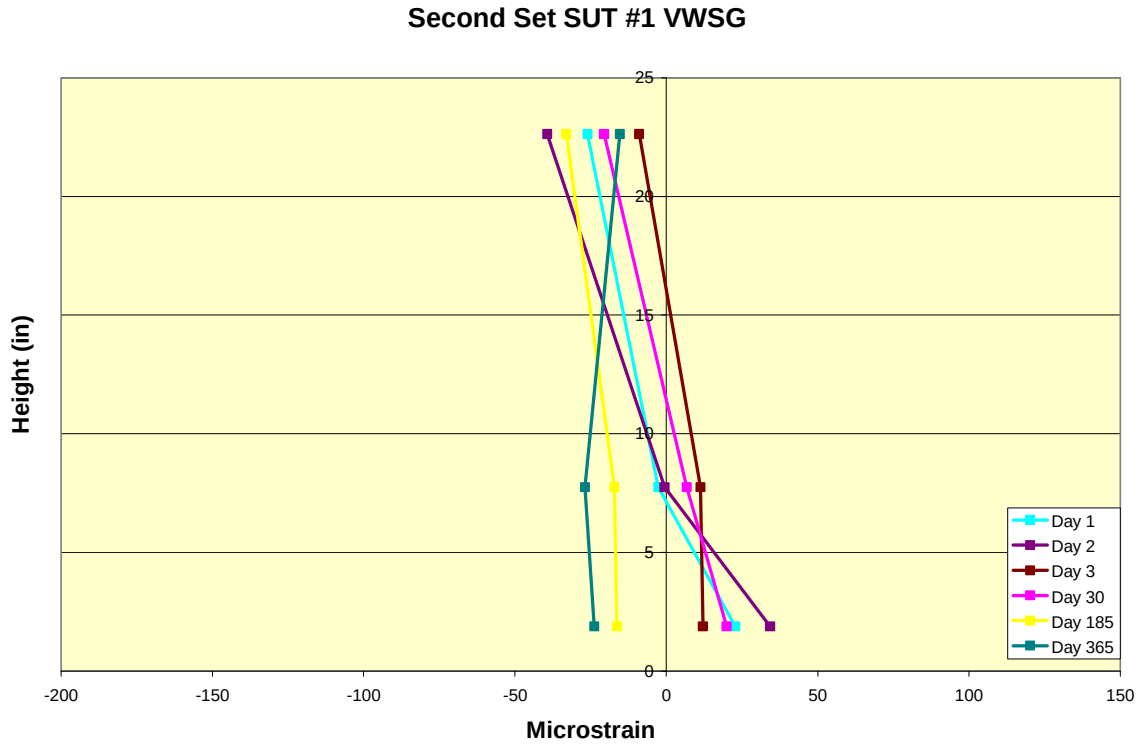

Figure 4.9 Second set SUT #1 concrete strains (change due to shrinkage losses)

Strains from the VWSGs were used to determine experimental prestress losses in the IT beams. Elastic shortening was the strain present in the bottom VWSG immediately after detensioning. Creep was the value from the tensioned IT specimens after elastic shortening and shrinkage readings were subtracted. Equation 4.3 was used to convert the VWSG strain into prestress loss.

$$\sigma = E\varepsilon \tag{4.3}$$

where:

σ = prestress loss

E = modulus of elasticity of prestress strand (28,500 ksi)

ε = strain reading

Experimental prestress losses were compared with ACI, PCI, and AASHTO code equations. The equations used can be seen in Appendix A.3. ACI and PCI results were the same, so they are placed together. Calculation of the prestress losses for the ACI, PCI, and AASHTO methods can be seen in Appendix A.4. Long-term losses can be seen in Table 4.2. Intermediate losses were also calculated for each set of beams, and the comparison between the experimental and theoretical effective prestress can be seen in Tables 4.3 and 4.4 for the first and second set of beams, respectively.

Table 4.2 Experimental prestress losses vs. code losses

Method	Elastic Shortening	Creep	Shrinkage	Relaxation	Effective Prestress
ACI/PCI	27.86	37.26	6.8	2.12	124
AASHTO	30.99	29.3	7.25	0.09	130
1st Set SCC	22.88	23.19	0	-	152*
2nd Set SCC	29.64	39.78	1.36	-	127
1st Set CON	27.53	25.29	0.18	-	145*
2nd Set CON	26.91	44.55	1.28	-	125

all values in ksi, *values at 6 months

Table 4.3 Effective prestress by day for first set of ITs

Day	ACI/PCI	AASHTO	SCC	CON
Transfer	170	167	175	170
21	152	152	167	160
49	147	148	166	157
185	139	142	152	145

all values in ksi

Table 4.4 Effective prestress by day for second set of ITs

Day	ACI/PCI	AASHTO	SCC	CON
Transfer	170	167	168	171
30	150	151	151	155
185	139	142	136	135
365	135	139	127	125

all values in ksi

Shrinkage strain values are lower than predicted due to the fact that the first readings were taken right before detensioning. This was four days after the beams were cast. During this time the beams would have experienced a large amount of shrinkage that wasn't recorded. The beams also could have been internally curing causing there to be less shrinkage. Losses for the first set of beams were less than predicted code losses. This can be explained by the fact that the code equations for long-term losses are for five years. Experimental losses of prestress were lower than the predicted long-term values for the specimens monitored for one year. Specimens were only monitored for one year, and the intermediate effective stresses are lower than the predicted code values. Results show that the lightweight beams in this study experienced larger prestress losses than predicted by the code equations. These losses at 1-year were 73 ksi for the CON specimens and 71 ksi for the SCC specimens, compared with AASHTO predicted value of 59 ksi. The main difference between the experimental values and the AASHTO values can be seen in the losses from creep. Both sets of 1-year specimens experienced creep losses of over 10 ksi more than the predicted AASHTO values.

CHAPTER 5 - Creep and Shrinkage Prisms

This section discusses theory and equations developed for creep and shrinkage. The ACI 209 Committee has formulated equations that predict the amount of creep and shrinkage a prestressed beam will undergo. These equations and their meaning will be discussed in this section.

5.1 Creep

Creep is defined as "the time-dependent increase of strain in hardened concrete subjected to sustained stress" (ACI Committee 209 2005). Prestressed beams experience a large amount of creep due to the prestressing force. It is important to know the amount of creep in a beam so that prestress losses due to creep can be estimated correctly. ACI Committee 209 (2005) has developed the following equation for predicting the amount of creep over time in a prestress beam:

$$v_t = \frac{t^{\psi}}{d + t^{\psi}} v_u \tag{5.1}$$

where:

v_t= creep coefficient at time t

d= constant (6 to 30 days)

ψ= constant (0.40 to 0.80)

t= time in days after loading

v_u= ultimate creep coefficient (1.30 to 4.15)

The procedure from ATSM C512 (2009) was followed in testing the creep specimens. Six creep specimens were cast for each set of IT beams that had been cast. These specimens were 4 in. x 4 in. square with a height of 24 inches. Three of the specimens were loaded at the time of detensioning the IT specimens and the remaining three were loaded at 28 days. During handling, several of the first set of prisms were damaged so the prisms for the first set of beams were only loaded on the detension day. The specimens were mounted with Whittemore points to

measure the strain. The top and bottom of each prism was sulfur-capped to provide an even surface to load the prisms on without causing any irregularities. Figure 5.1 shows the prisms being sulfur-capped at the Kansas State University laboratory. The prisms were loaded to 40% of their compressive strength in load frames that can be seen in Figure 5.2.

Figure 5.1 Sulfur-capping creep and shrinkage prisms

Figure 5.2 Creep prism in load frame

Whittemore readings were taken at the appropriate interval as prescribed by ASTM C512 (2009). Prisms for the first set of ITs were housed in an uncontrolled room, but the second set of prisms were housed in an environmental chamber. Humidity was maintained at $50 \pm 4\%$ and temperature was maintained at 73.4 ± 2.0 degrees Fahrenheit as stated in ASTM C512 (2009).

5.2 Shrinkage

ACI Committee 209 (2005) states, "Shrinkage, after hardening of concrete, is the decrease with time of the concrete volume." There are three types of shrinkage: "drying shrinkage due to moisture loss in the concrete, autogenous shrinkage caused by the hydration of cement, and carbonation shrinkage resulting as the various cement hydration products are carbonated in the presence of CO" (ACI Committee 209 2005). ACI Committee 209 (2005) developed Equation 5.2 to predict the amount of shrinkage over time in a concrete beam. The amount of shrinkage can decrease the prestress force in a prestressed beam and is an important parameter to estimate. Shrinkage prisms were cast at the same time as the creep prisms as seen in Figure 5.3.

$$\left(\varepsilon_{sh}\right)_t = \frac{t^{\alpha}}{f + t^{\alpha}}\left(\varepsilon_{sh}\right)_u \tag{5.2}$$

where:

$(\epsilon_{sh})_t$= shrinkage strain at time t

t= time after loading

f= constant (20 to 130 days)

α= constant (0.90 to 1.10)

$(\epsilon_{sh})_u$= ultimate shrinkage strain (415×10^{-6} to 1070×10^{-6})

Figure 5.3 Casting of creep and shrinkage prisms

Since each creep prism experienced shrinkage, a shrinkage prism was cast for each creep prism to be able to subtract the shrinkage from the creep values. The shrinkage prisms were mounted with Whittemore points and were measured at the same time as the creep prisms. The top and bottom of each prism was sulfur-capped to maintain the same volume-to-surface ratio as the creep prisms. The shrinkage prisms were housed in the same location as the creep prisms to prevent a variation in environmental changes. Figure 5.4 shows the second set of creep and shrinkage prisms in the environmental chamber.

Figure 5.4 Second set of creep and shrinkage prisms in environmental chamber

CHAPTER 6 - Creep and Shrinkage Results

6.1 Creep Results

Readings were taken from the creep specimens for one year. The creep readings included elastic shortening, creep strain, and shrinkage. The creep strains were calculated by subtracting the elastic shortening and shrinkage of the companion specimens from the total strain readings. ACI Committee 209 (2005) stated that the creep coefficient can be found by graphing Equation 5.1 and changing the variables ψ, d, and V_u until the values fit the actual data. The experimental creep coefficient is the ratio found by dividing creep strains by the elastic shortening strain. The variables in Equation 5.1 can be varied until the data fits the graph of the experimental data. The creep coefficient variables were found using a trial-and-error method for both sets of specimens. Since two SCC specimens were loaded for each case, graphs for all of the SCC #2 creep specimens can be seen in Appendix A.5. The first set of specimens were only loaded at detensioning, and the second set included specimens that were loaded at detensioning and at 28 days. Figures 6.1 and 6.2 show results from the first set of CON and SCC #1, respectively. Figures 6.3 and 6.4 show results from the second set of CON and SCC #1 specimens that were loaded at detensioning, respectively. Results from the CON and SCC #1 specimens from the second set that were loaded at 28 days can be seen in Figures 6.5 and 6.6, respectively. Figure 6.7 shows a summary of the creep ratios. Creep parameters for all of the specimens are summarized in Table 6.1. The CON specimens were loaded to a higher load since the mix had a higher compressive strength. This may be one reason why the CON creep coefficients are larger on average vs. the SCC specimens.

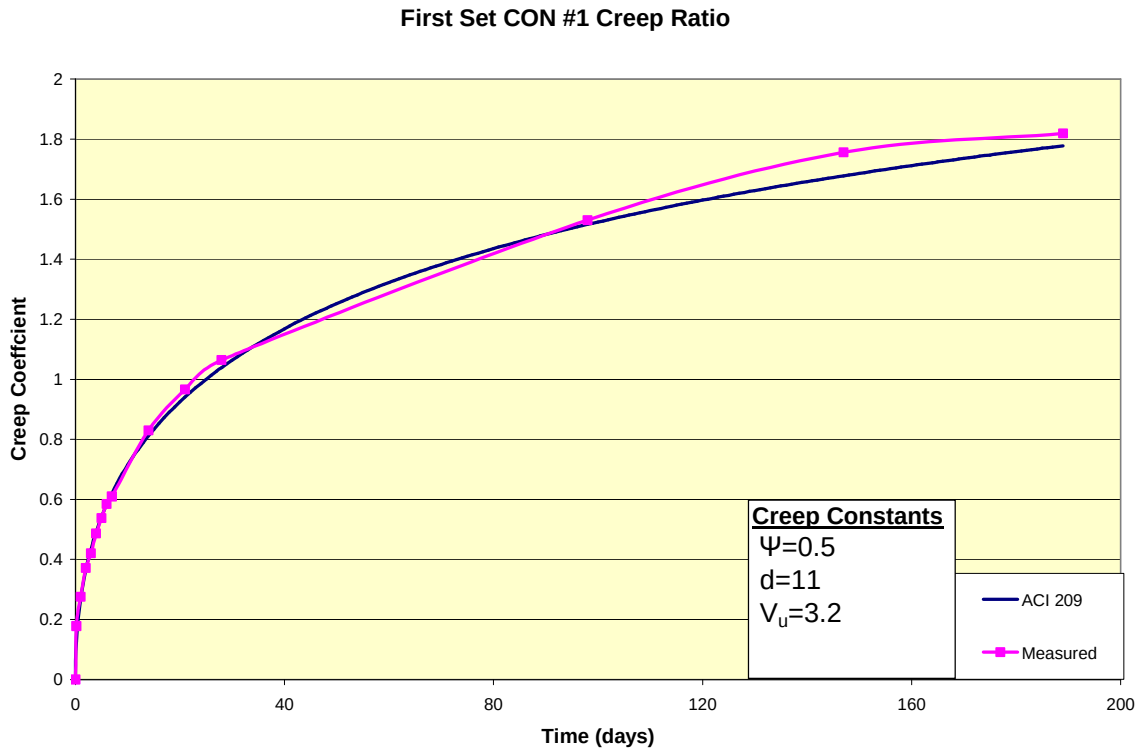

Figure 6.1 Creep coefficient of first set CON #1

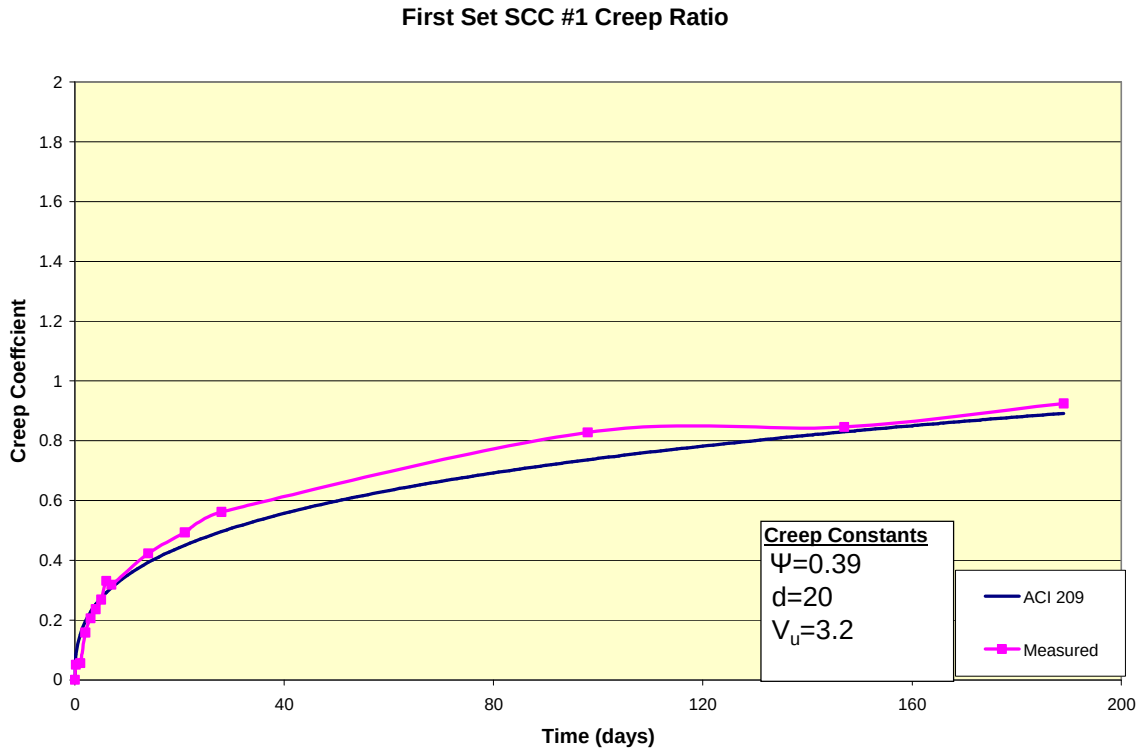

Figure 6.2 Creep coefficient of first set SCC #1

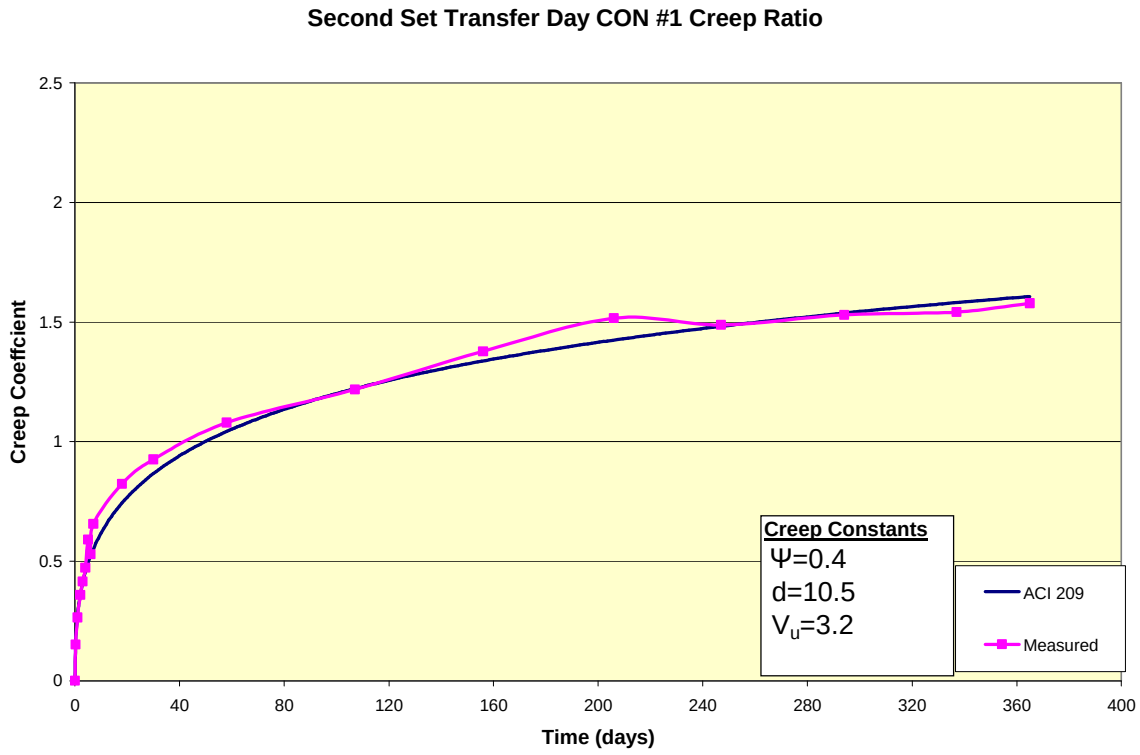

Figure 6.3 Creep coefficient of second set transfer day CON #1

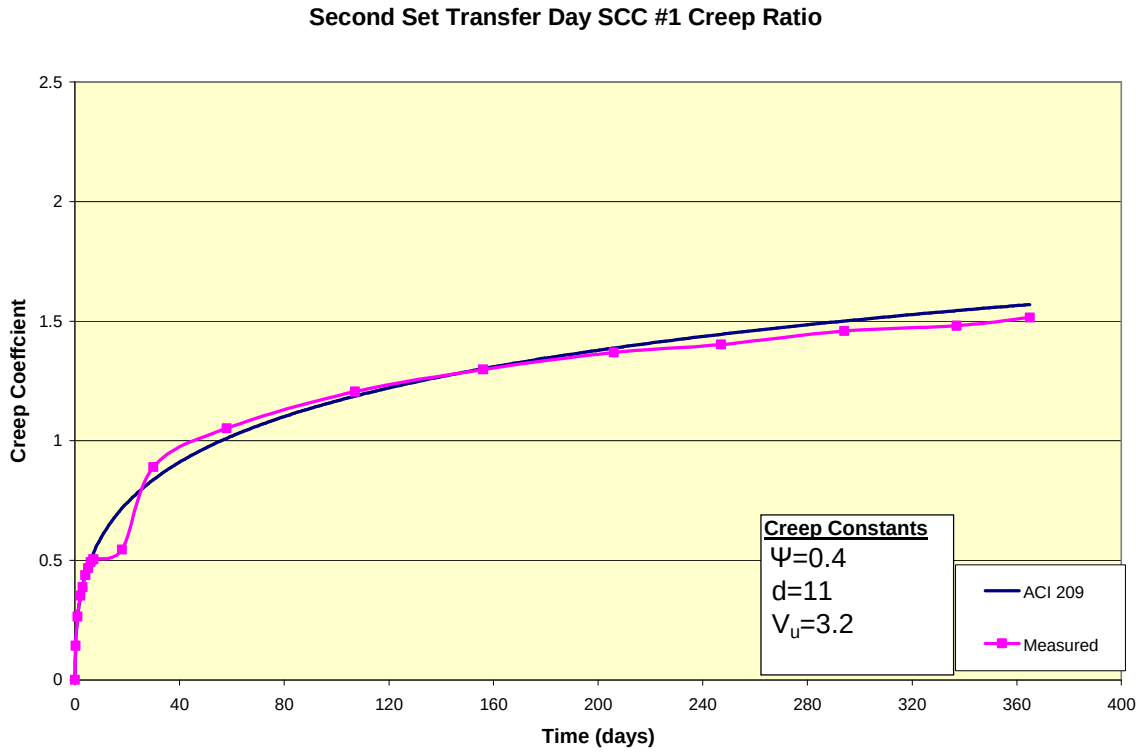

Figure 6.4 Creep coefficient of second set transfer day SCC #1

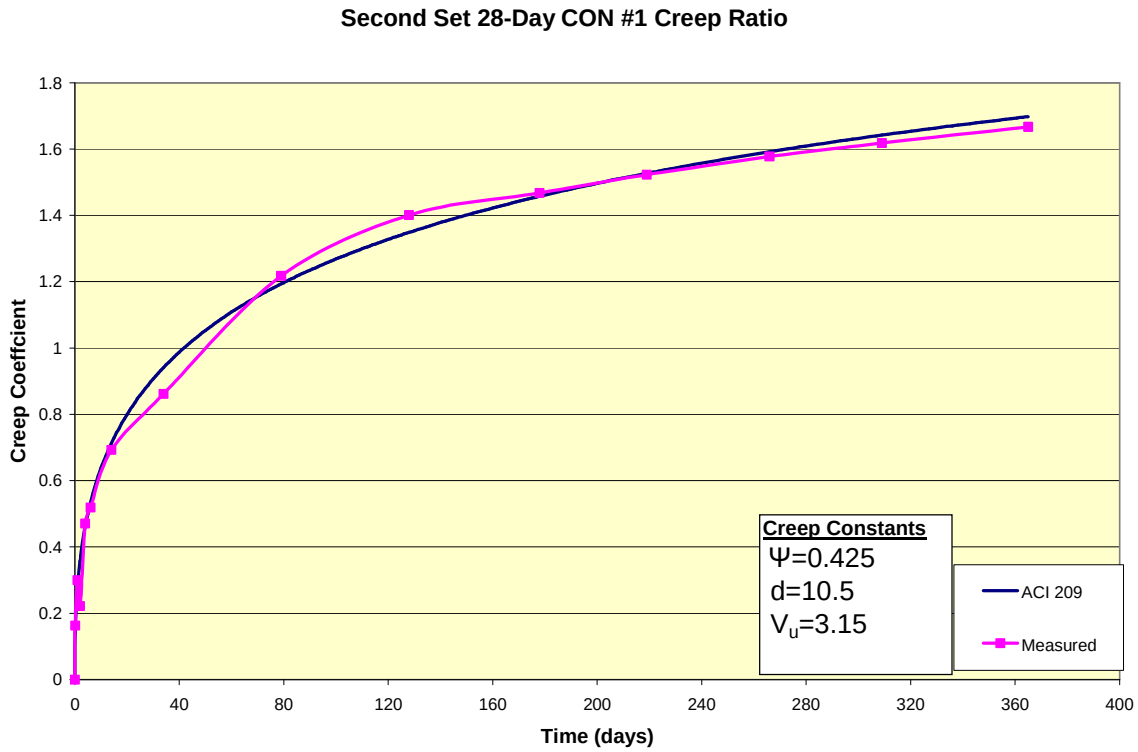

Figure 6.5 Creep coefficient of second set 28-day CON #1

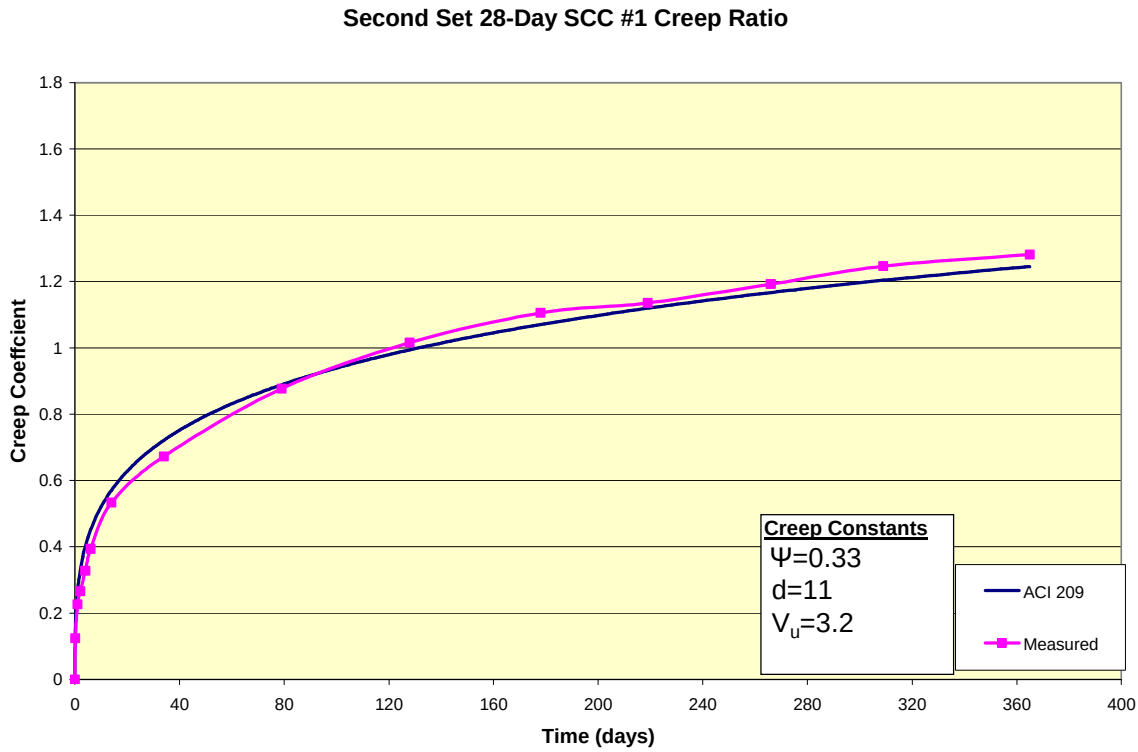

Figure 6.6 Creep coefficient of second set 28-day SCC #1

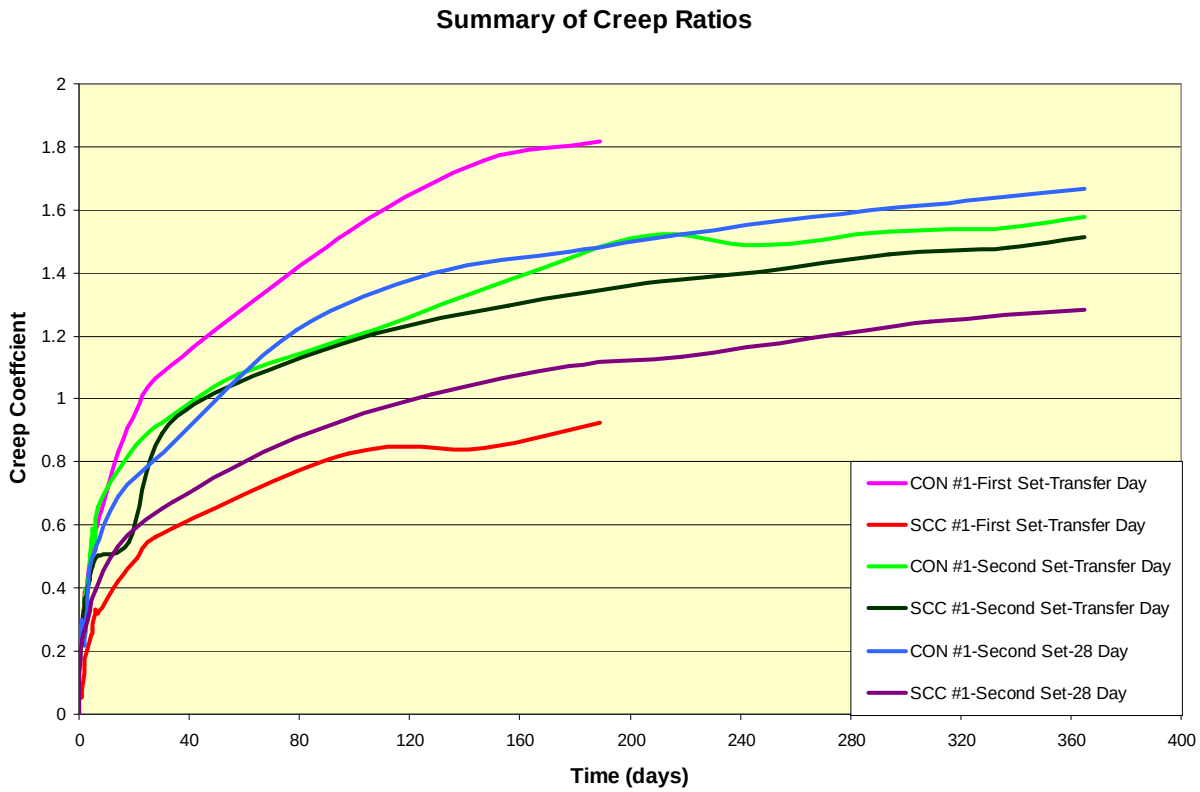

Figure 6.7 Summary of creep ratios

Table 6.1 Summary of creep parameters

Creep Set		CON #1 Transfer Day	SCC #1 Transfer Day	SCC #2 Transfer Day	CON #1 28-Day	SCC #1 28-Day	SCC #2 28-Day
First	ψ	0.5	0.39	0.51	-	-	-
	d	11	20	22	-	-	-
	v_u	3.2	3.2	3.15	-	-	-
Second	ψ	0.4	0.4	0.51	0.425	0.33	0.4
	d	10.5	11	10.25	10.5	11	11
	v_u	3.2	3.2	3.15	3.15	3.2	3.125

6.2 Shrinkage Results

Shrinkage readings were taken at the same time as the creep readings. Like the creep specimens, two SCC specimens were cast and measured for each set of specimens. Graphs for all SCC #2 shrinkage specimens can be seen in Appendix A.6. The measured strain readings

were compared to calculated values from ACI Committee 209 (2005) for each set of specimens. Using Equation 5.2, variables α, f, and $(\epsilon_{sh})_u$ were changed until the fit data resembled the experimental shrinkage data. Figures 6.8 and 6.9 show shrinkage results from the first set of CON and SCC #1 prisms. Figures 6.10 and 6.11 show shrinkage results from the second set of prisms measured, starting at detensioning. Figures 6.12 and 6.13 shows results from the second set of CON and SCC #1 prisms matched with the 28-day creep specimens. Figure 6.14 shows a summary of the shrinkage strains. Shrinkage parameters for all of the sets of specimens are summarized in Table 6.2.

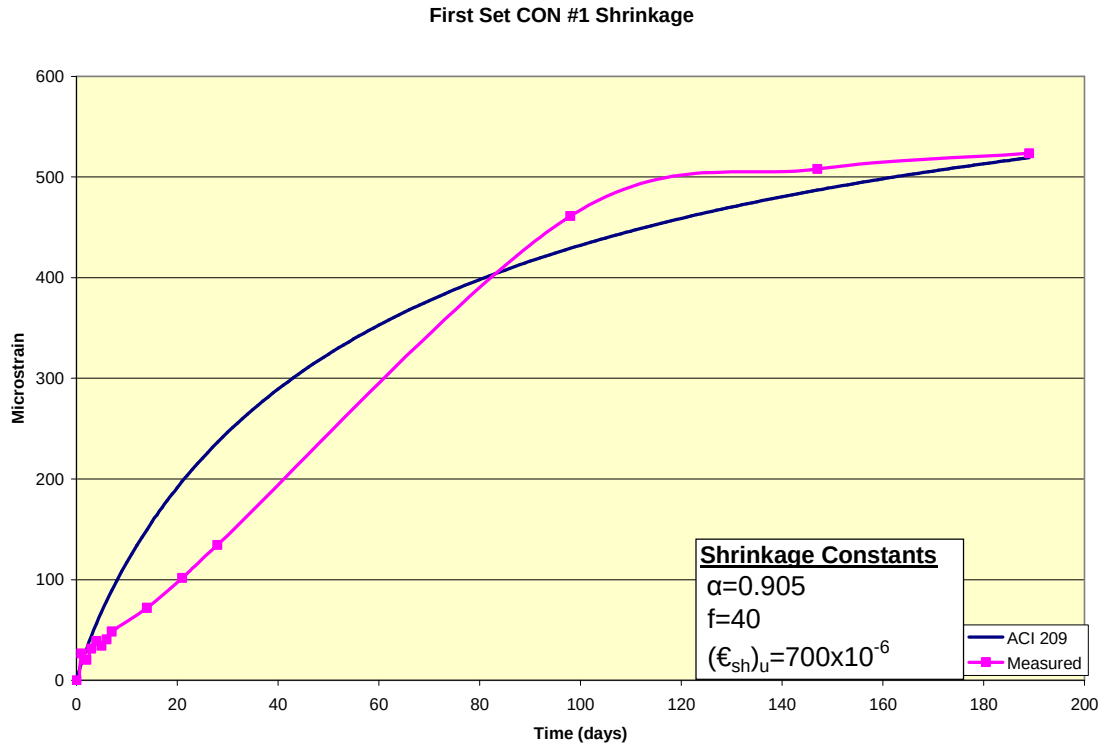

Figure 6.8 Shrinkage strains for first set CON #1 specimen

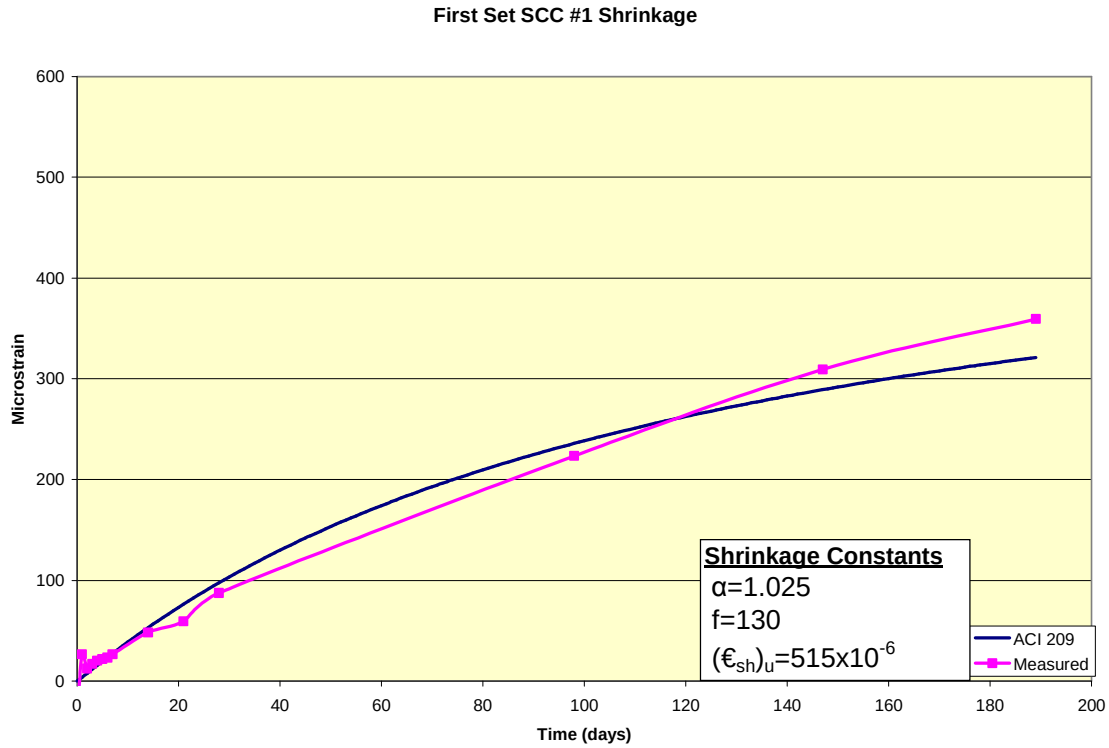

Figure 6.9 Shrinkage strains for first set SCC #1 specimen

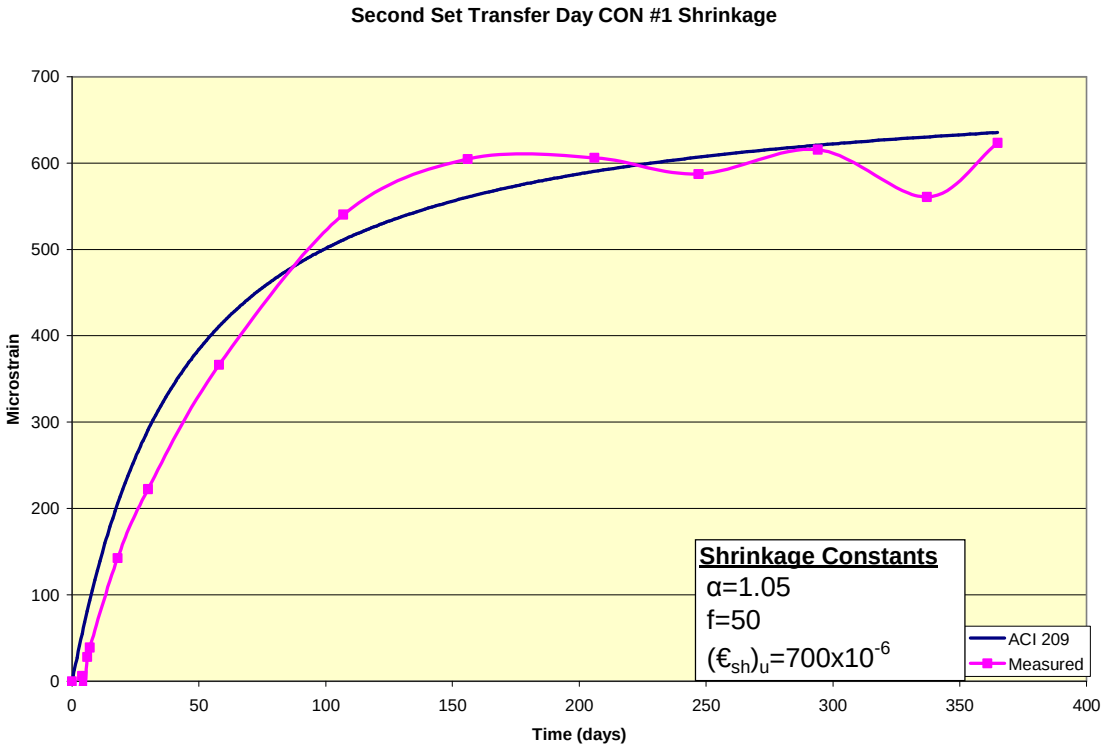

Figure 6.10 Shrinkage strains for second set transfer day CON #1 specimen

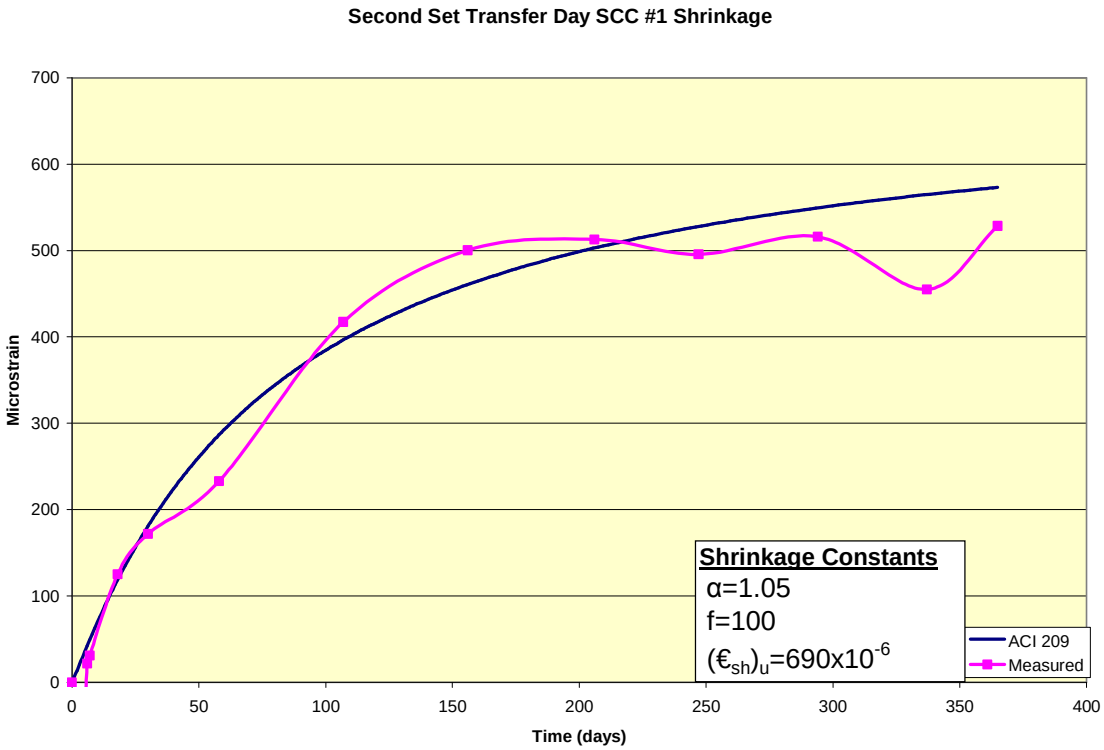

Figure 6.11 Shrinkage strains for second set transfer day SCC #1 specimen

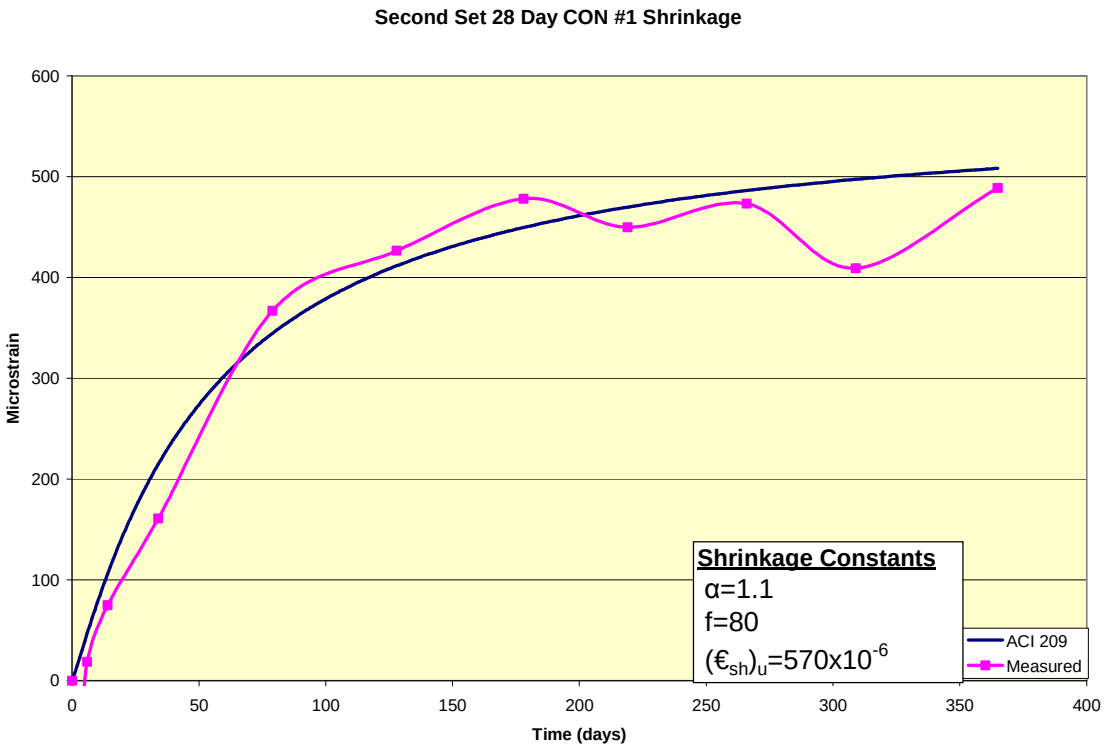

Figure 6.12 Shrinkage strains for second set 28-day CON #1 specimen

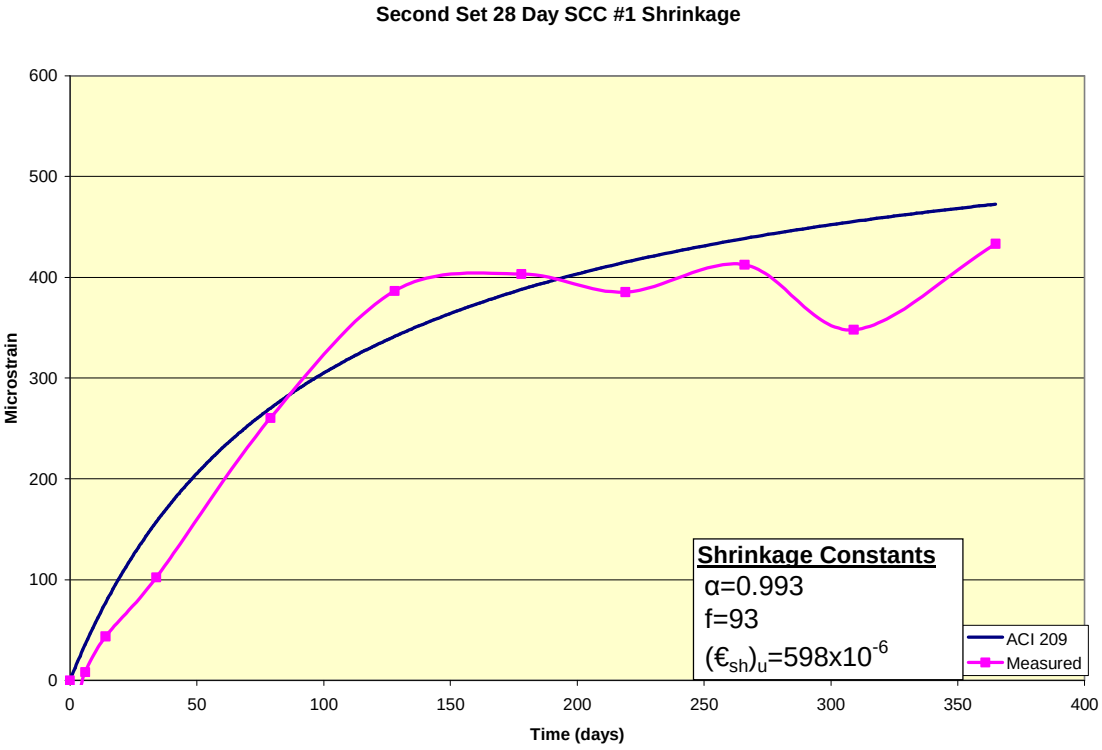

Figure 6.13 Shrinkage strains for second set 28-day SCC #1

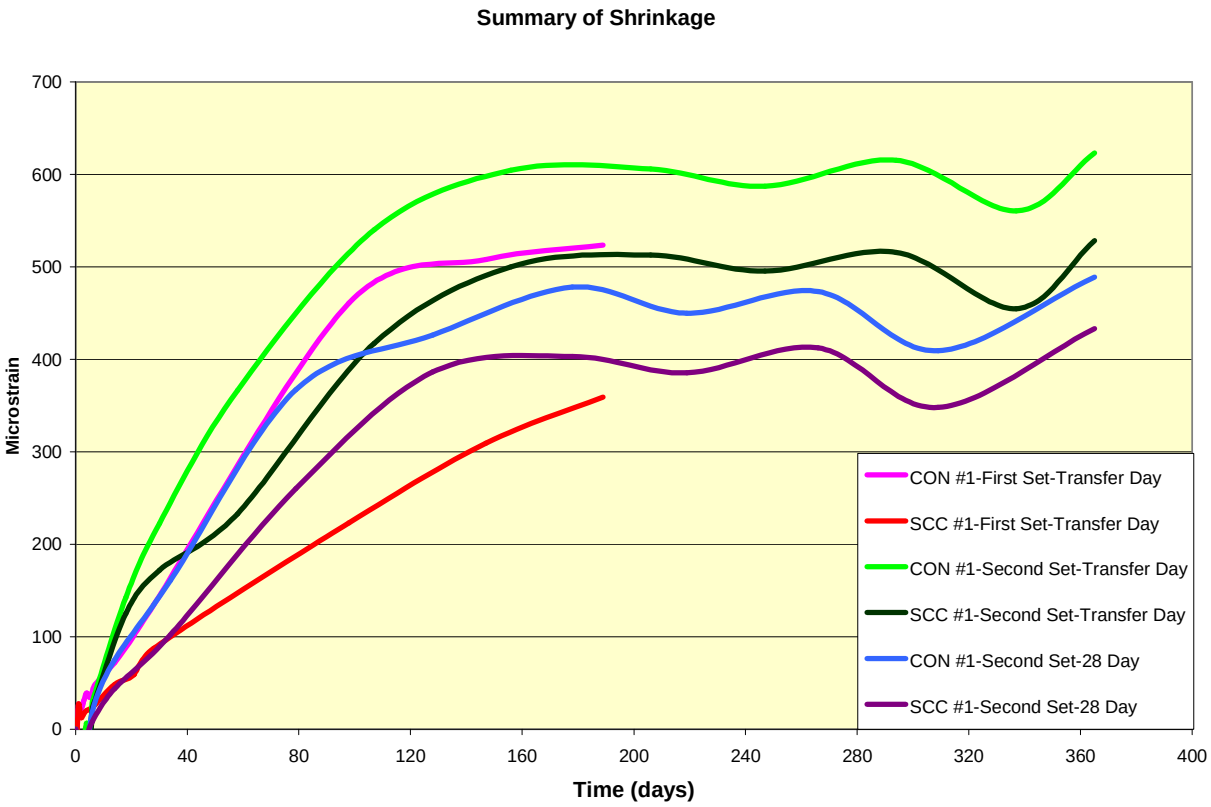

Figure 6.14 Summary of shrinkage strains

Table 6.2 Summary of shrinkage parameters

Shrinkage Set		CON #1 Transfer Day	SCC #1 Transfer Day	SCC #2 Transfer Day	CON #1 28-Day	SCC #1 28-Day	SCC #2 28-Day
First	f	40	130	125	-	-	-
	α	0.905	1.025	1.05	-	-	-
	$(€_{sh})_u$	700	515	550	-	-	-
Second	f	50	100	20	93	95	80
	α	1.05	1.05	0.995	0.993	1.1	1.1
	$(€_{sh})_u$	700	690	650	598	525	570

6.3 Summary of Creep and Shrinkage Findings

Average values for creep and shrinkage parameters were found during this study. Creep coefficients over time can be modeled with Equation 5.1 using the experimentally determined average values of ψ, d, and V_u for each of the two lightweight mixes. Shrinkage behavior of the

two lightweight mixes can be estimated with Equation 5.2 using the experimentally determined average values of α, f, and $(\epsilon_{sh})_u$. These values can be seen in Table 6.3 along with the values for the creep parameters. The shrinkage values for the second set transfer day SCC #2 specimen were not used since they varied from the other three specimens.

Table 6.3 Summary of average experimental creep and shrinkage parameters

Average of Experimental Values		CON Transfer Day	SCC Transfer Day	CON 28-Day	SCC 28-Day
Shrinkage	f	45	118	80	94
	α	0.99	1.04	1.1	1.05
	$(\epsilon_{sh})_u$	700	585	570	562
Creep	ψ	0.45	0.46	0.43	0.37
	d	10.75	10.63	10.5	11
	v_u	3.2	3.17	3.15	3.16

6.4 ACI 209 Prestress Loss Summary

ACI Committee 209 has a method for predicting prestress losses based on parameters found from creep and shrinkage prisms. The equations used for these losses use the creep coefficient and the ultimate shrinkage strains to predict the long term losses. The calculations of these losses can be seen in Appendix A.7. Table 6.4 shows a comparison between the ACI 209 predicted losses and the experimental losses from the second set of beams. The values from the second set of ITs were used because they were measured for a longer period of time. The ACI 209 predicted losses due to elastic shortening were close to the experimental results. The creep and shrinkage losses predicted by ACI 209 were highly conservative when compared to the experimental findings. The experimental results were based on one year losses where as the ACI 209 losses are based on long term losses (five years). The experimental losses may increase overtime to become closer to the ACI 209 predicted values.

Table 6.4 Comparison between ACI 209 prestress losses vs. experimental losses

Method	Elastic Shortening	Creep	Shrinkage	Relaxation	Effective Prestress
ACI 209 SCC	31	55.65	11.07	5	95
2nd Set SCC	29.64	39.78	1.36	-	127
ACI 209 CON	31	56.18	13.24	5	93
2nd Set CON	26.91	44.55	1.28	-	125

CHAPTER 7 - Flexure Beam Design and Fabrication

This section discusses design and fabrication of the flexure beams tested for this project at KSU. Twelve total beams were fabricated, including four with a T-beam cross section and eight with a rectangular cross section. These beams were later tested to verify the transfer length and development length of the SCC mix. The beams were cast at Prestressed Concrete, Inc. in Newton, Kan., on the afternoon of January 20, 2010.

7.1 Rectangular Section Design

Eight beams having a rectangular cross section were cast and tested. Four of these had a 100% development length and the remaining four had an 80% development length. For each length of beam, there were two SCC and two CON beams cast. The various specimens will be referred to as SCC #1 100% L_d, CON #2 80% L_d, etc. The beams were designed to have a minimum of 3.5% strain in the prestressing steel at nominal capacity. The cross section of the rectangular cross section was 8 inches x 12 inches with a single ½-inch-diameter prestressed strand 10 inches from the top of the beam. Dimensions of the beams are shown in Figure 7.1. The rectangular cross section beams didn't have any shear reinforcement. Shear capacity of the beams was found to be greater than the amount of shear present when the beam was loaded to nominal moment and the calculations can be seen in Appendix A.8. The nominal moment capacities of each beam can be seen in Appendix A.9. The prestress loss calculations used to find the effective prestress force, which was used for the nominal moment calculations for the rectangular beams, can be seen in Appendix A.10. Transfer and development lengths were calculated using ACI code equations and can be seen in Appendix A.10.

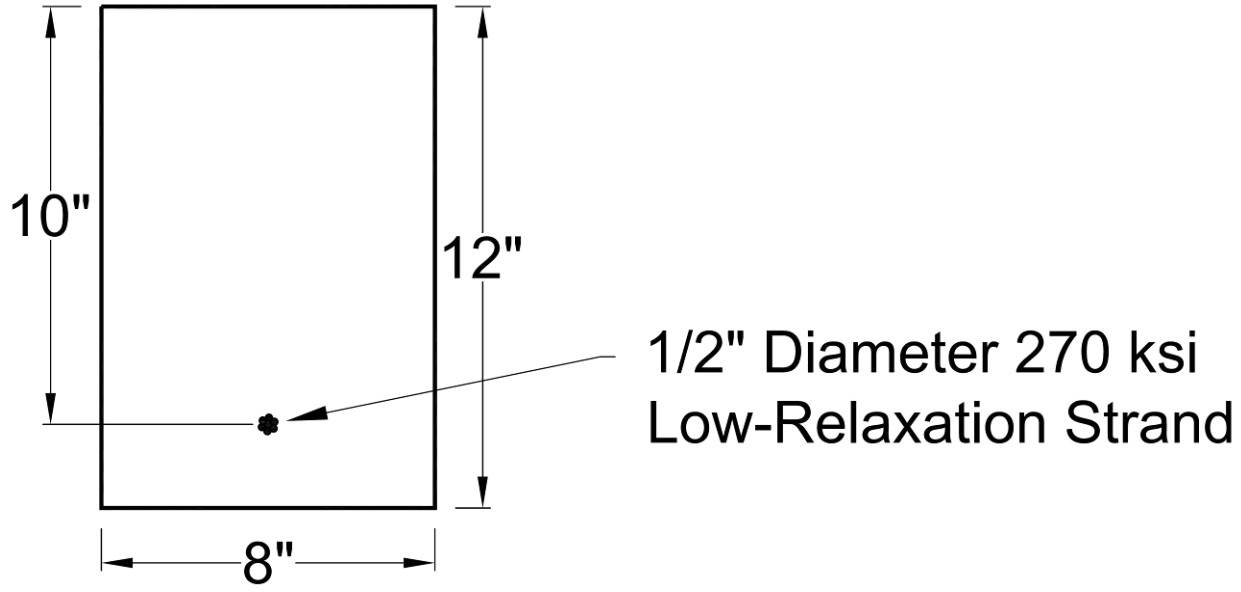

Figure 7.1 Rectangular beam cross section

7.2 T-Beam Section Design

Four beams having a T-shape cross section were cast and tested. Two of these were SCC and the remaining two were CON. The specimens will be referred to as SCC #1 T-beam, CON #2 T-beam, etc. The beams were designed to have a minimum of 3.5% strain in the prestressing steel at nominal capacity and had some shear reinforcement in them consisting of #4 bars at six-inch centers. The T-beams had a total height of 21 inches and a flange depth of 6 ½ inches, with a flange width of 36 inches. The web was 16 inches wide with a height of 14 ½ inches. The section included compression steel along with five ½-inch-diameter prestress steel 19 inches from the top of the specimen. The cross section of the T-beams can be seen in Figure 7.2. As with the rectangular beams, transfer lengths and development lengths were calculated. These calculations can be seen, along with the prestress loss calculations for the T-beams, in Appendix A.10. Shear capacity was calculated to be greater than the amount of shear present when the beam was loaded to nominal moment, and calculations for the nominal moment capacity can been seen in Appendix A.11.

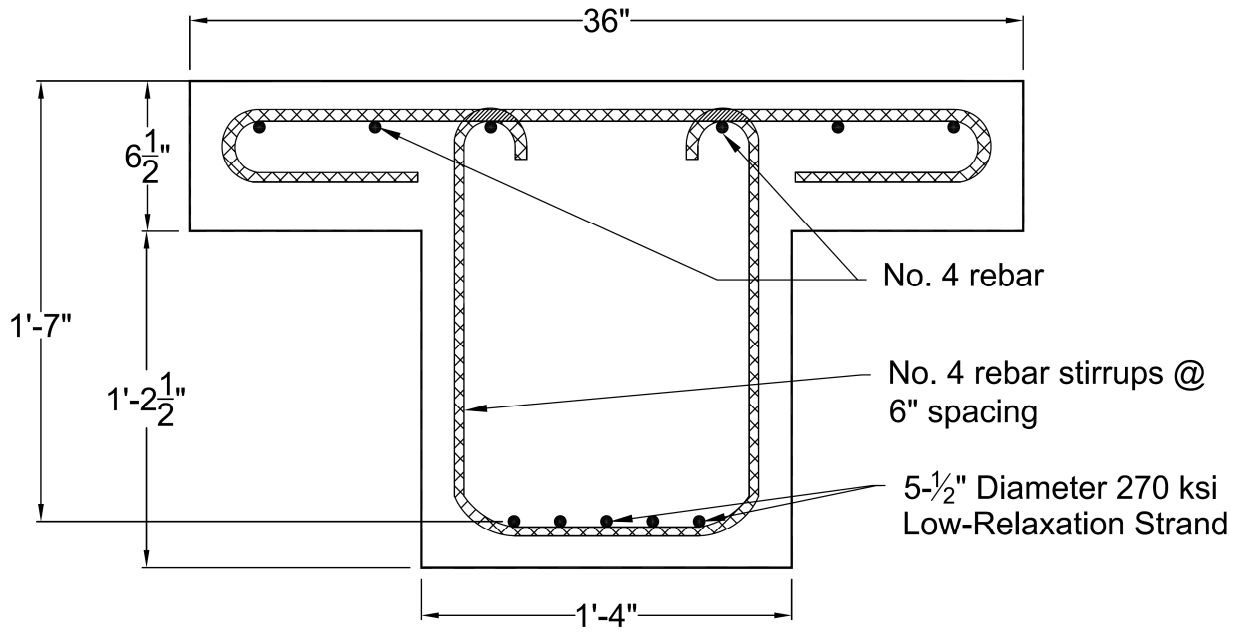

Figure 7.2 T-beam cross section

7.3 Flexure Beam Fabrication

The 12 flexure beams were cast at PCI on January 20, 2010. They were cast in steel prestress forms that were fitted with wood inserts to provide the correct dimensions. Crack formers were placed in each set of beams at the loading locations to cause a crack at each edge of the constant moment region. The crack formers can be seen in the rectangular beams' forms in Figure 7.3. The forms were heated with steam before and after casting the specimens. The forms used to cast the T-beams can be seen in Figure 7.4, and the forms used for the rectangular beams can be seen in Figure 7.5.

Figure 7.3 Crack formers in rectangular beams' form

Figure 7.4 T-beams' form with reinforcement

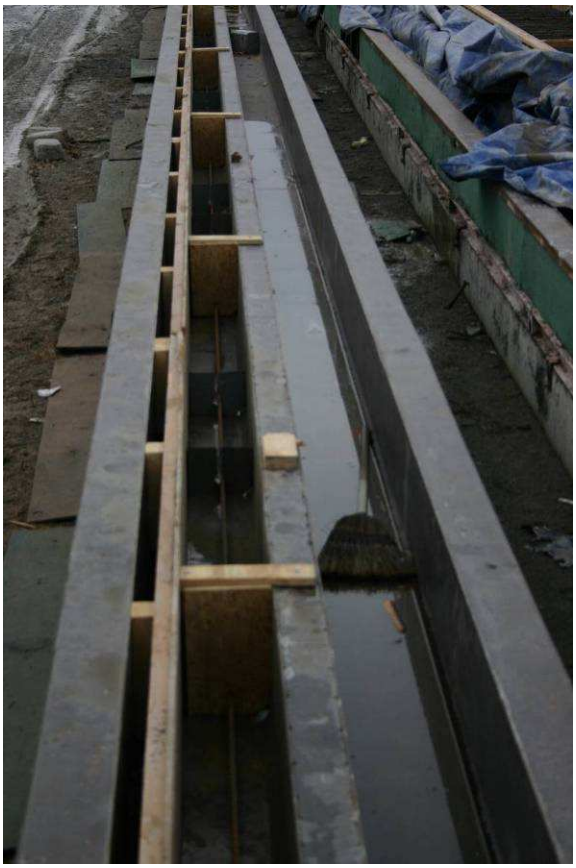

Figure 7.5 Rectangular beams' forms

The SCC beams were cast first and the CON beams were cast second. Figures 7.6 through 7.8 show the casting of the flexural beams. Each mix was tested for slump/spread, air, and unit weight. Compressive cylinders were also made for each set of beams. Testing was done following the ASTMs used in Chapter 3 of this study. Mix proportions of the flexure beams can be seen in Table 7.1. The properties of the mixes used for the flexure beams can be seen in Table 7.2.

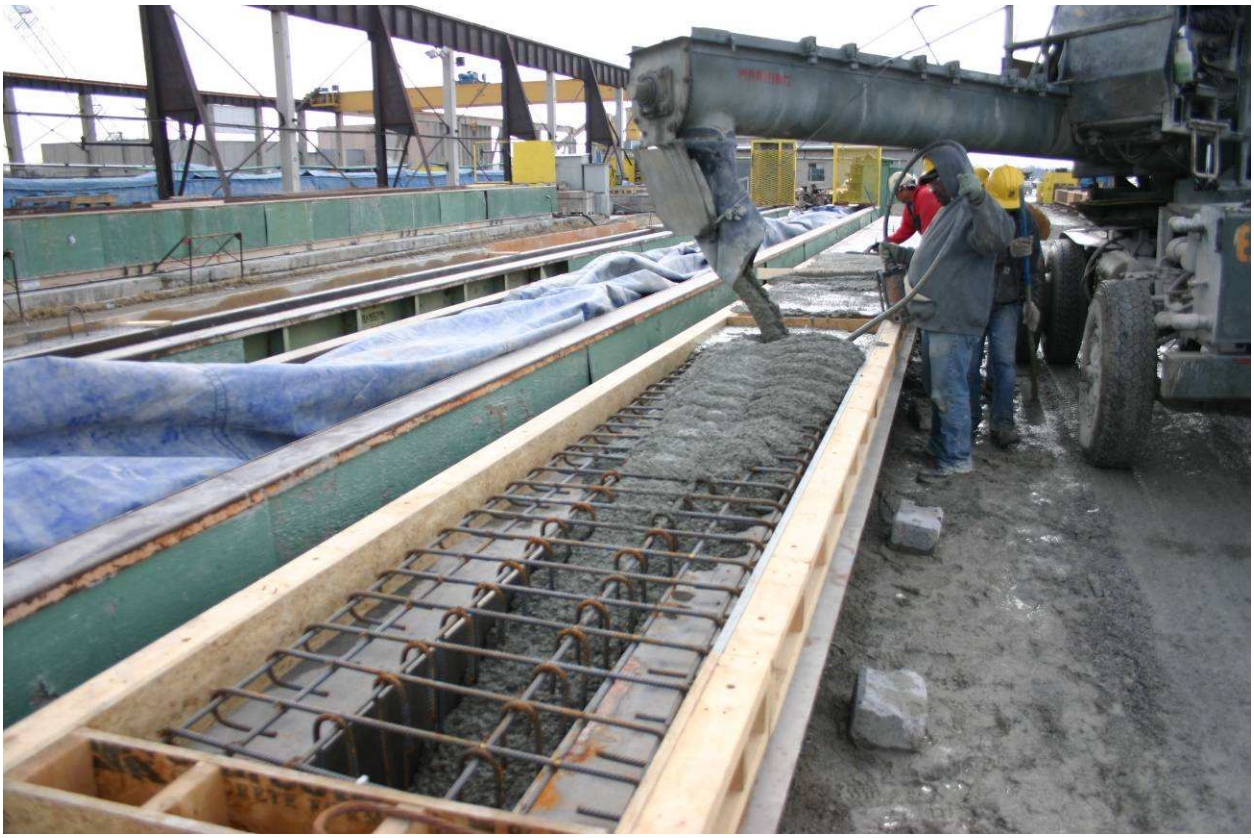

Figure 7.6 Casting of the T-beam specimens

Figure 7.7 Casting of T-beam specimen

Figure 7.8 Casting of rectangular beam

Table 7.1 Mix proportions of flexure beams

Batch (per yd^3)		Dry Sand (lbs)	Surface Dry Marquette (lbs)	Type III Cement (lbs)	Water (lbs)	Adva Cast 530 (oz)	Adva Flow 555 (oz)	Air Entrainer (oz)	Theoritical unit weight (pcf)	Theoretical water to cement ratio
Flexure Beams Cast on January 20, 2010	SCC #1	1337	829	632	203	113	0	5.2	113.5	0.32
	SCC #2	1349	816	640	202	106	0	5.3	113.6	0.315
	SCC #3	1352	819	640	202	115	0	4.4	113.6	0.315
	CON #1	1671	694	657	218	0	91	6	122.1	0.331
	CON #2	1675	695	657	214	0	91	6.1	122.3	0.325

Table 7.2 Batch properties of flexure beams

Batch		Spread/ Slump (in)	Air (%)	Unit Weight (pcf)	1-Day Compressive Strength (psi)	4-Day Release Strength (psi)	28-Day Compressive Strength (psi)
Flexure Beams Cast on January 20, 2010	SCC #1	24	4.5	114.1	3264	4325	2744
	SCC #2	24.5	-	110.2	3310	4456	5246
	SCC #3	20.5	5	111.5	3208	4425	5053
	CON #1	7.5	6.5	112.3	2415	3575	5128
	CON #2	7.5	7	109.8	2348	3508	4818

There were five total pours since the capacity of the pan mixer at PCI was four cubic yards. There were three SCC batches and two CON batches. Beams cast from each batch can be seen in Table 7.3. The finished beams can be seen in Figures 7.9 and 7.10. The beams were finished and the forms were covered with heavy tarps to insulate them as they steam-cured.

Table 7.3 Summary of specimens cast with each mix

Mix Design	Specimens Cast
SCC #1	SCC T-Beam #1
SCC #2	SCC T-Beam #2
SCC #3	All SCC Rectangular Beams
CON #1	All CON T-Beams
CON #2	All CON Rectangular Beams

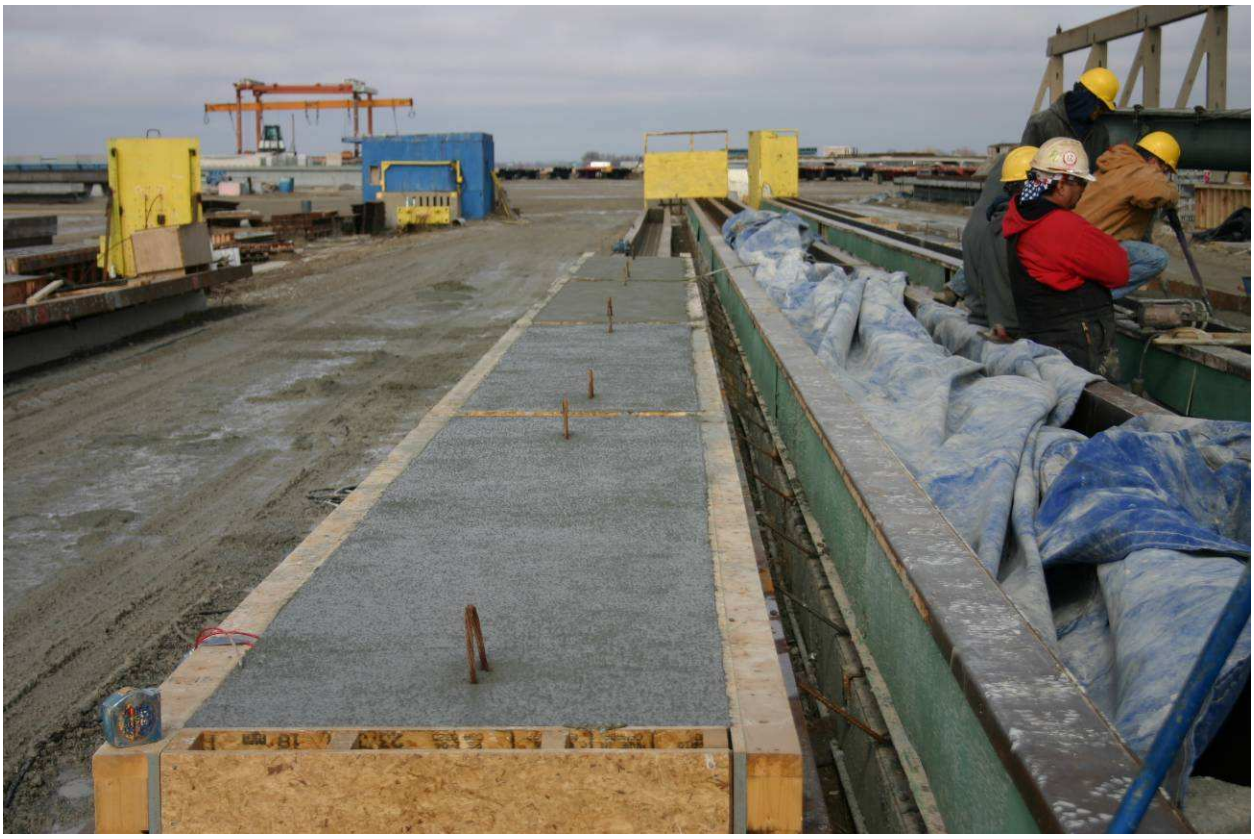

Figure 7.9 Finished T-beam specimens

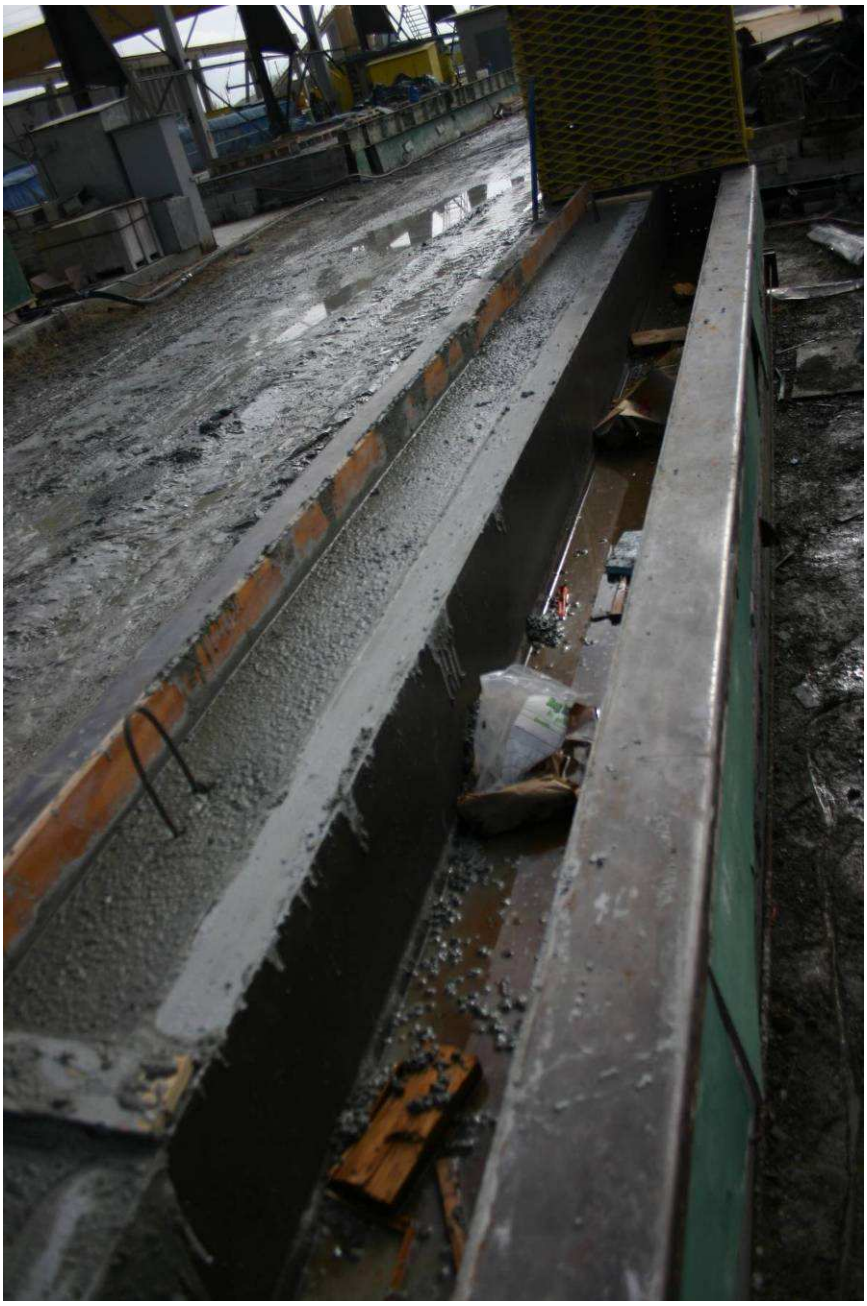

Figure 7.10 Finished rectangular beams

Compressive strength of the beams was tested after one day. The concrete compressive strength was too low to detension, so the forms continued to be heated until the beam strand were detensioned after four days. The one-day and release-compressive strengths can be seen in Table 7.1, along with the release and 28-day strengths. The beams were delivered to Kansas State University via flatbed semi truck. They were unloaded and stored inside the Civil Engineering Structures Lab to prevent freezing of the specimens, which would disrupt the curing process.

CHAPTER 8 - Flexure Beam Testing and Results

This section explains the testing procedure used to test the flexure beams poured at PCI in Newton, Kan. The beams were tested in the Civil Engineering Structural Lab at Kansas State University using MTS servo hydraulic testing equipment. Each set of flexure beams were tested using a different test setup but same loading condition, due to the difference in the beams' lengths and nominal moment capacities.

8.1 Flexure Beam Test Setup

The rectangular beams were tested using a computer-controlled servo hydraulic cylinder with a maximum capacity of 22 kips, which was twice the nominal capacity of the beams. The rectangular beams were set up with a three-foot spreader beam to create a constant moment region in the beam. The beams were supported by a roller on each end to prevent adding addition horizontal forces due to friction. The roller support was located two inches from the end of the beams. Figure 8.1 shows the test setup for the rectangular beams with 100% development length (L_d) while the test setup for the rectangular beams with 80% L_d is shown in Figure 8.2. The T-beams were loaded with a hydraulic cylinder that was computer-controlled, as was the 22-kip cylinder, but had a capacity of 150 kips, which was 50% more than the nominal capacity of the T-beams. The T-beams were loaded with a 26 inch spreader beam and had roller supports two inches from the end, just as the rectangular beams did. Figure 8.3 shows the testing diagram for the T-beams.

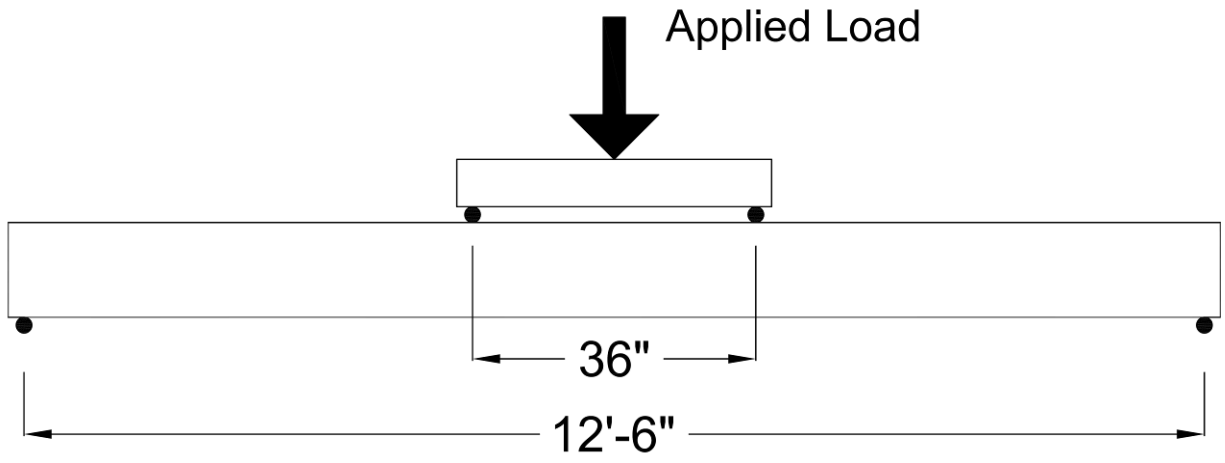

Figure 8.1 Loading conditions for 80% L_d beams

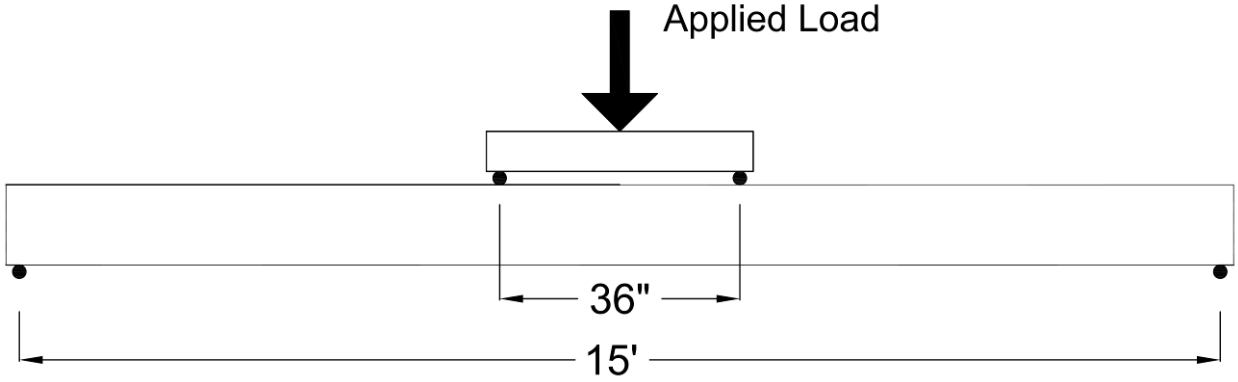

Figure 8.2 Loading conditions for 100% L_d beams

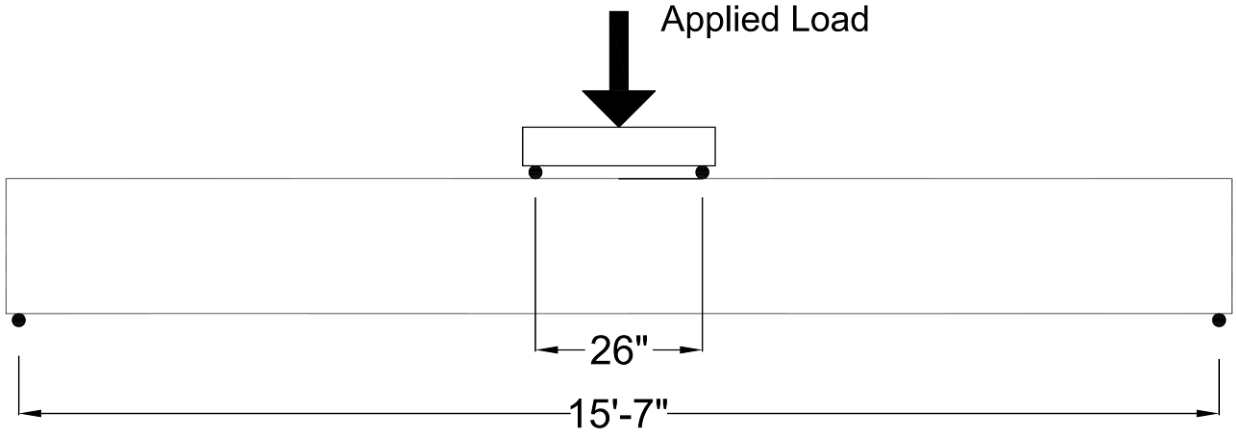

Figure 8.3 Loading conditions for T-beams

8.1.1 100% L_d Test Setup

The 100% L_d beams were loaded in a two-part loading. The first part used a faster load rate, and the second part required a slower load rate to be sure to accurately record any possible

end-slip. The beam was loaded at 100 pounds per minute up to 75% of nominal moment. The loading rate was then changed to 10 pounds per minute until failure.

8.1.2 80% L_d Test Setup

The 80% L_d beams were also loaded in a two-part loading. The beam was loaded at 100 pounds per minute up to 75% of nominal moment. The loading rate was then changed to 10 pounds per minute until failure.

8.1.3 T-Beam Test Setup

The T-beams were also loaded in a two-part loading. The beam was loaded at 750 pounds per minute up to 75% of nominal moment. The loading rate was then changed to 50 pounds per minute until failure.

8.2 100% L_d Beam Test Results

After loading the 100% L_d beams to failure, data from the beams was exported to Excel to be able to graph results from the tests. A graph of the experimental moment vs. mid-span deflection was produced for each beam. The end-slip for each end was also plotted on the same graph to show any end-slip that may have occurred. The mid-span deflection was calculated by taking the average of the two linear variable differential transformers (LVDTs) that were placed at the center of each beam. The experimental moment was in the constant moment region of the beam, which was half of the force applied multiplied by the moment arm. The calculated nominal moment of each beam was also plotted on the same graph. The nominal moment of each of the beams was calculated using strain compatibility, and the calculations can be seen in Appendix A.9. Figures 8.4 and 8.6 show results for the two CON 100% L_d beams. CON 100% L_d was unloaded and reloaded due to malfunction of the testing equipment. Figures 8.5 and 8.7 show the two CON 100% L_d beams after failure. The two Con 100% L_d beams reached 98% and 97% of nominal, respectively. Con #1 100% L_d failed due to a shear crack developing and can be seen in Figure 8.5. Con #2 100% L_d failed in the compression block and its failure can be seen in Figure 8.7. Figures 8.8 and 8.10 show the moment vs. deflection graphs for the two SCC 100% L_d beams. SCC #1 100% L_d was cracked during handling which decreased the initial stiffness of the specimen. The two SCC 100% L_d beams reached 96% and 99% of nominal, respectively. SCC #1 100% L_d failed in the compression block and its failure can be seen in

Figure 8.9. SCC #2 100% L_d failed when a flexure crack developed into a shear, causing failure which can be seen in Figure 8.11. The comparison between nominal and experimental results can be seen in Table 8.1, along with the other flexure beams. Figure 8.12 shows a summary of the 100% L_d specimens' moment versus deflection.

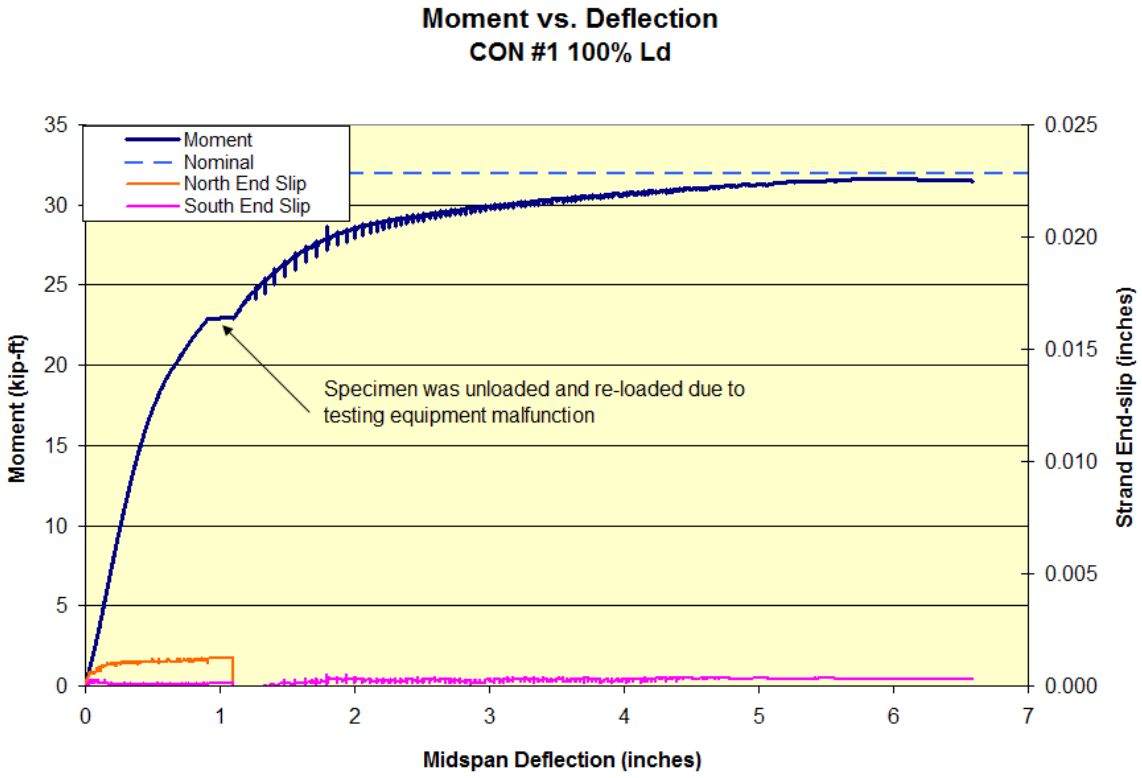

Figure 8.4 Moment versus deflection for CON #1 100% L_d specimen

Figure 8.5 Failure of CON #1 100% L_d specimen

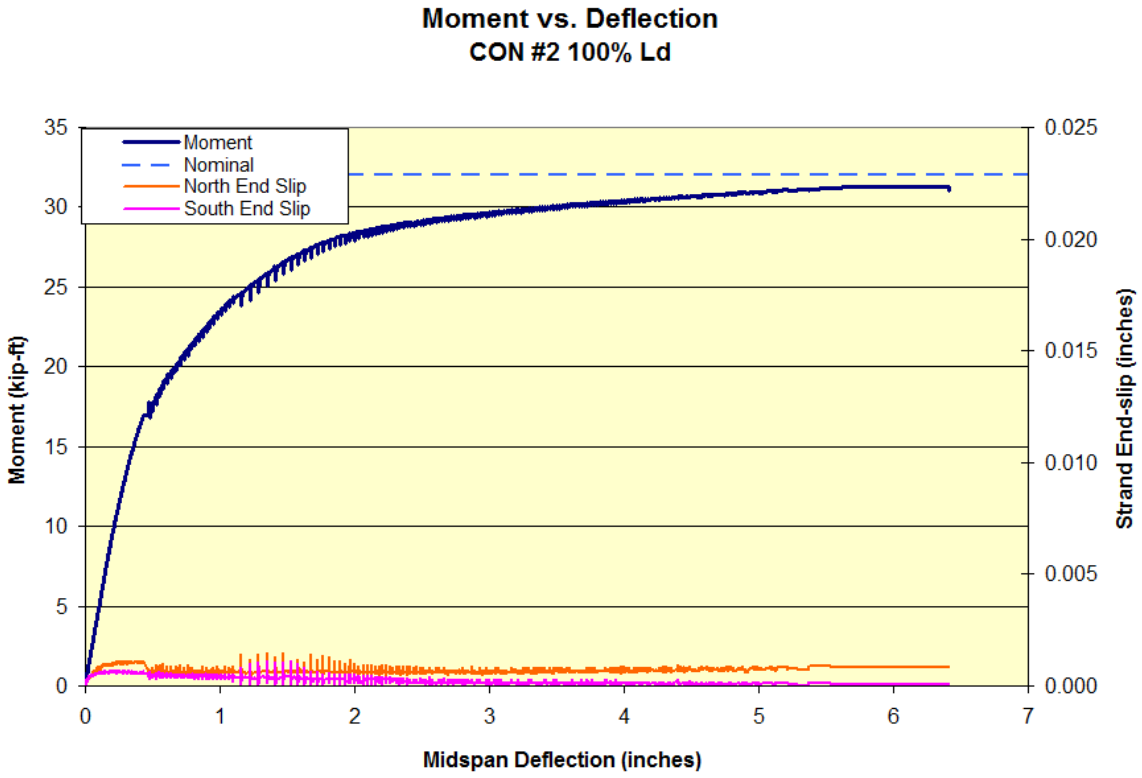

Figure 8.6 Moment versus deflection for CON #2 100% L_d specimen

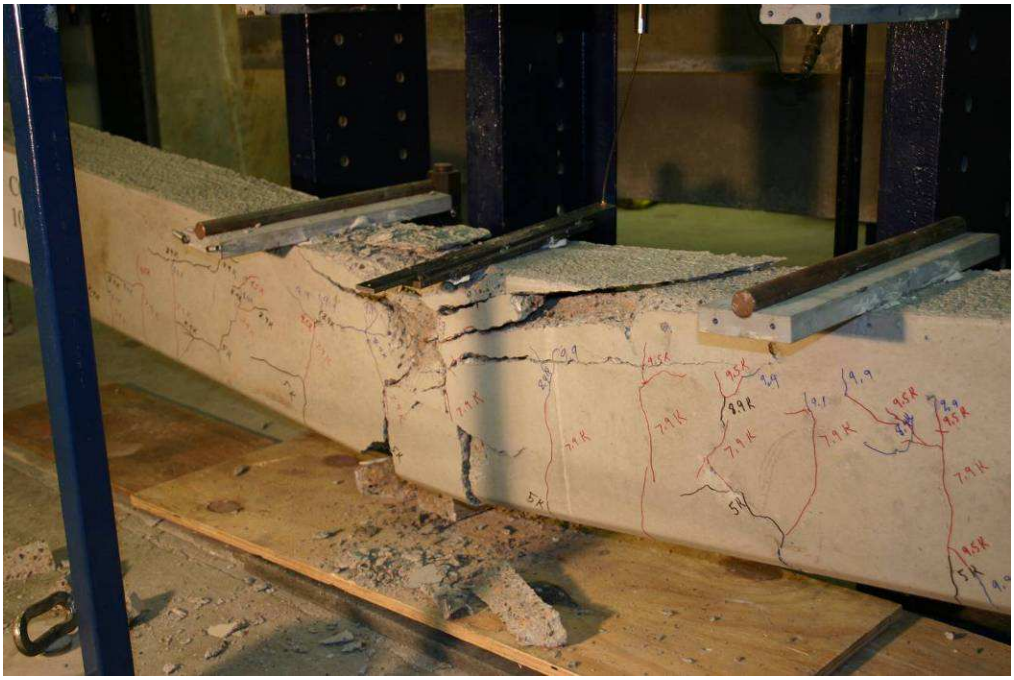

Figure 8.7 Failure of CON #2 100% L_d specimen

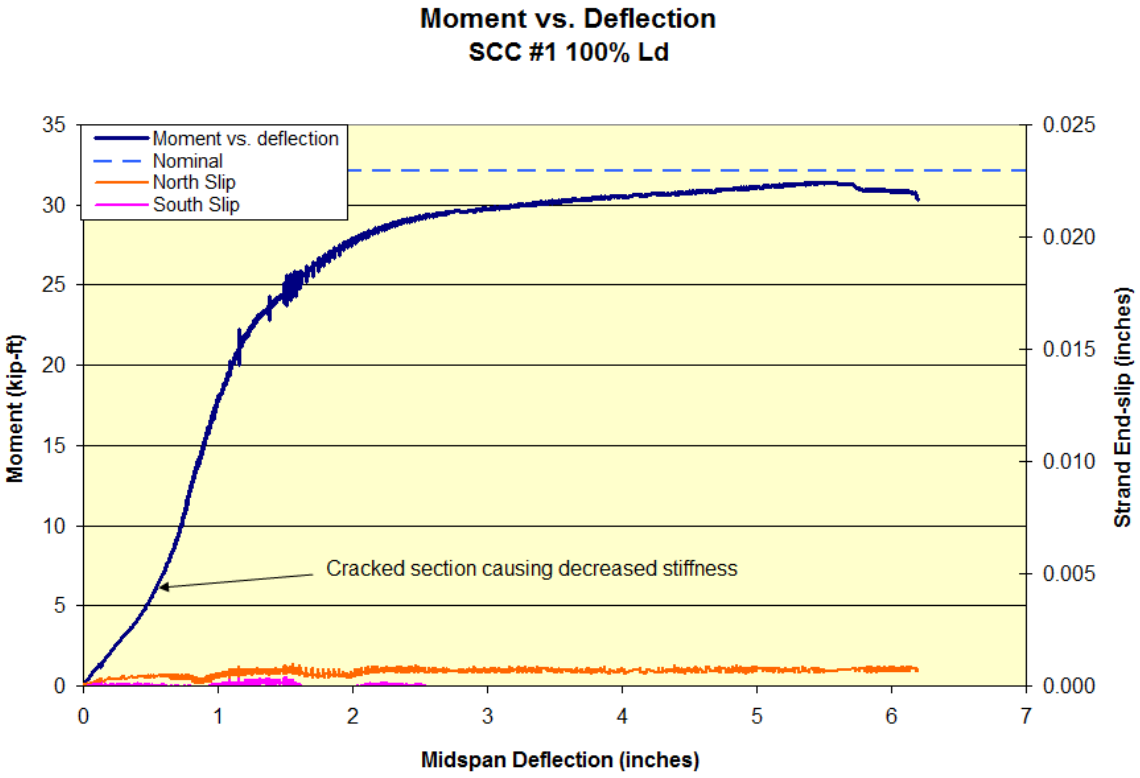

Figure 8.8 Moment versus deflection for SCC #1 100% L_d specimen

Figure 8.9 Failure of SCC #1 100% L_d specimen

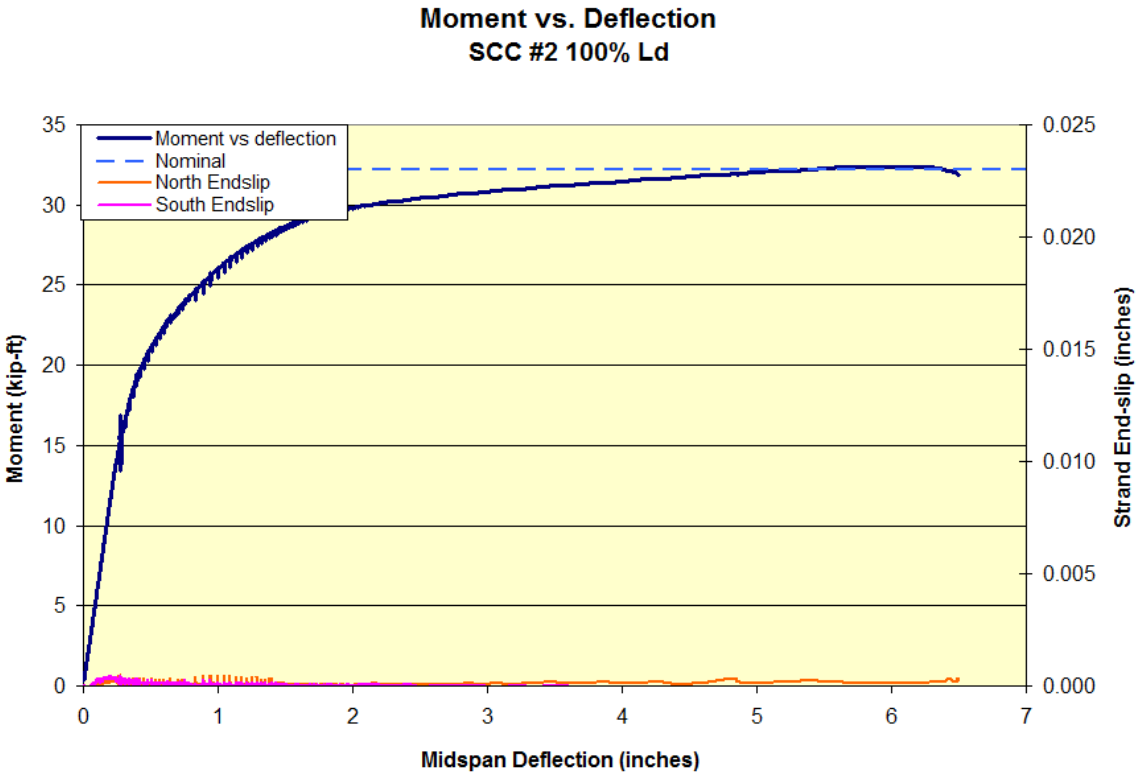

Figure 8.10 Moment versus deflection for SCC #2 100% L_d specimen

Figure 8.11 Failure of SCC #2 100% L_d specimen

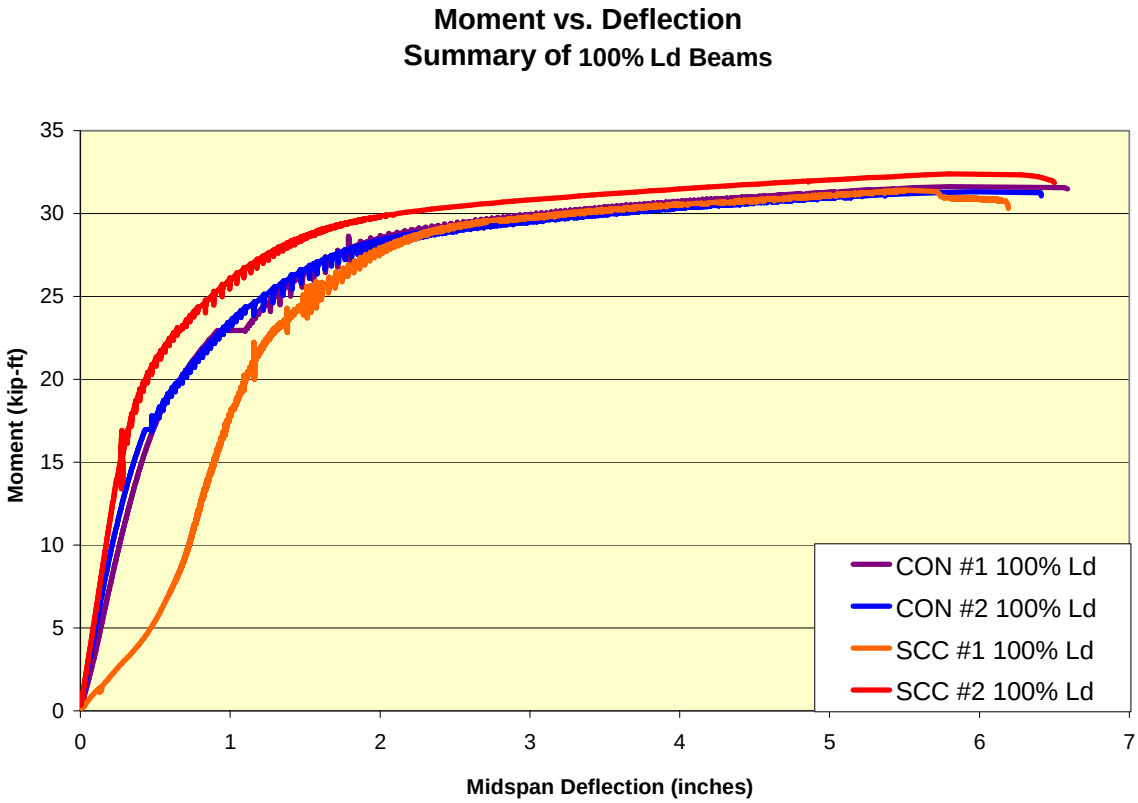

Figure 8.12 Summary of 100% L_d specimens' moment versus deflection

8.3 80% L_d Test Results

The 80% L_d beam data was analyzed the same as the 100% L_d and an experimental moment vs. deflection graph was produced. The moment arm was smaller for the 80 % L_d since the beams were shorter. The nominal moment was calculated using a reduced prestress force in the beams. Figures 8.13 and 8.15 show moment vs. deflection curves for the CON 80% L_d beams. CON #1 80% L_d reached nominal and failed as a flexure crack developed into a shear crack. This can be seen in Figure 8.14. CON #2 80% L_d only reached 77% of nominal; it failed due to end-slip, which can be seen in Figure 8.15. Figure 8.16 shows CON #2 80% L_d after failure due to end-slip, which caused a shear crack to develop and cause failure. Figures 8.17 and 8.19 show moment vs. deflection curves for the 80% L_d SCC beams. Both beams reached nominal capacity. SCC #1 80% L_d failed from a shear crack developing and its failure can be seen in Figure 8.18. SCC #2 80% L_d failed in the compression block and can be seen in Figure

8.20. Table 8.1 shows the comparison of experimental versus nominal moments for each of the beams, along with failure modes of each beam. Figure 8.21 shows a summary of the 80% L_d specimens' moment versus deflection.

Table 8.1 Summary of flexure beam breaks

Specimen	Batch Number	Date Tested	Compressive Strength at break (psi)	Nominal Moment (kip-ft)	Max Experimental Moment (kip-ft)	Exp. / Nominal	Failure Type
SCC #1 80% Ld	SCC #3	April 16, 2010	5645	28.84	32.02	1.11	Shear
SCC #2 80% Ld	SCC #3	May 3, 2010	5681	28.85	31.52	1.09	Compression
CON #1 80% Ld	CON #2	April 20, 2010	4501	28.46	30.31	1.07	Shear
CON #2 80% Ld	CON #2	May 4, 2010	4724	28.55	21.94	0.77	Bond
SCC #1 100% Ld	SCC #3	February 17, 2010	5019	32.14	30.97	0.96	Compression
SCC #2 100% Ld	SCC #3	February 24, 2010	5238	32.23	32.00	0.99	Comp / Shear
CON #1 100% Ld	CON #2	February 20, 2010	4738	31.97	31.18	0.98	Comp / Shear
CON #2 100% Ld	CON #2	February 25, 2010	4752	32.01	30.93	0.97	Compression
SCC #1 T Beam	SCC #1	April 21, 2010	5922	315.84	249.10	0.79	Bond
SCC #2 T Beam	SCC #2	May 7, 2010	5634	315.30	281.80	0.89	Bond
CON #1 T-Beam	CON #1	May 6, 2010	4917	313.66	212.20	0.68	Bond
CON #2 T-Beam	CON #1	May 11, 2010	4966	313.79	233.00	0.74	Bond

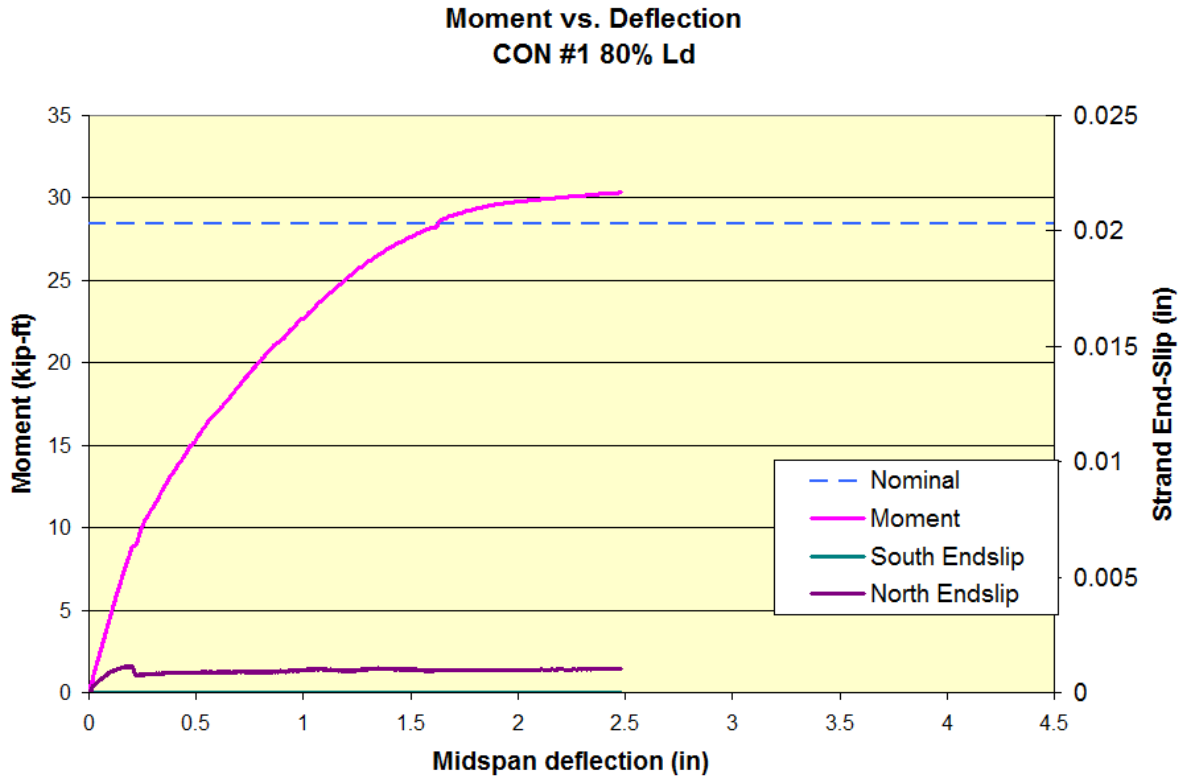

Figure 8.13 Moment versus deflection for CON #1 80% L_d specimen

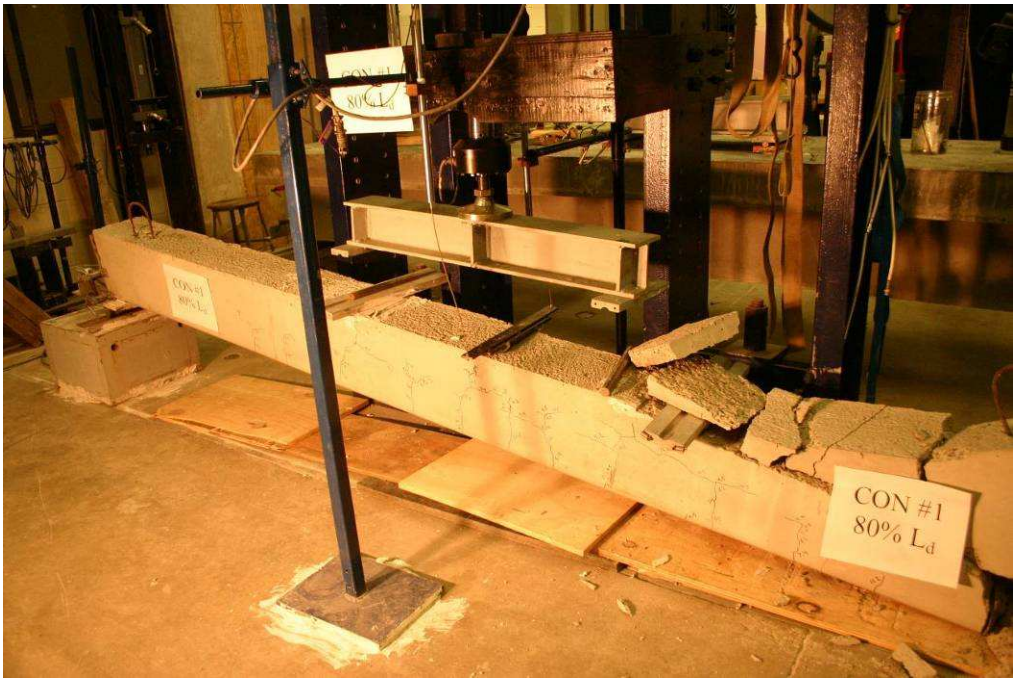

Figure 8.14 Failure of CON #1 80% L_d specimen

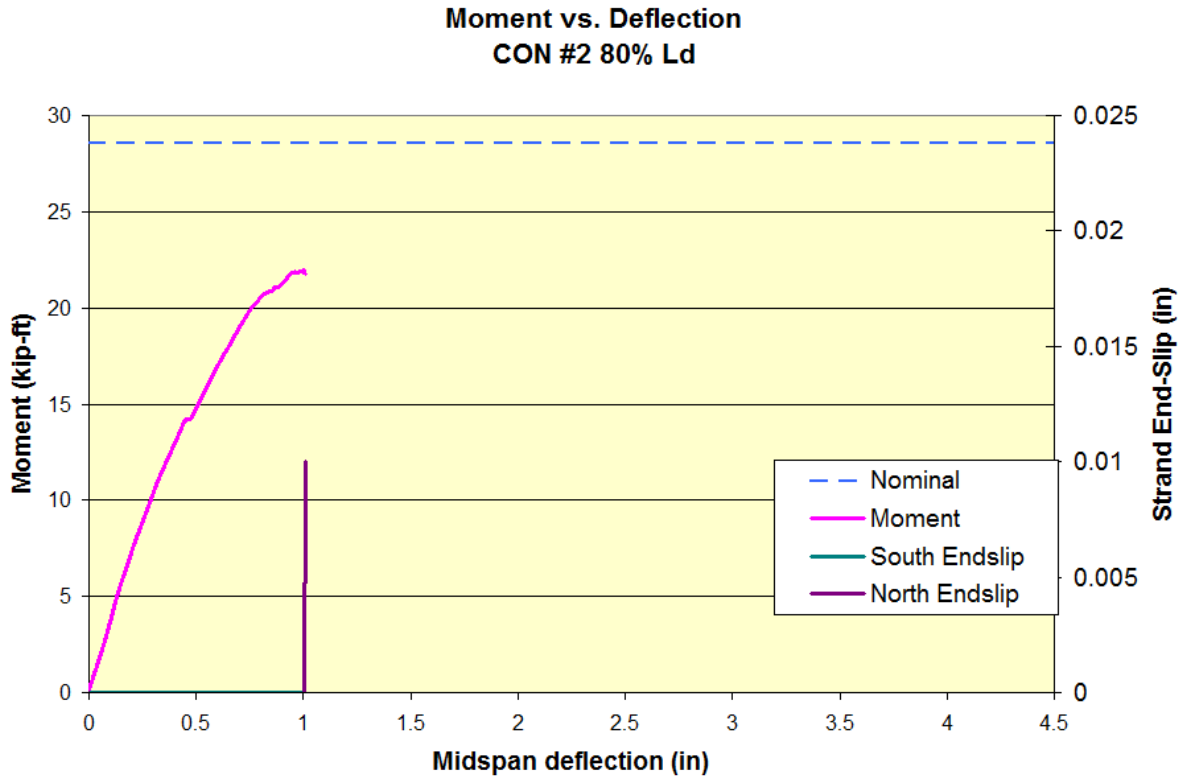

Figure 8.15 Moment versus deflection for CON #2 80% L_d specimen

Figure 8.16 Failure of CON #2 80% L_d specimen

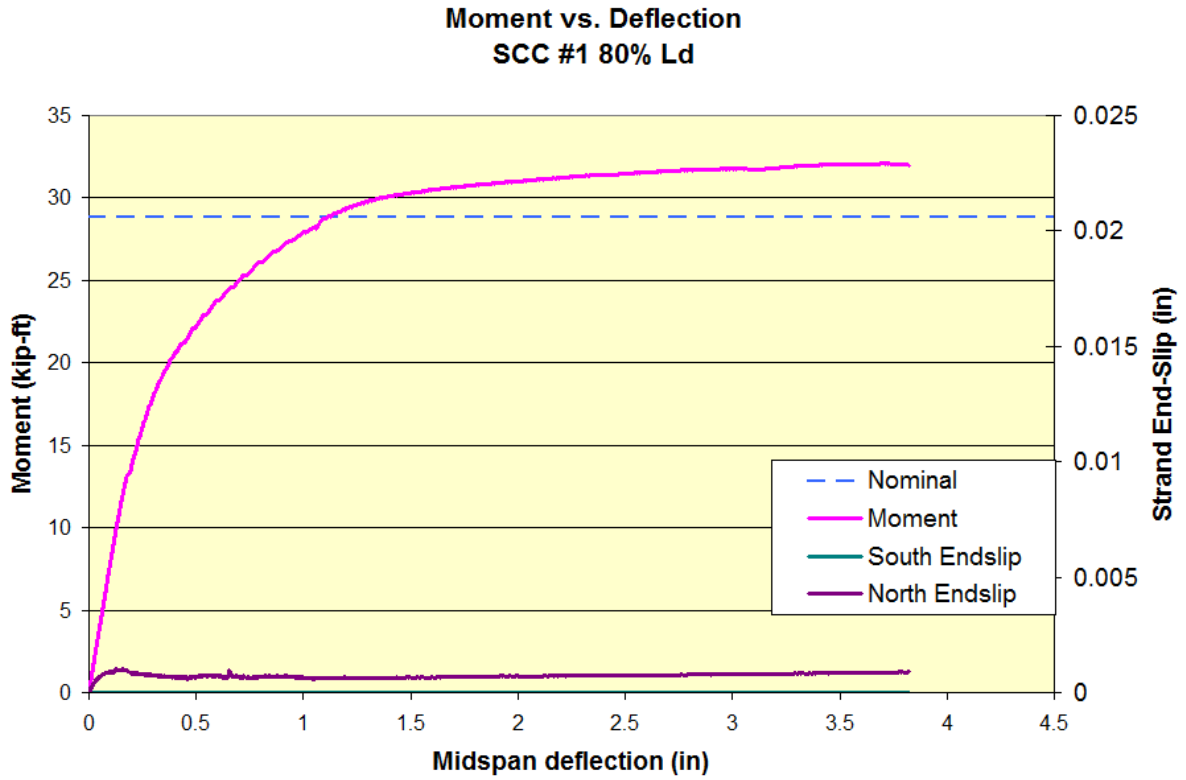

Figure 8.17 Moment versus deflection for SCC #1 80% L_d specimen

Figure 8.18 Failure of SCC #1 80% L_d specimen

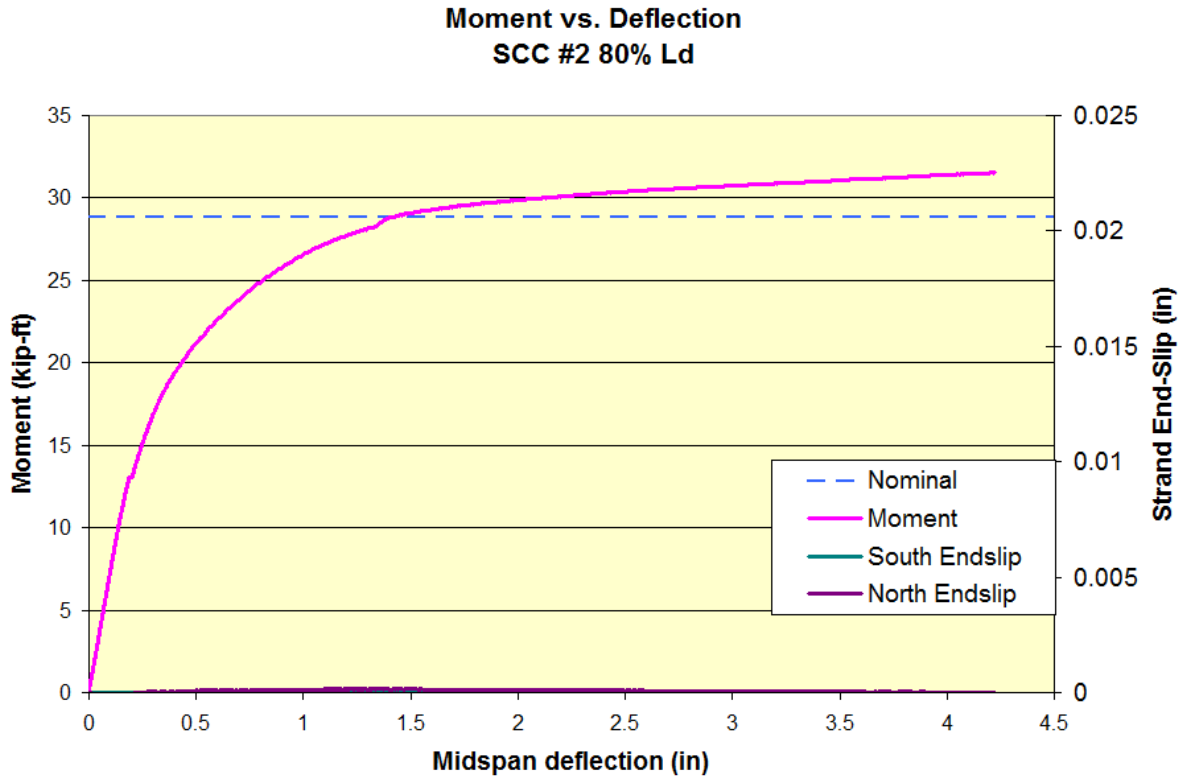

Figure 8.19 Moment versus deflection for SCC #2 80% L_d specimen

Figure 8.20 Failure of SCC #2 80% L_d specimen

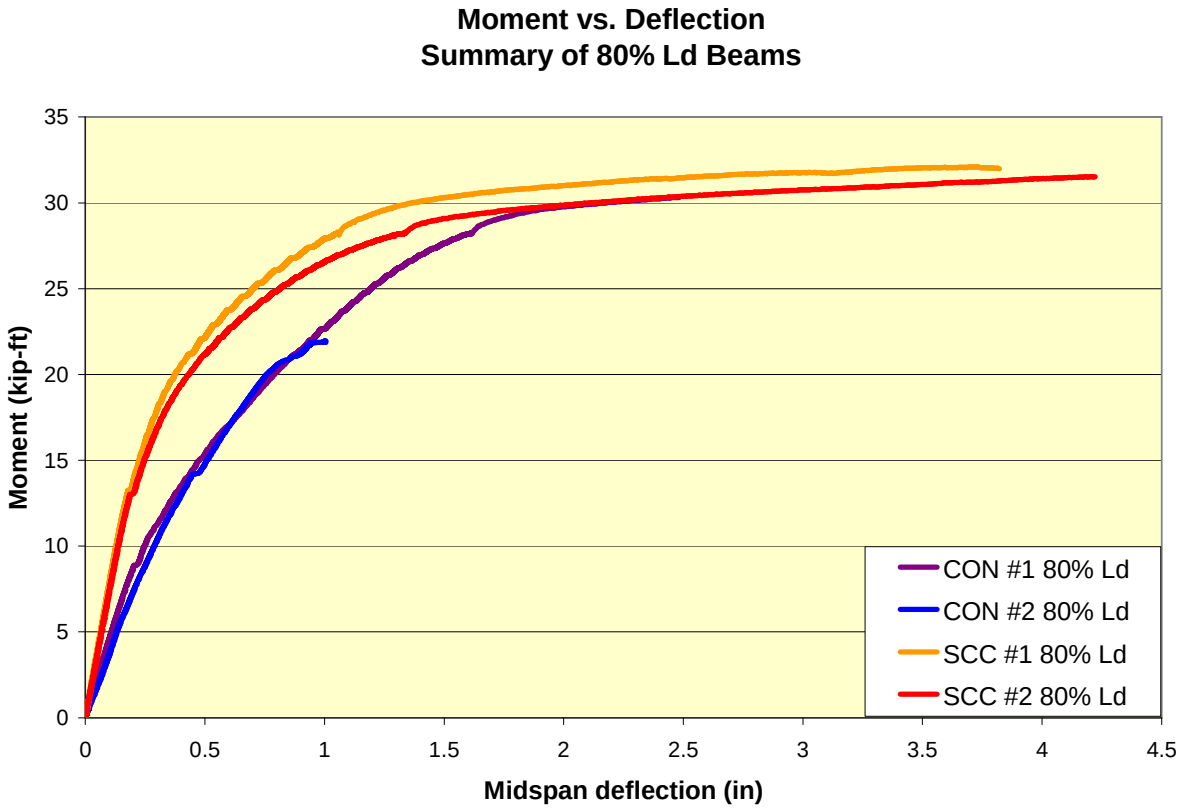

Figure 8.21 Summary of 80% L_d specimens' moment versus deflection

8.4 T-Beam Test Results

T-beam data was analyzed just like the rectangular beams, except there were five end-slip LVDTs graphed for each end of the beam. Figures 8.22 and 8.24 show moment vs. deflection curves for the two CON T-beams. Both beams failed due to the strands slipping, which caused the prestress force to be lost causing shear failure. Both beams failed to reach nominal capacity, with CON #1 reaching 68% and CON #2 reaching 74% of nominal capacity. In CON #1, one end of the beam had strand slip and in Con #2, both ends experienced strand slip, which can be seen in Figures 8.22 and 8.24, respectively. Figures 8.23 and 8.25 show the CON T-beams after failure. Figures 8.26 and 8.28 show moment vs. deflection curves for the two SCC T-beams. Like the CON T-beams, both SCC T-beams failed due to strand slip. SCC #1 reached 79% and SCC #2 reached 89% of nominal capacity. Both SCC T-beams had one end experience strand slip. Their failures can be seen in Figures 8.27 and 8.29. Table 8.1 shows a summary of results

from the T-beam tests, along with results from the rectangular beam tests. Figure 8.30 shows a summary of the T-beam specimens' moment versus deflection.

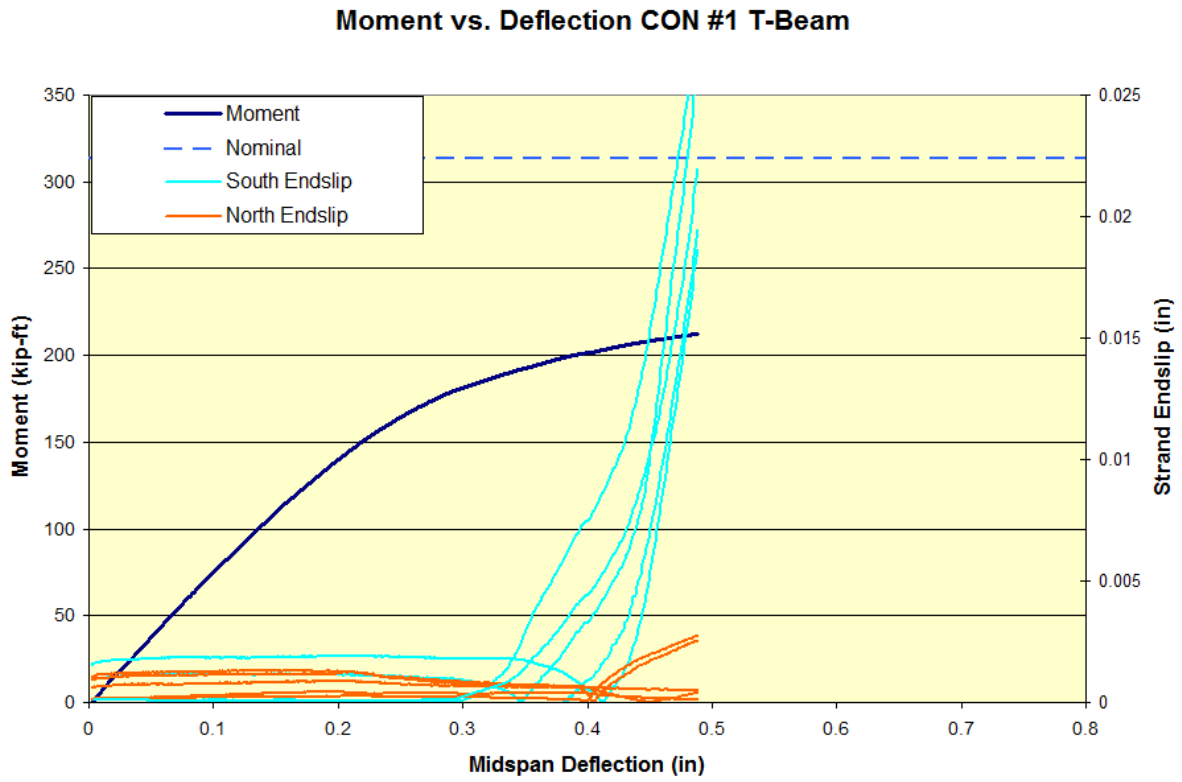

Figure 8.22 Moment versus deflection for CON #1 T-beam specimen

Figure 8.23 Failure of CON #1 T-beam specimen

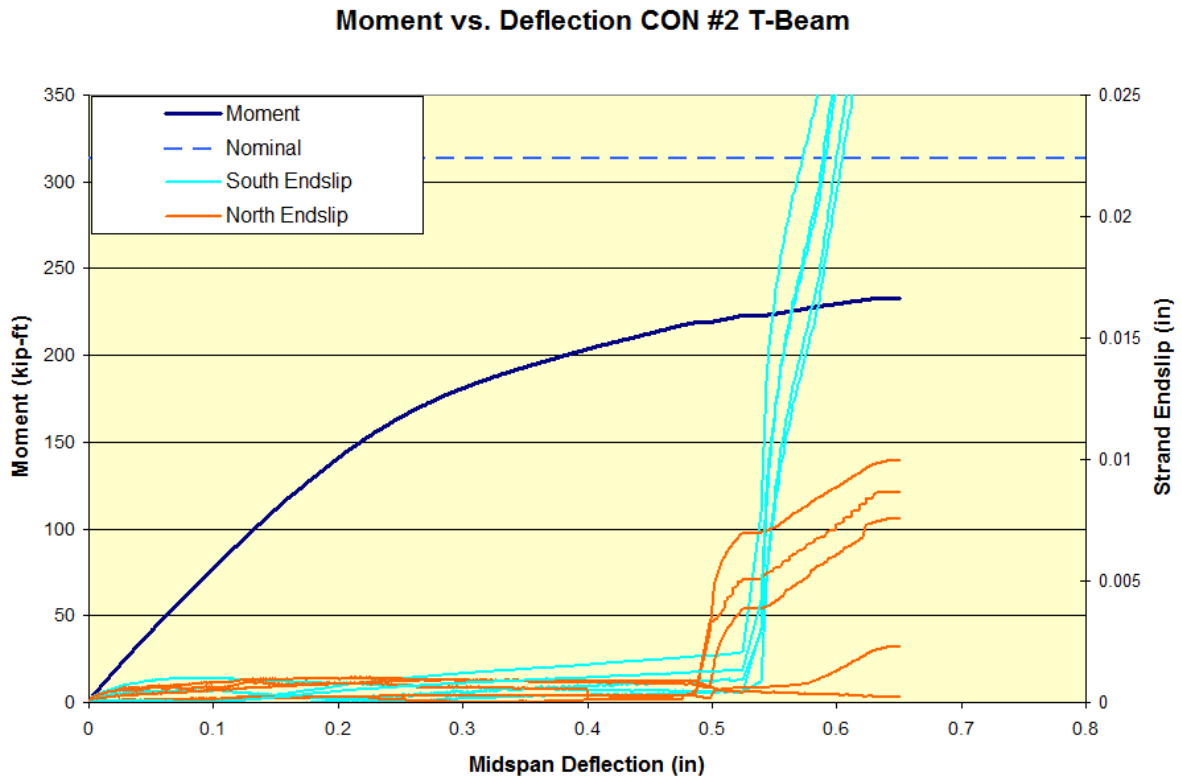

Figure 8.24 Moment versus deflection for CON #2 T-beam specimen

Figure 8.25 Failure of CON #2 T-beam specimen

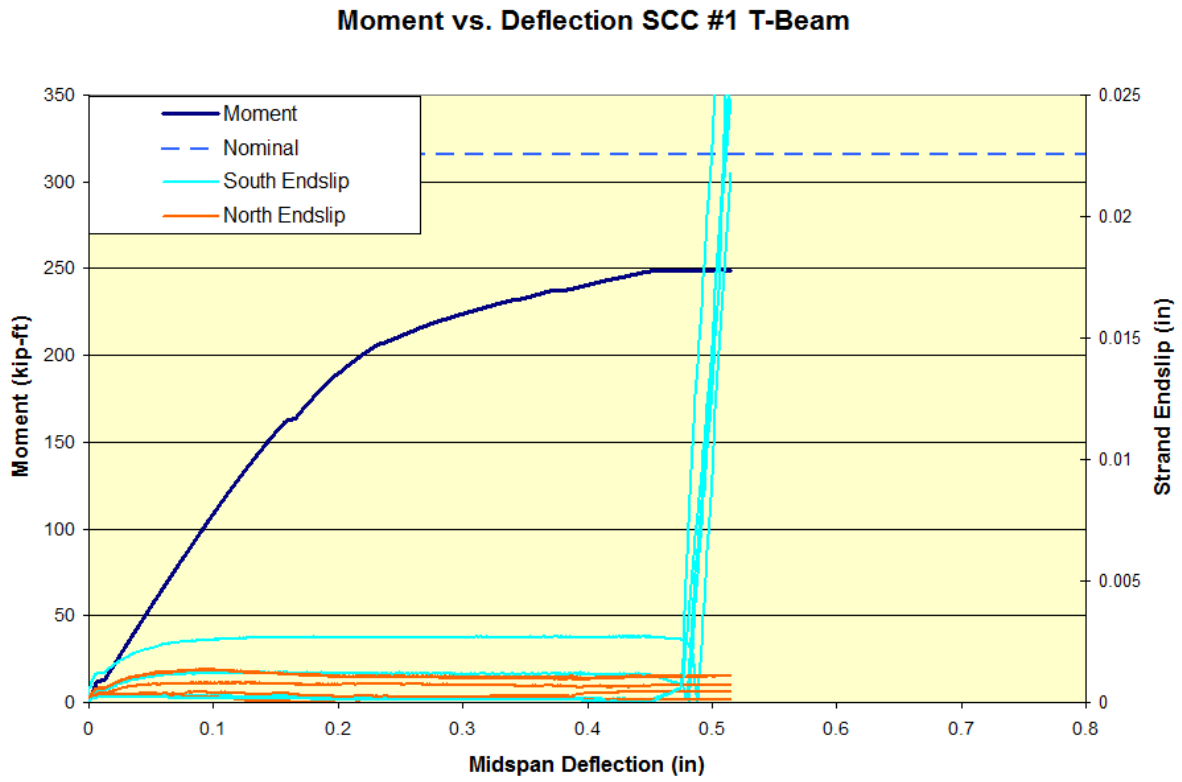

Figure 8.26 Moment versus deflection for SCC #1 T-beam specimen

Figure 8.27 Failure of SCC #1 T-beam specimen

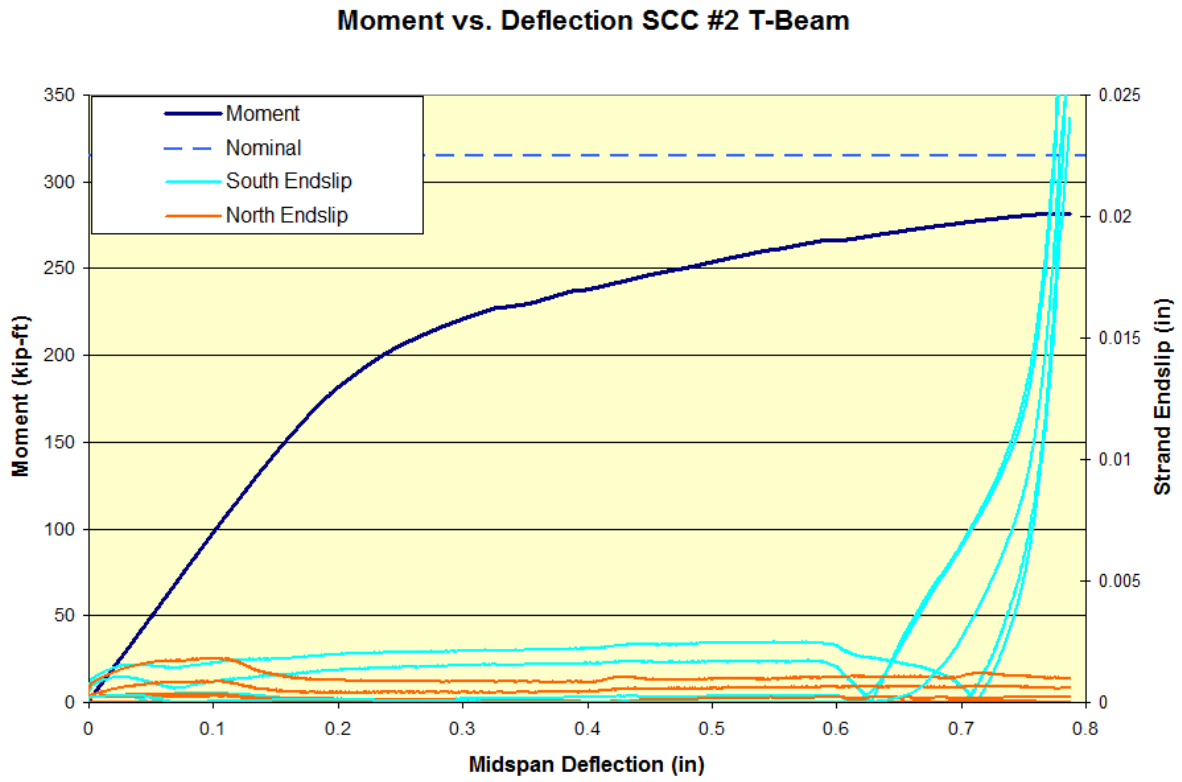

Figure 8.28 Moment versus deflection for SCC #2 T-beam specimen

Figure 8.29 Failure of SCC #2 T-beam specimen

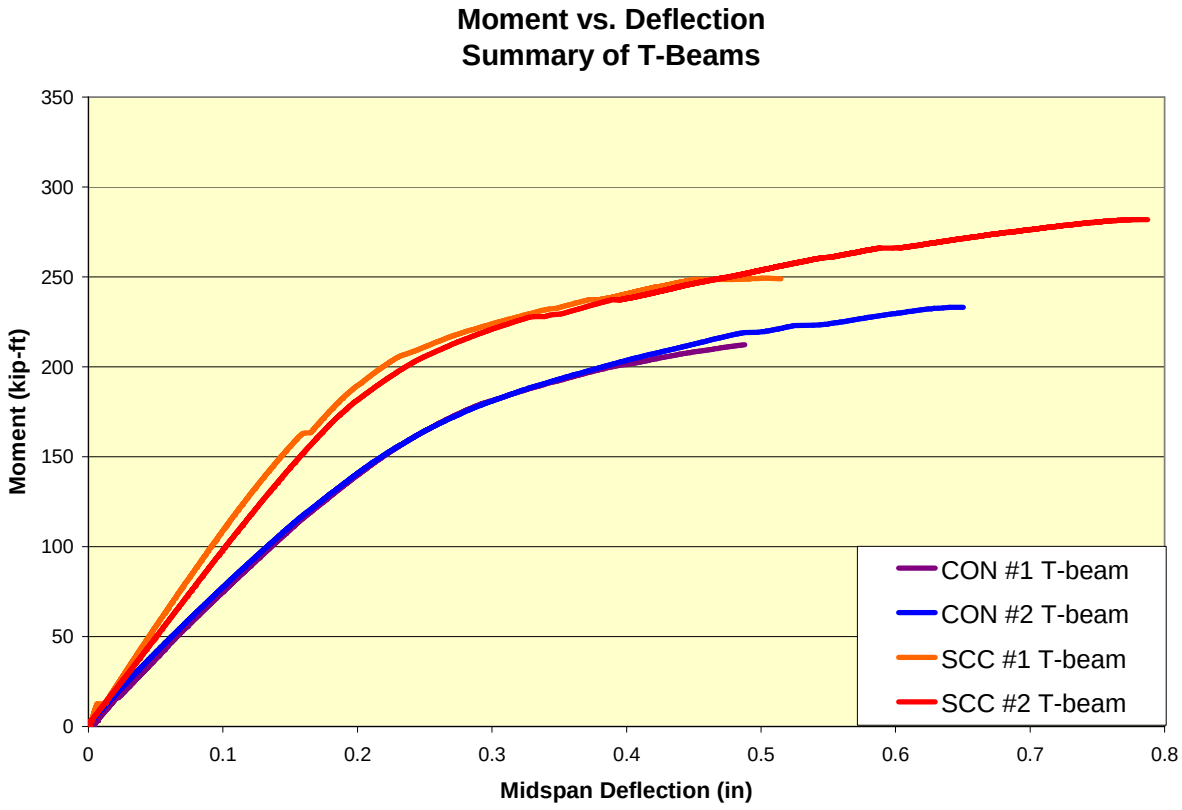

Figure 8.30 Summary of T-beam specimens' moment versus deflection

Ends of the T-beams showed possible signs of excessive moisture in the mixes. Water being released from the aggregate could cause this increase in moisture since excess moisture wasn't observed during the casting of the beams. This moisture caused the beams to be discolored around the strand at each end which is shown in Figure 8.31. The movement of water could cause an increase in the water-to-cement ratio around the strand causing the strength of the of the concrete to decrease. Decrease in concrete strength near the strand could cause a decrease in the bond capacity of the concrete with the strand causing the specimen to failure prematurely through bond failure. Figure 8.32 shows the T-beam end with the end-slip LVDTs after bond failure.

Figure 8.31 Discoloration of T-Beam ends

Figure 8.32 T-beam end after bond failure

CHAPTER 9 - Conclusions and Recommendations

9.1 Conclusions

This test program revealed many interesting results and led to development of several conclusions as listed below. The IT specimens provided beneficial results on transfer length and prestress losses associated with lightweight concrete mixes. Creep and shrinkage prisms provided data to accurately predict long term creep and shrinkage of the lightweight mixes in this study. Flexure beam tests determined the bond characteristics of the lightweight mixes.

1. IT specimens showed code equations used for transfer length and prestress losses were not conservative in predicting the behavior of the lightweight concrete mixes in this study. The experimental transfer lengths were found to be 19% to 30% longer than the recommended value of $60d_b$ or 30 inches by AASHTO (2004). Low concrete strengths at release could provide one reason for the increased transfer lengths.
2. VWSG results were used to determine the experimental prestress losses. The shrinkage losses were found to be much lower than the predicted code values. Reasons for this difference would include the timeline at which initial readings were taken and the presence of internal curing. The initial shrinkage readings may have been taken after a majority of the shrinkage had taken place. Elastic shortening losses were found to be close to the predicted code equations but the losses due to creep were over 10 ksi larger than the values predicted. The one year experimental losses for the SCC and CON mixes were found to be 71 ksi and 73 ksi, respectively. AASHTO code equation losses for one year were calculated to be 59 ksi.
3. Creep and shrinkage prisms supplied information about the long term characteristics of the lightweight concrete mixes. The data from the prisms were used with ACI 209 equations to determine the creep and shrinkage parameters. These parameters conservatively predicted the long term prestress losses of the lightweight mixes used in this study.

4. Flexure beam results showed that the development length equations were not conservative in predicting the behavior of the lightweight concrete and mixes evaluated in this study. All of the T-beams tested in this study exhibited bond failures. Excess moisture released by the aggregate after placement in the forms may have caused a higher water-to-cement ratio in the paste near the prestress strand. The additional water may have caused the bond strength to decrease, causing premature failure.

9.2 Recommendations & Areas of Further Investigation Before Implementation

Flexural tests revealed that the lightweight concrete in this study performed poorly when compared to AASHTO, ACI and PCI code predictions. Findings from this study can be a benchmark for future research projects but several items require further research.

1. Additional trial runs should be performed at precast plant before casting more test samples. Time between trial test mixes and test sample cast dates should be minimized.
2. Cast additional test specimens to determine if new, higher-strength, mix will result in acceptable bond performance.
3. Additional transfer length tests should be performed to confirm the findings from this study. Use of longer specimens will show plateau in transfer length graphs.
4. The source of excess moisture that appeared in the T-beams needs be determined to prevent girders from having a sudden bond failure.
5. Use of dry-lightweight aggregate should be investigated to decrease excess moisture in the mix.
6. Violent failure of several of the beams caused by strand end-slip warrants future research be done on the lightweight mixes before they can be successfully implemented in Kansas' bridges.
7. The issue with low concrete strengths must be resolved before lightweight concrete girders can be implemented on Kansas roads.
8. Lightweight mixes used in this study should not be used for Kansas bridges.

References

1. AASHTO. “LRFD Bridge Design Specifications,” American Association of State Highway and Transportation Officials. 2004.
2. ACI Committee 209. *Report on Factors Affecting Shrinkage and Creep of Hardened Concrete*, ACI 209.1R-05, American Concrete Institute, 2005.
3. ACI Committee 318. *Building Code Requirements for Structural Concrete*, 318-08, American Concrete Institute, 2008.
4. ASTM C31 Standard Practice for Making and Curing Concrete Test Specimens in the Field, 2009.
5. ASTM C39 Standard Test Method for Compressive Strength of Cylindrical Concrete Specimens, 2009.
6. ASTM C138 Standard Test Method for Density, Yield, and Air Content (Gravimetric) of Concrete, 2009.
7. ASTM C143 Standard Test Method for Slump of Hydraulic-Cement Concrete, 2009.
8. ASTM C173 Standard Test Method for Air Content of Freshly Mixed Concrete by the Volumetric Method, 2009.
9. ASTM C192 Standard Practice for Making and Curing Concrete Test Specimens in the Laboratory, 2009.
10. ASTM C330 Standard Specification for Lightweight Aggregates for Structural Concrete, 2009.
11. ASTM C496 Standard Test Method for Splitting Tensile Strength of Cylindrical Concrete Specimens, 2009.
12. ASTM C512 Standard Test Method for Creep of Concrete in Compression, 2009.
13. ASTM C1611 Standard Test Method for Slump Flow of Self-Consolidating Concrete, 2009.
14. ASTM C1621 Standard Test Method for Passing Ability of Self-Consolidating Concrete by J-Ring, 2009.

15. Barnes, R.W., J. W. Grove, and N. H. Burns. “Experimental Assessment Factors Affecting Transfer Length,” *ACI Structural Journal* 100.6, 2003: 740-748.
16. Buckner, D. “A Review of Strand Development Length for Pretensioned Concrete Members.” *PCI Journal* 40.2, 1995: 84-105.
17. Cousins, T.E., M. H. Badaux, and S. Moustafa. “Proposed Test for Determining Bond Characteristics of Prestressing Strand.” *PCI Journal* 37.1, 1992: 66-73.
18. Girgis, A.F.M., and C. Y. Tuan. “Bond Strength and Transfer Length of Pretensioned Bridge Girders Cast with Self-Consolidating Concrete.” *PCI Journal* 50.6, 2005: 72-87.
19. Grace, N.F. “Transfer Length of /CFRP/CFCC Strands for Double-T Girders.” *PCI Journal* 45.5, 2000: 110-126.
20. Interim Guidelines for the Use of Self-Consolidating Concrete in Precast/Prestressed Concrete Institute Member Plants, First Edition, Chicago, IL, 2003.
21. Kahn, L.F., and M. Lopez. “Prestress Losses in High-Performance Lightweight Concrete Pretensioned Bridge Girders.” *PCI Journal* 50.5, 2005: 84-95.
22. Kamel, M.R., and M. K. Tadros. “The Inverted-Tee Shallow Bridge System for Rural Areas.” *PCI Journal* 41.5, 1996: 28-43.
23. Khayat, K.H., J. Assaad, and J. Daczko. “Comparison of Field-Oriented Test Methods to Asses Dynamic Stability of Self-Consolidating Concrete.” *ACI Materials Journal* 101.2, 2004: 168-176.
24. Larson, K.H. “Evaluating the Time-Dependent Deformations and Bond Characteristics of a Self-Consolidating Concrete Mix and the Implication for Pretensioned Bridge Applications.” Kansas State University. 2006.
25. Larson, K.H., R. J. Peterman, and A. Esmaeily. “Bond Characteristics of Self-Consolidating Concrete for Prestressed Bridge Girders.” *PCI Journal* 52.4, 2007: 44-57.
26. Logan, D. R. “Acceptance Criteria for Bond Quality of Strand for Pretensioned Prestressed Concrete Applications.” *PCI Journal* 42.2, 1997: 52-90.

27. Martin, L., and N. Scott. “Development of Prestressing Strand in Pretensioned Members.” *ACI Journal* 73.8, 1976, 453-456.
28. Mitchell, D., W. D. Cook, A. A. Khan, and T. Tham. “Influence of High-Strength Concrete on Transfer and Development Length of Pretensioning Strand.” *PCI Journal* 38.3, 1993: 52-66.
29. Mitchell, D. W., and H. Marzouk. “Bond Characteristics of High-Strength Lightweight Concrete.” *ACI Structural Journal* 104.1, 2007:22-29.
30. Moustafa, S. “Pull-Out Strength of Strand and Lifting Loops.” Concrete Technology Associates Technical Bulletin, 1974: 74-B5.
31. Ouchi, M. “Self-Compacting Concrete Development, Applications and Investigations.” *Proceedings of the Fourth International Conference on Materials Engineering for Resources* 1, 2001: 53-58.
32. PCI Industry Handbook Committee. *PCI Design Handbook*, Sixth Edition, Chicago, IL, Precast/Prestress Concrete Institute, 2004.
33. Perkins, J. “Concrete Fluidity Effects on Bond of Prestress Tendons for Lightweight Bridge Girders.” Kansas State University, 2008.
34. Peterman, R.J. “Effects of As-Cast Depth and Concrete Fluidity on Strand Bond.” *PCI Journal* 52.3, 2007: 72-101.
35. Peterman, R.J., J. A. Ramirez, and J. Olek. “Influence of Flexure-Shear Cracking on Strand Development Length in Prestressed Concrete Members.” *PCI Journal* 45.5, 2000: 76-94.
36. Research Department, State Highway Commission of Kansas, *Availability and Suggested Usage of Lightweight Aggregate Concrete for Kansas highway Construction*, 1953.
37. Russell, B.W., and N. H. Burns. “Measured Transfer Lengths of 0.5-in. and 0.6-in. Strands in Pretensioned Concrete.” *PCI Journal* 41.5, 1996: 44-65.
38. Shing, P.B., D. M. Frangopol, M. L. McMullen, W. Hutter, D. E. Cooke, and M. A. Leonard. “Strand Development and Transfer Length Tests on High-Performance Concrete Box Girders.” *PCI Journal* 45.5, 2000: 96-109.
39. Steinberg, E., J. T. Beier, and S. Sargand. “Effects of Sudden Prestress Force Transfer in Pretensioned Concrete Beams.” *PCI Journal* 46.1, 2001: 64-75.

40. Weerasekera, I.R.A., A. Sabesh, and R. E. Loov. “Reliability of Bond Measuring Devices in Pretensioned Prestressed Concrete.” *Innovations in Structural Engineering and Construction* 1, 2008: 333-338.

Appendix A - Supplementary Table, Figures, and Calculations

A.1 IT Beams' Transfer Length Graphs

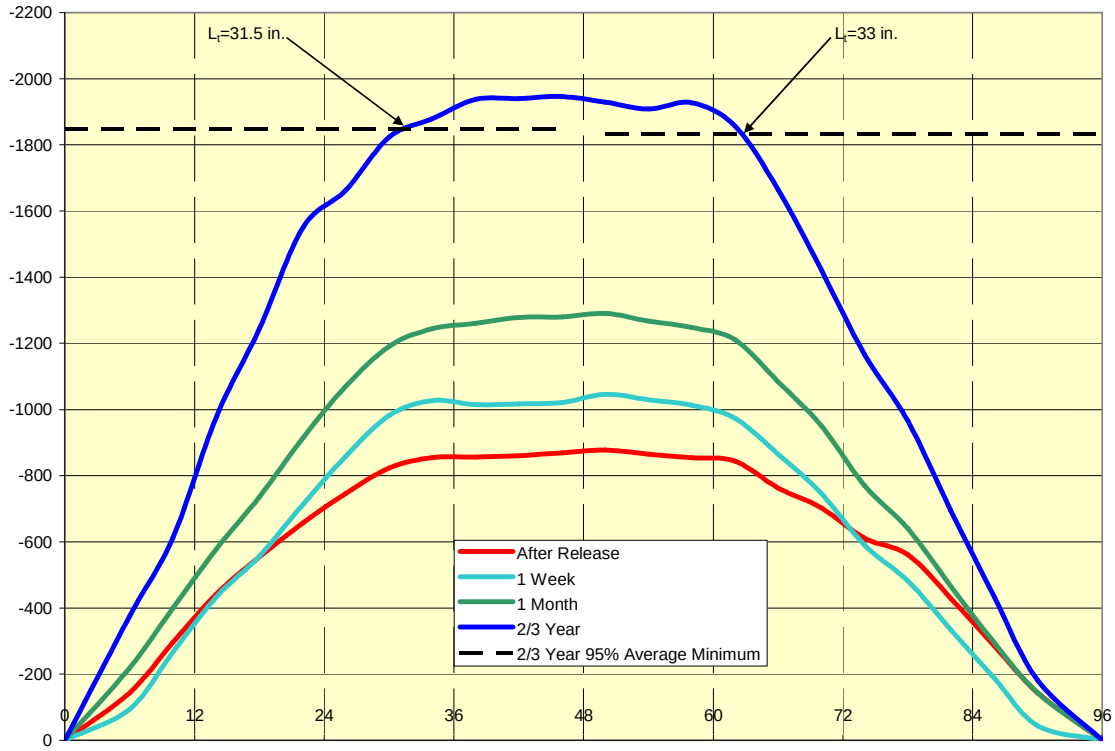

Figure 9.1 Transfer length for first set CT #2

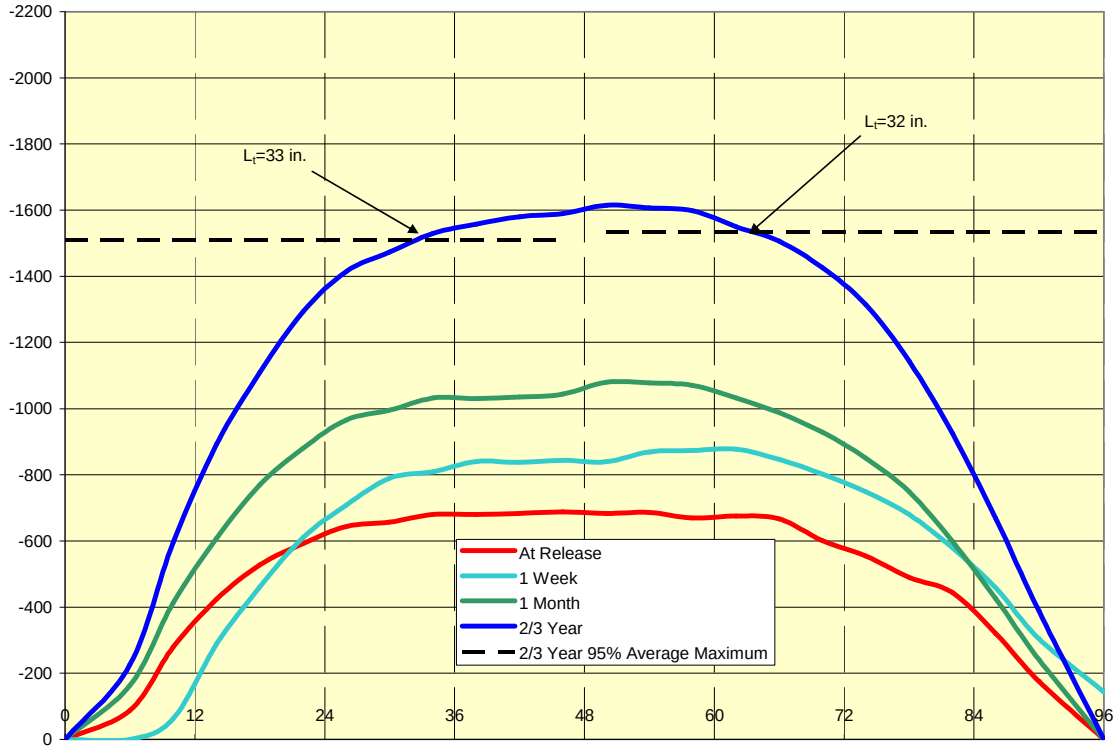

Figure 9.2 Transfer length of first set ST #2

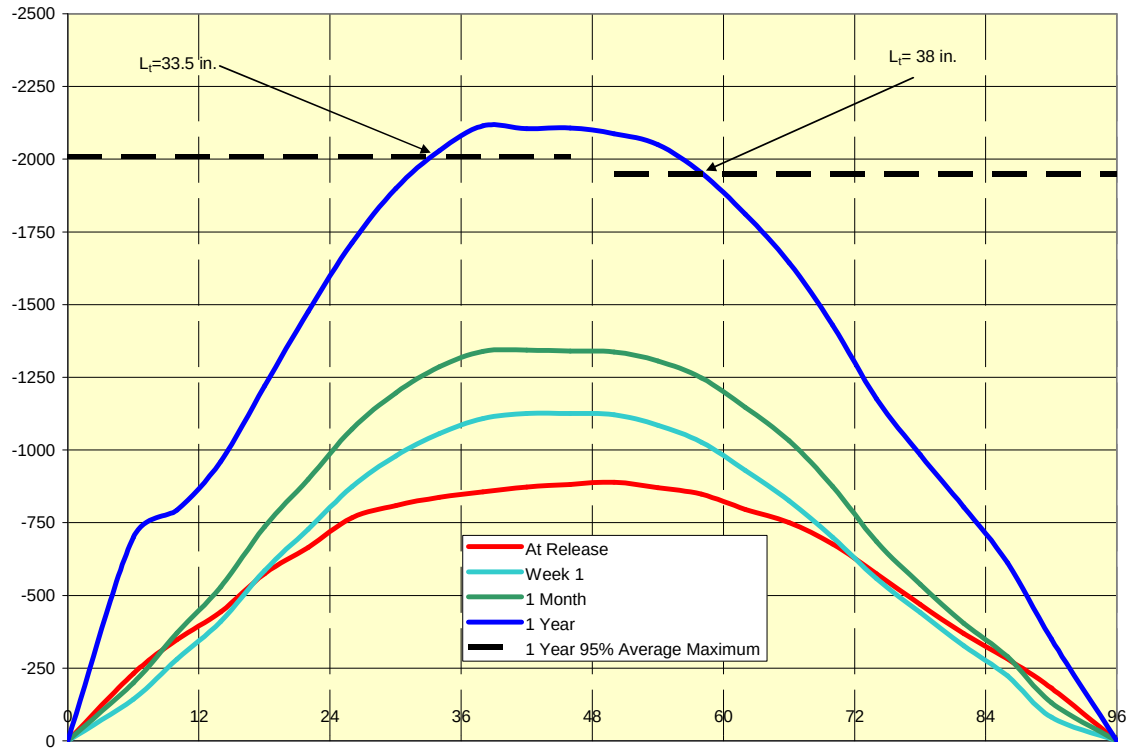

Figure 9.3 Transfer length of second set CT #2

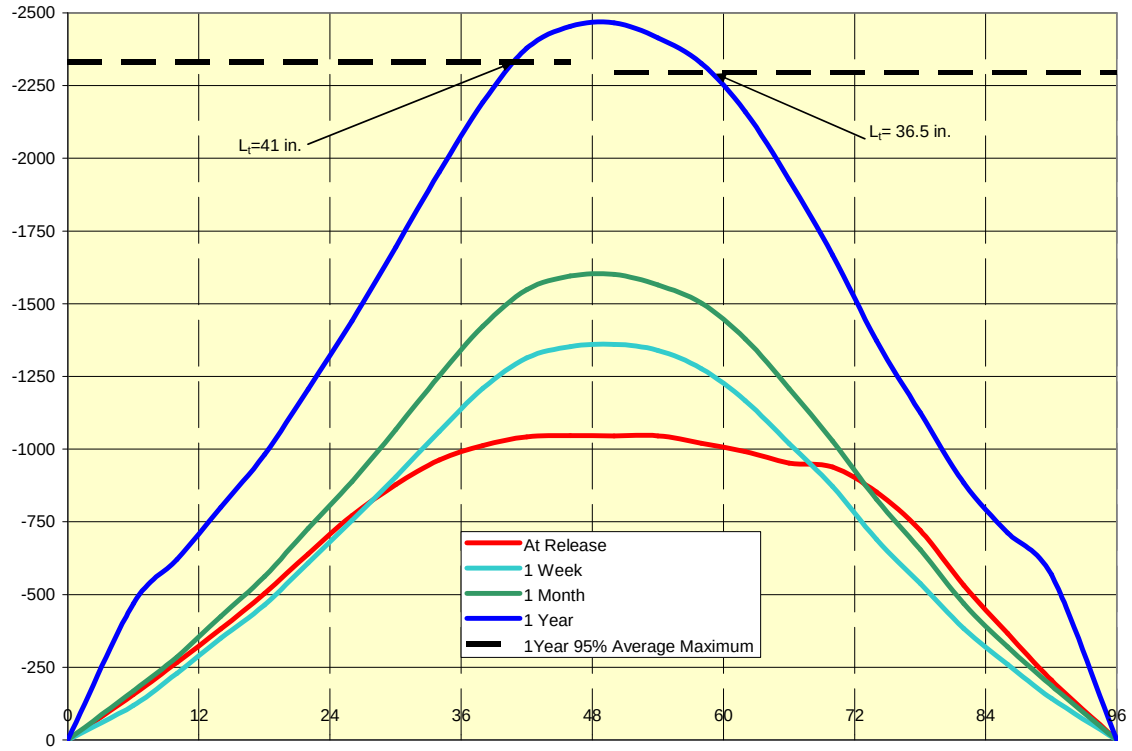

Figure 9.4 Transfer length of second set ST #2

A.2 IT Beams' VWSG Graphs

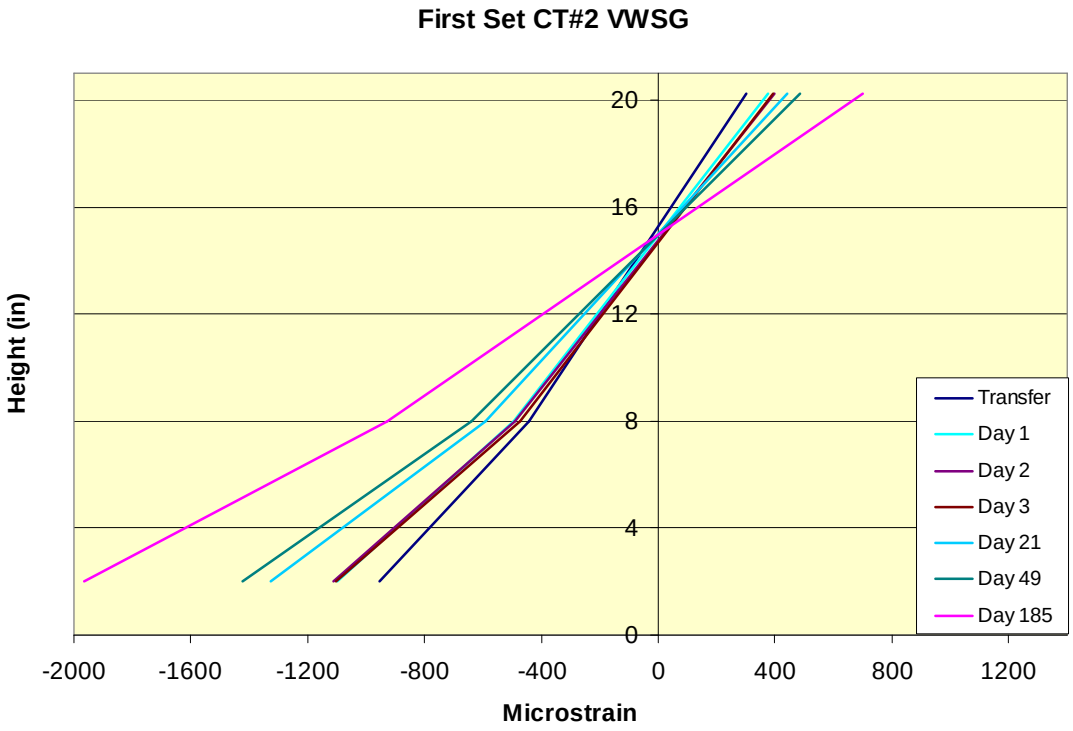

Figure 9.5 VWSG for first set CT #2 (creep, shrinkage, and elastic shortening losses)

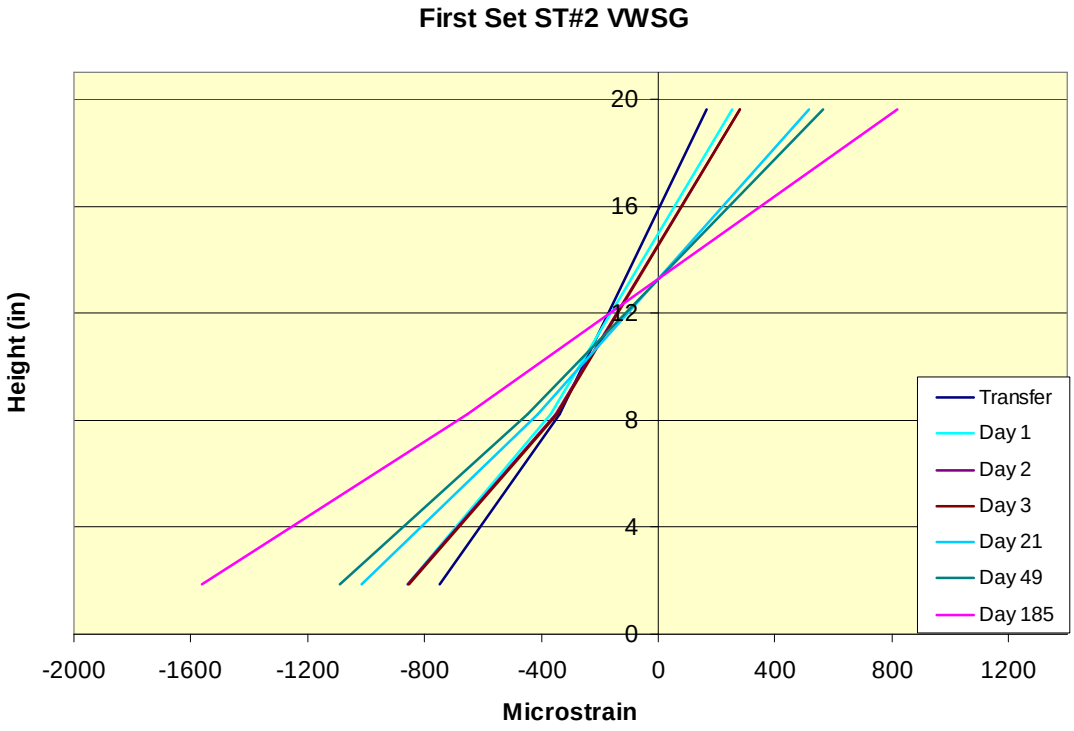

Figure 9.6 VWSG for first set ST #2 (creep, shrinkage, and elastic shortening losses)

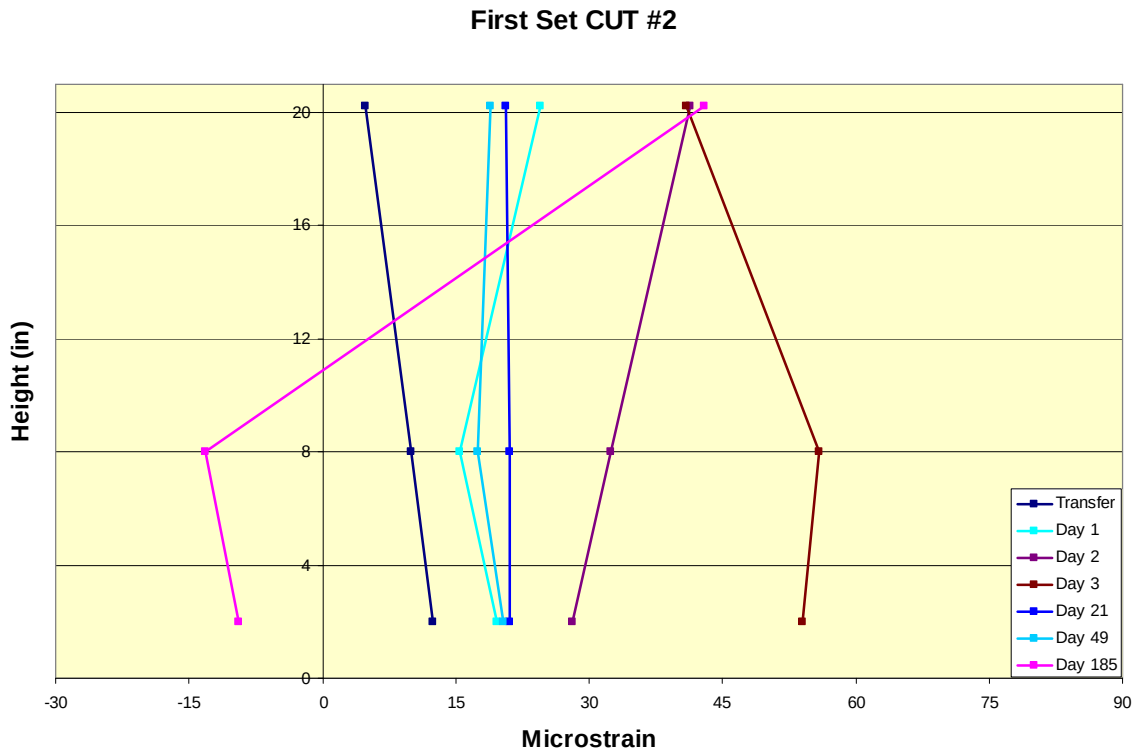

Figure 9.7 VWSG for first set CUT #2 (change due to shrinkage losses)

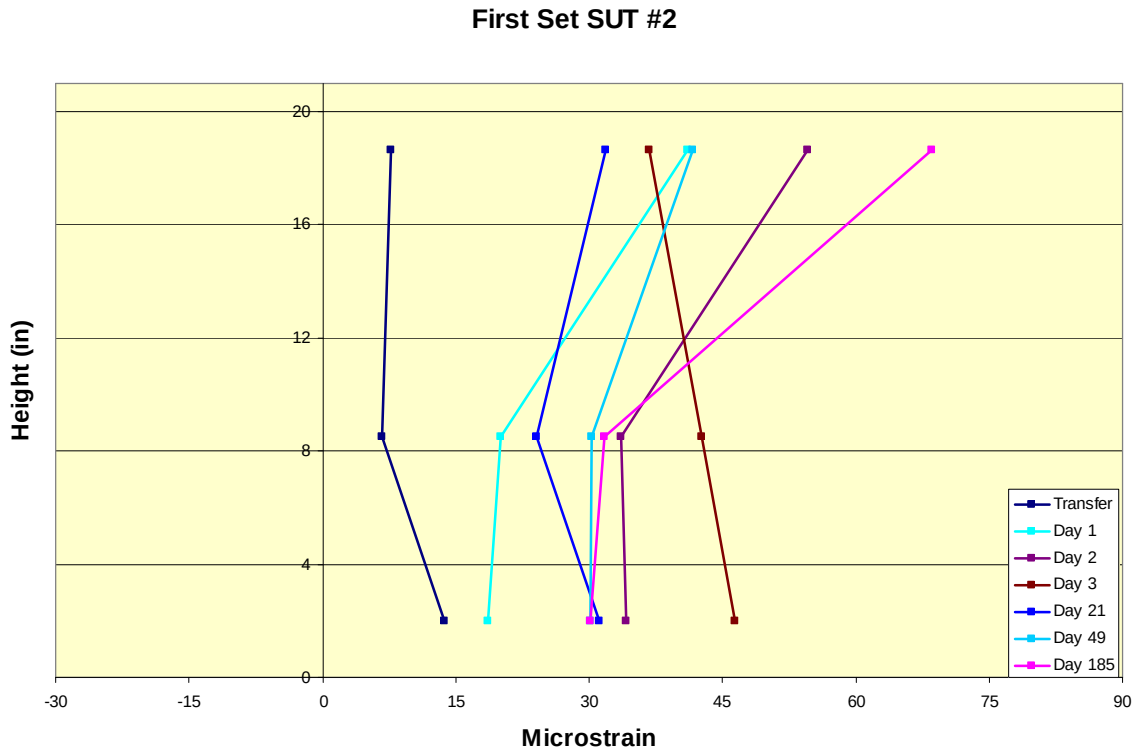

Figure 9.8 VWSG for first set SUT #2 (change due to shrinkage losses)

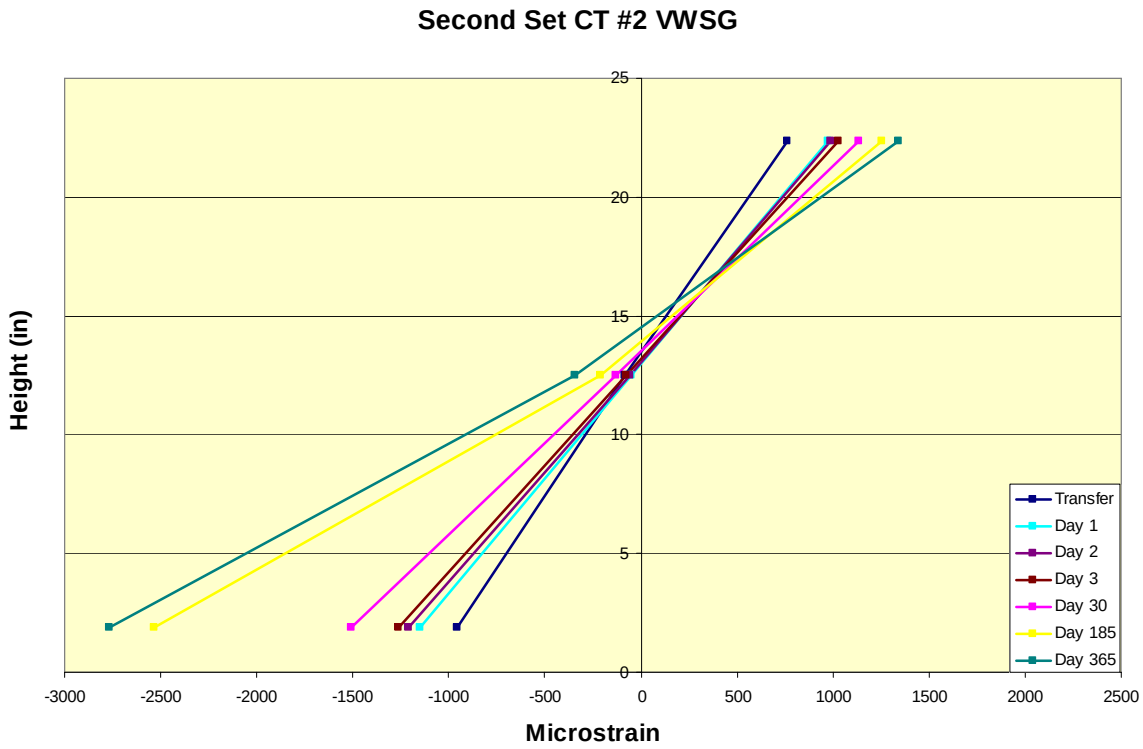

Figure 9.9 VWSG for second set CT #2 (creep, shrinkage, and elastic shortening losses)

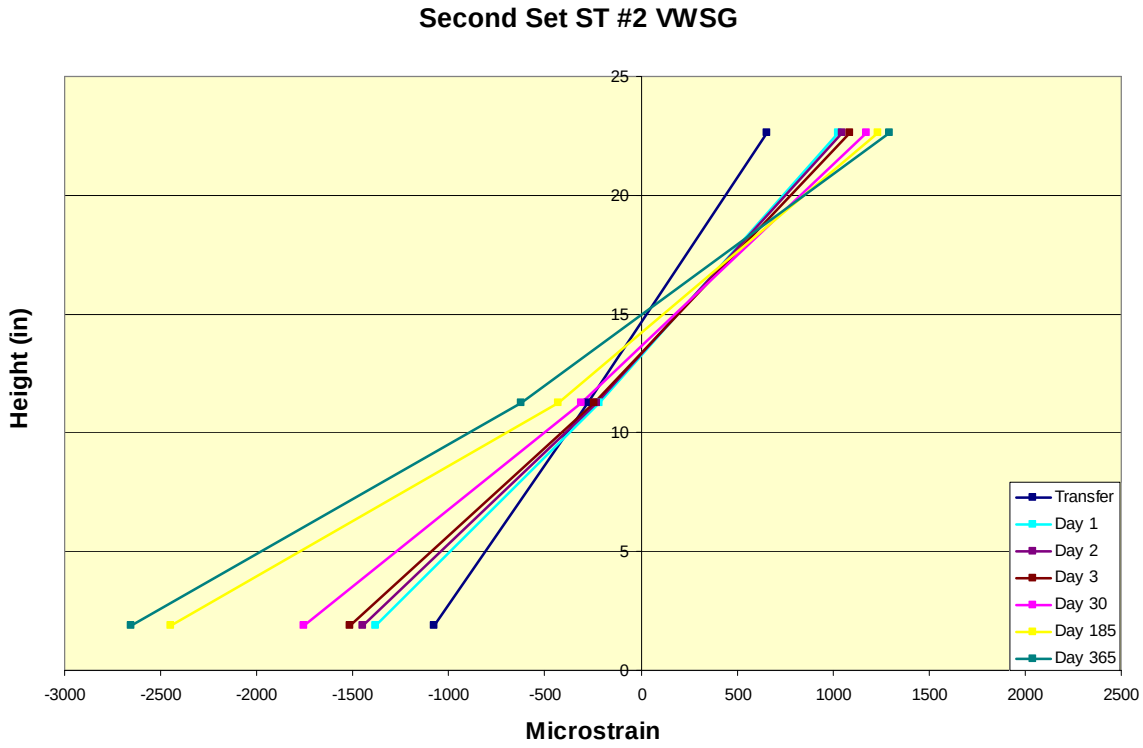

Figure 9.10 VWSG for second set ST #2 (creep, shrinkage, and elastic shortening losses)

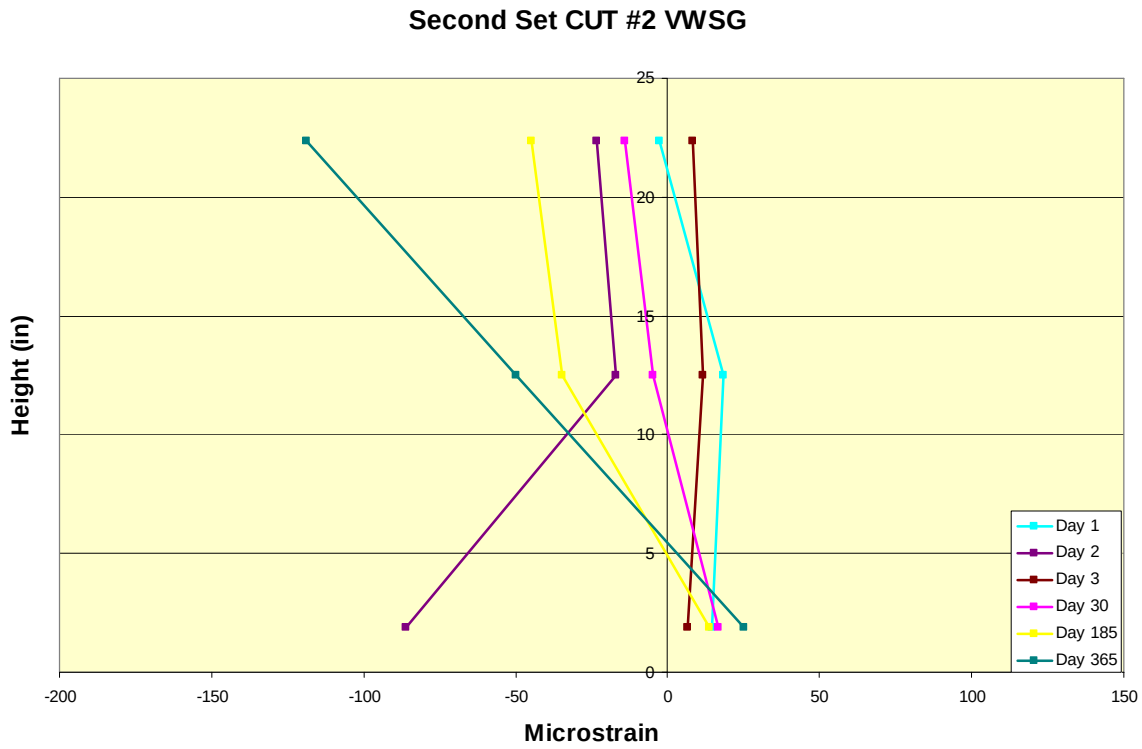

Figure 9.11 VWSG for second set CUT #2 (change due to shrinkage losses)

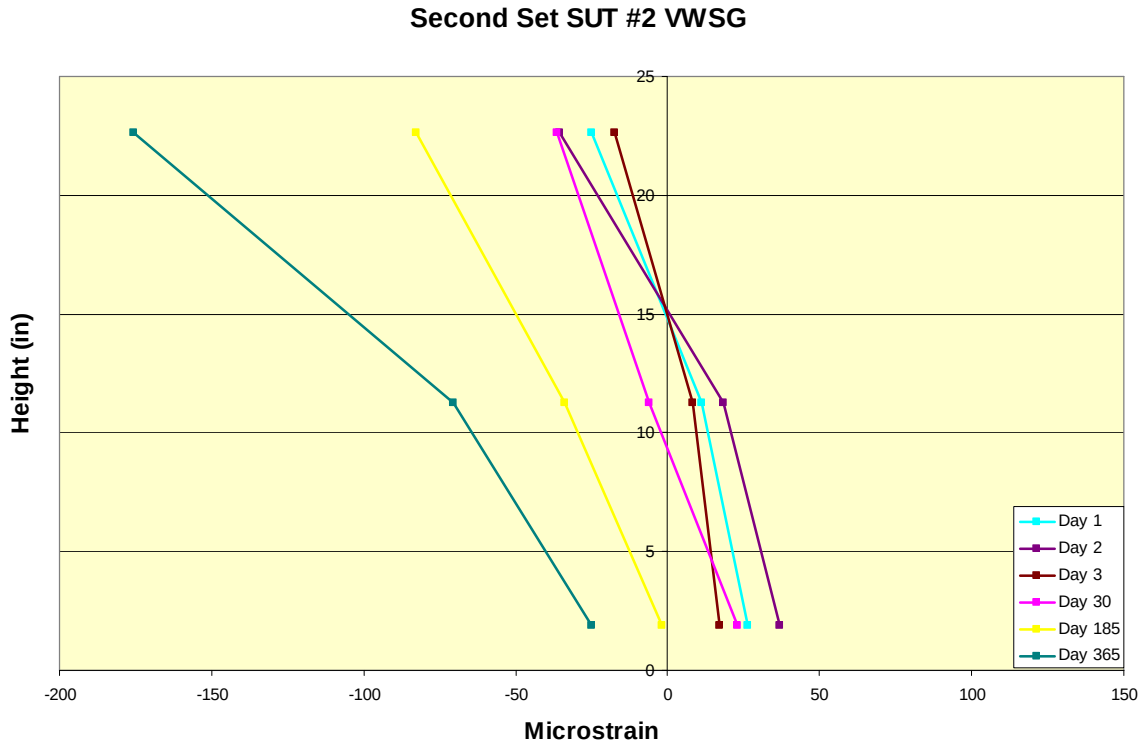

Figure 9.12 VWSG for second set SUT #2 (change due to shrinkage losses)

A.3 Prestress Loss Equations

ACI and PCI Methods

(ACI Committee 318, 2005 and PCI Design Handbook, 2004)

Elastic Shortening of Concrete (ES):

$$ES = K_{es} E_s \frac{f_{cir}}{E_{ci}}$$

where:

K_{es}= 1.0 for pretensioned members

E_{ci}= modulus of elasticity of concrete at time prestress is applied

E_s= modulus of elasticity of prestressing tendons

$$f_{cir} = K_{cir} f_{cpi} - f_g$$

where:

K_{cir}= 0.9 for pretensioned members

Creep of Concrete (CR):

Members with bonded tendons:

$$CR = K_{cr} \frac{E_s}{E_c} \times [f_{cir} - f_{cds}]$$

where:

K_{cr}= 1.6 for lightweight concrete

Shrinkage of Concrete (SH):

$$SH = \left(8.2 \times 10^{-6}\right) \times K_{sh} \times E_{ps} \times \left[1 - 0.06 \times \frac{V}{S}\right] \times [100 - RH]$$

where:

K_{sh}= 1.0 for pretensioned members

V/S= volume-to-surface ratio

RH= average ambient relative humidity

Relaxation of Tendons (RE):

$$RE = \left[K_{re} - J \times \left(SH + CR + ES \right) \right] \times C$$

where:

K_{re}, J, and C are taken from tables in PCI Handbook (2004)

AASHTO Method

From Third Edition AASHTO (2004)

$$\Delta f_{pT} = \Delta f_{pES} + \Delta f_{pSR} + \Delta f_{pCR} + \Delta f_{pR2}$$

where:

Δf_{pT}= total loss (ksi)

Δf_{pES}= loss due to elastic shortening (ksi)

Δf_{pSR}= loss due to shrinkage (ksi)

Δf_{pCR}=loss due to creep of concrete (ksi)

Δf_{pR2}= loss due to relaxation of steel after transfer (ksi)

Elastic Shortening (Δf_{pES}):

$$\Delta f_{pES} = \frac{E_p}{E_{ci}} \times f_{cgp}$$

where:

fcpg= sum of stresses in concrete at the center of gravity of the prestressing tendons due to the prestressing force at transfer and the self weight of the member at the section of maximum moment (ksi)

Ep= modulus of elasticity of prestressing steel (ksi)

Eci= modulus of elasticity of concrete at transfer (ksi)

Shrinkage (Δf_{pSR}):

$$\Delta f_{pSR} = \left[17.0 - 0.150 \times H \right]$$

where:

H= average annual ambient relative humidity

Creep (Δf_{pCR}):

$$\Delta f_{pCR} = 12.0 \times f_{cgp} - 7.0 \times \Delta f_{cdp} \geq 0$$

where:

f_{cgp}= concrete stress at center of gravity of prestressing steel at transfer

Δf_{cdp}= change in concrete stress at center of gravity of prestressing steel due to permanent loads with the exception of the load acting at the time the prestressing force is applied. Values of Δf_{cdp} should be calculated at the same section or at sections at which f_{cgp} is calculated (ksi)

Relaxation (Δf_{pR2}):

$$\Delta f_{pR2} = 20.0 - 0.4 \times \Delta f_{pES} - 0.2 \times \left[\Delta f_{pSR} + \Delta f_{pCR} \right]$$

where:

$_{\Delta}f_{pES}$= loss due to elastic shortening (ksi)

Δf_{pSR}= loss due to shrinkage (ksi)

Δf_{pCR}= loss due to creep of concrete (ksi)

A.4 Prestress Loss Calculations for IT Beams

<u>Elastic Shortening of Concrete (ES):</u>

$$ES = K_{es} E_s \frac{f_{cir}}{E_{ci}}$$

K_{es}= 1.0 for pretensioned members

$$E_{ci} = 33 w^{1.5} \sqrt{f_c'} = 33 \times 110^{1.5} \times \sqrt{3500} = 2250 ksi \text{ (ACI 318 2008)}$$

E_s= 28,500 ksi

$$f_{cir} = K_{cir} f_{cpi} - f_g$$

K_{cir}= 0.9 for pretensioned members

$$f_{cir} = 0.9 \times \left[\frac{484}{256} + \frac{484 \times 3.86^2}{12822} \right] - \frac{1.7 \times 12 \times 3.86}{12822} = 2.20 ksi$$

$$ES = 1 \times 28500 \times \frac{2.20}{2250} = 27.86 ksi$$

Creep of Concrete (CR):

$$CR = K_{cr} \frac{E_s}{E_c} \times [\, f_{cir} - f_{cds} \,]$$

K_{cr}= 1.6 for lightweight concrete

$$f_{cds} = 0 ksi$$

$$CR = 1.6 \times \left[\frac{28500}{2692} \right] \times (2.2 - 0) = 37.26 ksi$$

Shrinkage of Concrete (SH):

$$SH = \left(8.2 \times 10^{-6}\right) \times K_{sh} \times E_{ps} \times \left[1 - 0.06 \times \frac{V}{S} \right] \times [100 - RH]$$

K_{sh}= 1.0 for pretensioned members

V/S= 2.87

RH= 65%

$$SH = \left(8.2 \times 10^{-6}\right) \times 1 \times 28500 \times [1 - 0.06 \times 2.87] \times [100 - 65] = 6.8 ksi$$

Relaxation of Tendons (RE):

$$RE = \left[K_{re} - J \times (SH + CR + ES) \right] \times C$$

$$K_{re} = 5.0$$

$$J = 0.04$$

$$C = 1.0$$

$$RE_L = \left[5 - 0.04 \times (6.8 + 37.26 + 27.86) \right] \times 1 = 2.12 ksi$$

Total Losses:

$$TL = 27.86 + 37.26 + 6.8 + 2.12 = 74.04$$

$$f_{se} = f_{pj} - TL = 202.5 - 74.04 \approx 128 ksi$$

AASHTO Method

$$\Delta f_{pT} = \Delta f_{pES} + \Delta f_{pSR} + \Delta f_{pCR} + \Delta f_{pR2}$$

Elastic Shortening (Δf_{pES}):

$$\Delta f_{pES} = \frac{E_p}{E_{ci}} \times f_{cgp}$$

$$f_{cgp} = \left[\frac{484}{256} + \frac{484 \times 3.86^2}{12822} \right] - \frac{1.7 \times 12 \times 3.86}{12822} = 2.44 ksi$$

$$\Delta f_{pES} = \frac{28500}{2250} \times 2.44 = 30.99 ksi$$

Shrinkage (Δf_{pSR}):

$$\Delta f_{pSR} = \left[17.0 - 0.150 \times 0.65 \right] = 7.25 ksi$$

Creep (Δf_{pCR}):

$$\Delta f_{pCR} = 12.0 \times 2.44 - 7.0 \times 0 \geq 0$$

$$\Delta f_{pCR} = 29.3 ksi$$

Relaxation (Δf_{pR2}):

$$\Delta f_{pR2} = \left\{ 20.0 - 0.4 \times 30.99 - 0.2 \times \left[7.25 + 29.3 \right] \right\} \times 0.3 = 0.09 ksi$$

Total Losses

$$\Delta f_{pT} = 30.99 + 7.25 + 29.3 + 0.09 = 67.63 ksi$$

$$f_{se} = 198 - 67.63 = 130.37 ksi$$

A.5 Creep Coefficient Graphs

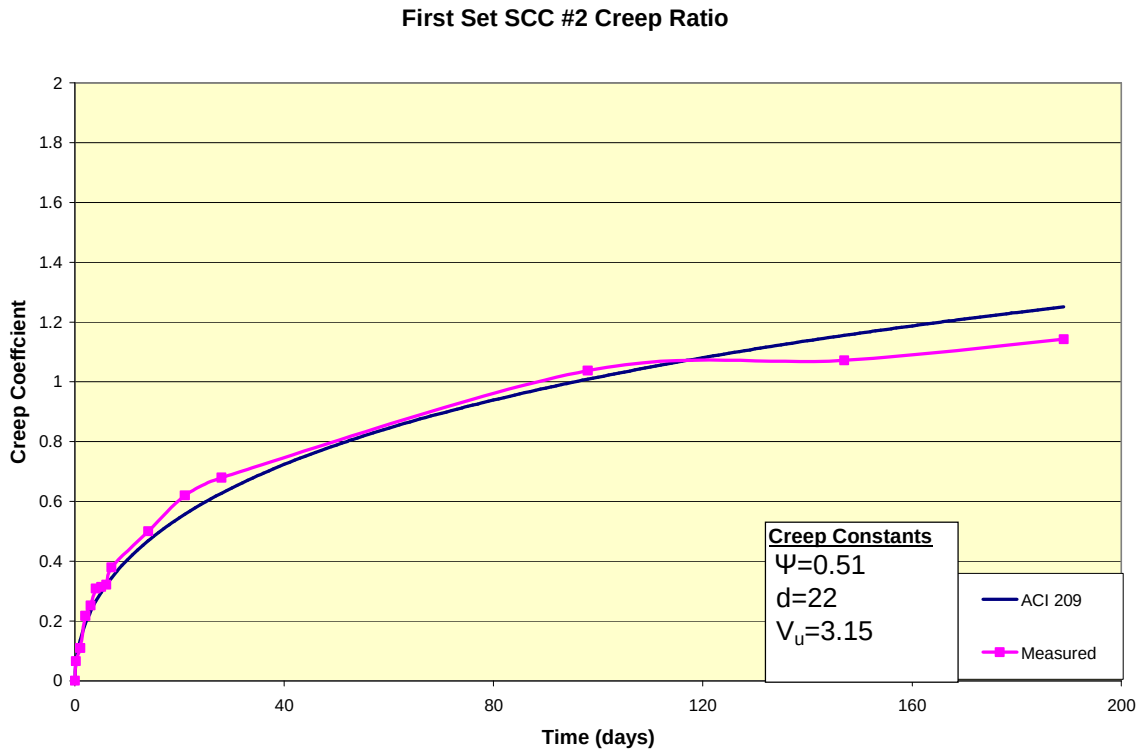

Figure 9.13 First set SCC #2 creep ratio

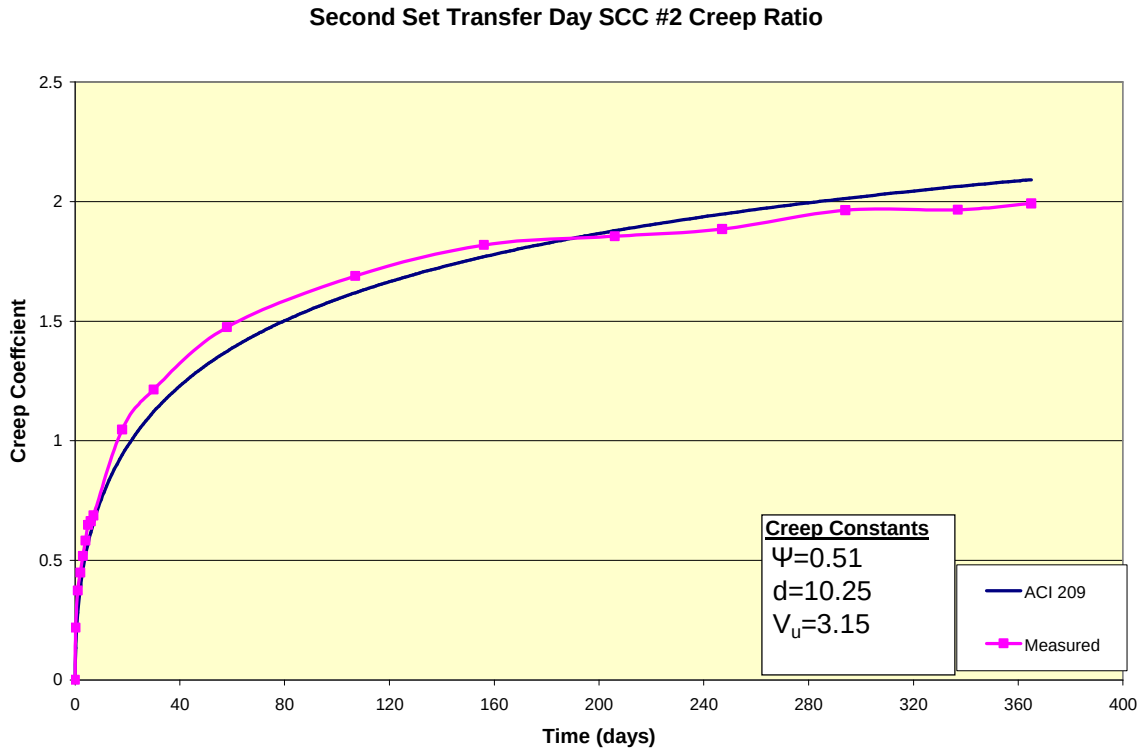

Figure 9.14 Second set SCC #2 creep ratio for transfer day

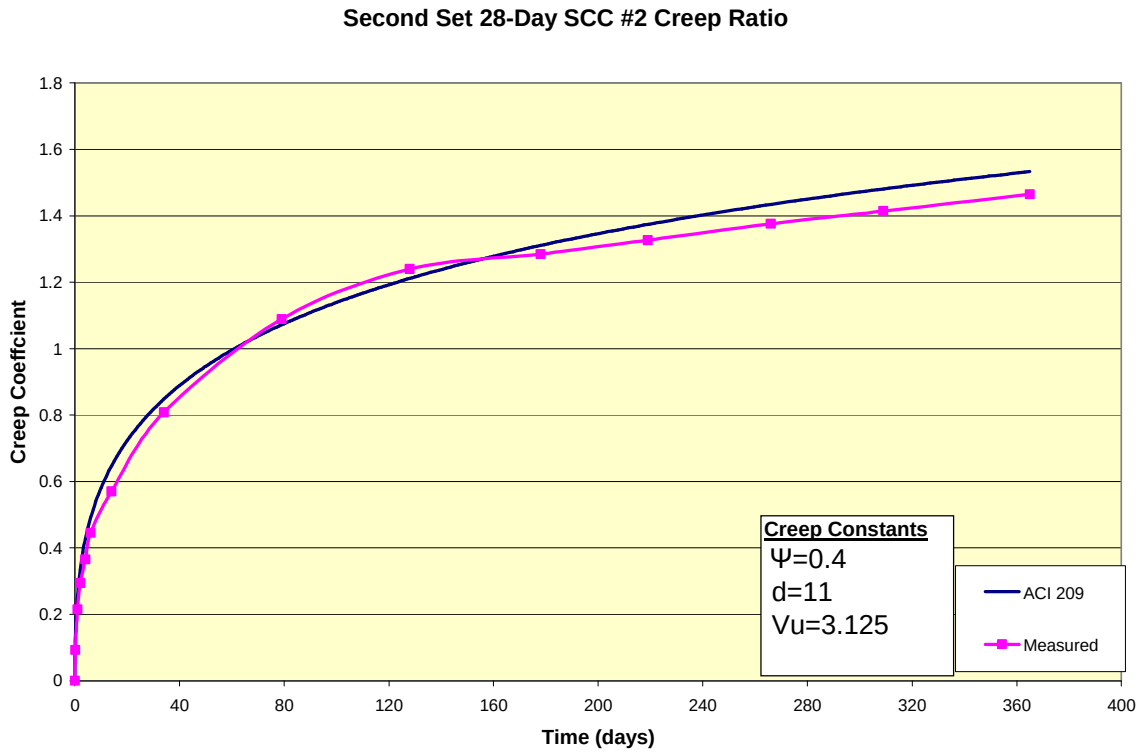

Figure 9.15 Second set SCC #2 creep ratio for 28-day

A.6 Shrinkage Prism Graphs

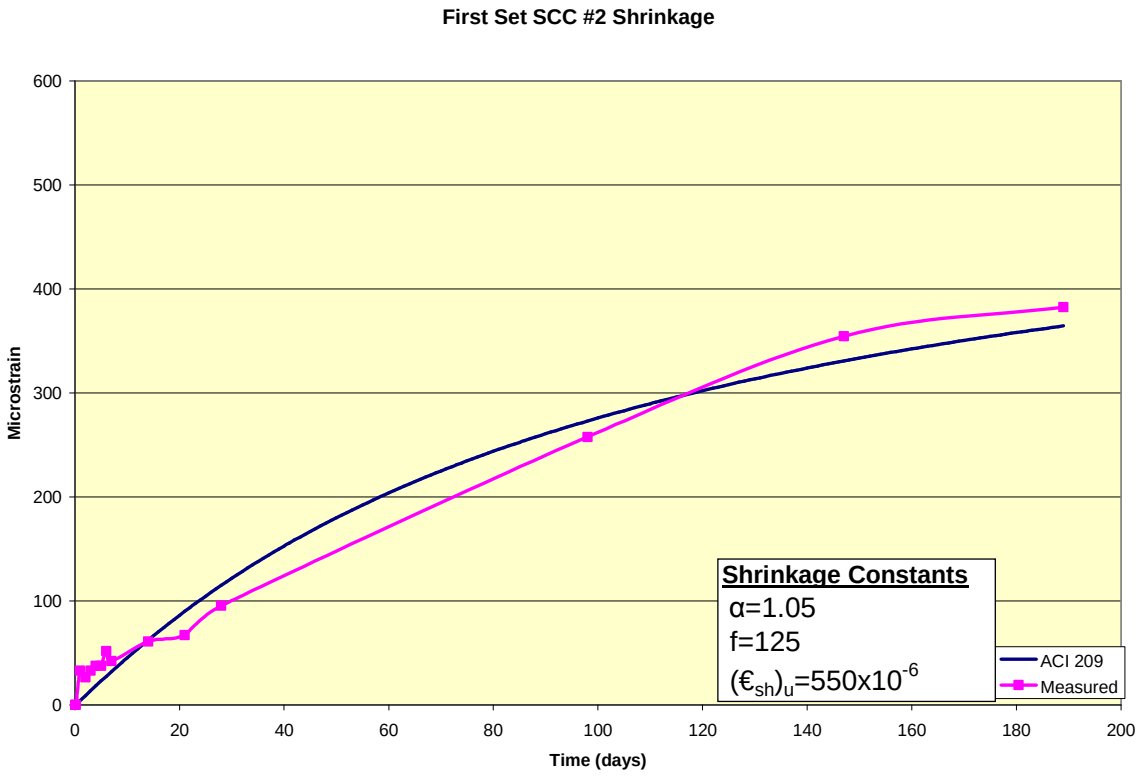

Figure 9.16 First set SCC #2 shrinkage strains

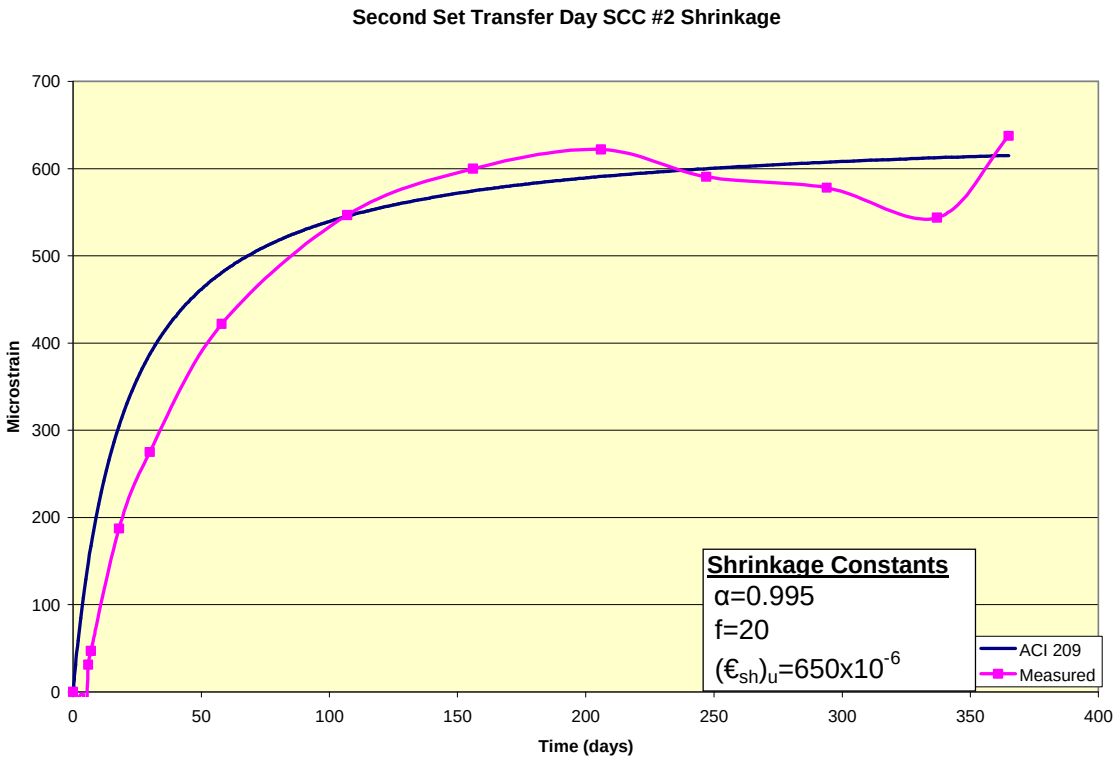

Figure 9.17 Second set SCC #2 shrinkage strains for transfer day

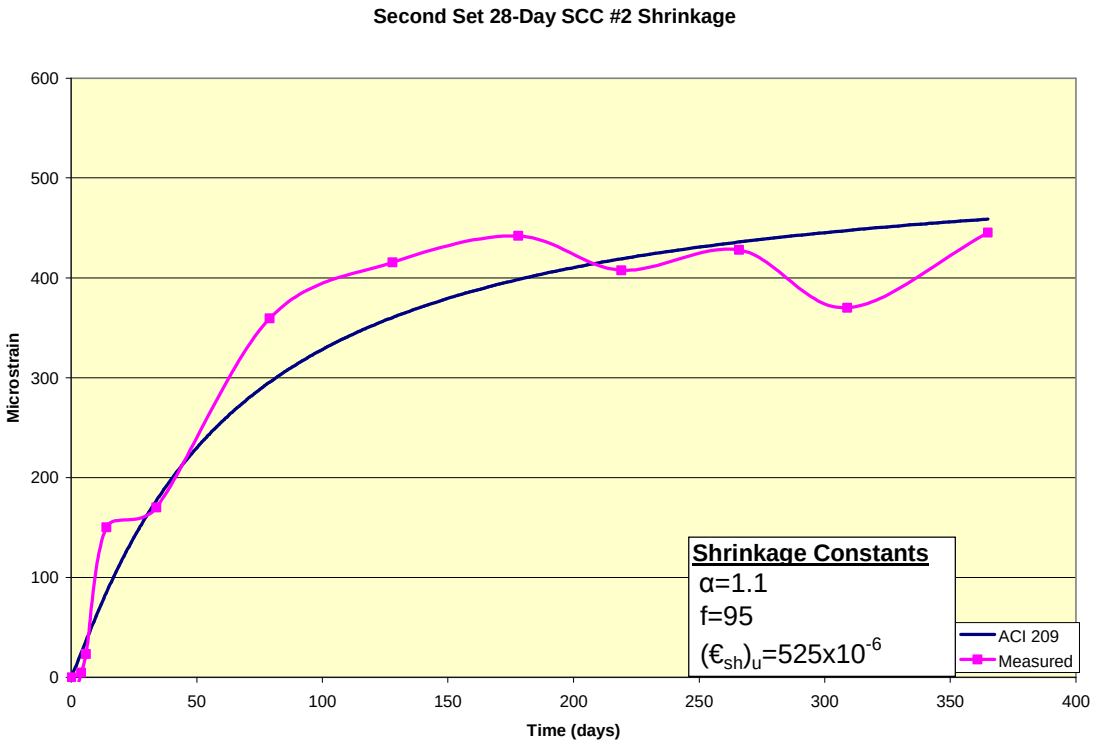

Figure 9.18 Second set SCC #2 shrinkage strains for 28-day

A.7 ACI 209 Prestress Loss Equations and Calculations

$$\lambda_u = \left[(nf_c) + (nf_c) v_u \left(1 - \frac{F_u}{2F_o} \right) + \frac{(\varepsilon_{SH})_u E_s}{(1 + n\rho\xi_s)} + (f_{sr})_u \right]$$

where:

λ_u = total losses in ksi

n = modular ratio, E_s/E_{ci}, at the time of loading

f_c = concrete stress such as at steel c.g.s due to prestress and precast beam dead load

v_u = ultimate creep coefficient

F_u = total ultimate (in time) loss of prestress minus the initial elastic loss

F_o = prestress force at transfer, after elastic loss

$(\varepsilon_{SH})_u$ = ultimate (in time) shrinkage strain in (in./in.)

E_s = modulus of elasticity of steel

ρ = reinforcement ratio

ξ_s = cross section shape coefficient

$(f_{sr})_u$ = ultimate (in time) stress loss due to steel relaxation on prestressed members

<u>Elastic shortening:</u>

$$ES = nf_c$$

$$n = \frac{28500}{2250} = 12.67$$

$$f_c = \frac{F_i}{A_t} + \frac{F_i e^2}{I_t} - \frac{M_D e}{I_t}$$

$$f_c = \frac{484}{256} + \frac{484 * 3.86^2}{12822} - \frac{1.7 * 12 * 3.86}{12822} = 2.44 ksi$$

$$ES = 12.67 * 2.44 = 31.0 ksi$$

Creep:

$$CR = (nf_c)v_u\left(1-\frac{F_u}{2F_o}\right)$$

$$n = \frac{28500}{2692} = 10.58$$

$$f_c = 2.44ksi$$

$v_{ui} = 3.2$ for CON and 3.17 for SCC

volume to surface correction:

Prisms: v/s=1 inch

$\lambda_{\frac{v}{s}} prism$ =correction factor for v/s ratio from Table 2.5.5.2 (ACI Committee 209)

Beams: v/s=2.87 inch

$\lambda_{\frac{v}{s}} beam$ =correction factor for v/s ratio from Table 2.5.5.2 (ACI Committee 209)

Creep $\lambda_{\frac{v}{s}} = \frac{\lambda_{\frac{v}{s}} beam}{\lambda_{\frac{v}{s}} prism} = \frac{0.83}{1.09} = 0.76$

$v_u = Creep\lambda_{\frac{v}{s}} * v_{ui} = 2.432$ for CON and 2.40 for SCC

$\frac{F_u}{F_o} = 0.21$ from Table 4.4.1.2 (ACI 209 Committee)

$$CR = (10.58 * 2.44)v_u\left(1-\frac{0.21}{2}\right)$$

CR= 56.18 ksi for CON and 55.65 ksi for SCC

Shrinkage:

$$SH = \frac{(\varepsilon_{SH})_u E_s}{(1 + n\rho\xi_s)}$$

$n = 10.58$

$E_s = 28500$

$$\rho = \frac{14 * 0.153}{6.25 * 21} = 0.016$$

$$\xi_s = 1 + \frac{e^2}{r^2} = 1 + \frac{3.84^2}{\left(\frac{12822}{256}\right)} = 1.30$$

$$SH = \frac{(\varepsilon_{SH})_u * 28500}{(1 + 10.58 * 0.016 * 1.30)}$$

volume to surface correction:

Prisms: v/s=1 inch

$\lambda_{\frac{v}{s}} prism$ =correction factor for v/s ratio from Table 2.5.5.2 (ACI Committee 209)

Beams: v/s=2.87 inch

$\lambda_{\frac{v}{s}} beam$ =correction factor for v/s ratio from Table 2.5.5.2 (ACI Committee 209)

Shrinkage $\lambda_{\frac{v}{s}} = \frac{\lambda_{\frac{v}{s}} beam}{\lambda_{\frac{v}{s}} prism} = \frac{0.86}{1.06} = 0.81$

$(\varepsilon_{SH})_u = Shrinkage \lambda_{\frac{v}{s}} * (\varepsilon_{SH})_{ui} = 567$ x 10^{-6} for CON and 473 x 10^{-6} for SCC

$SH = 13.24$ ksi for CON and 11.07 for SCC

Relaxation:

$RE = (f_{sr})_u$

$(f_{sr})_u = 0.025(f_{si})$ from Table 4.4.1.3 (ACI 209 Committee)

$RE = 0.025 * 198 = 4.95 ksi$

Total Losses:

CON:

$\lambda_u = 31.0 + 56.18 + 13.24 + 4.95 = 105.37 ksi$

SCC:

$\lambda_u = 31.0 + 55.65 + 11.07 + 4.95 = 102.67 ksi$

A.8 Shear Calculations for Single-Strand Flexure Beams

$L_{test} = 15\, ft$

$a_{test} = 6\, ft$

$M_D + M_L = M_N = 32.06 kip - ft$

$$\frac{w \times l^2}{8} + \frac{P_F \times a}{2} = M_N$$

$$\frac{0.08 \times 15^2}{8} + \frac{P_F \times 6}{2} = 32.06$$

$P_F = 9.94 kips$

$$V_{\max} = w \times a + \frac{P_F}{2} = 0.08 \times 6 + \frac{9.94}{2} = 5.45 kips$$

$$V_c = 2 \times \lambda \times \sqrt{f_c^{'}} \times b \times d = 2 \times 0.85 \times \sqrt{5000} \times 8 \times 10 = 9.61 kips$$

$V_c > V_{\max} \rightarrow (OK)$

A.9 Nominal Moment Calculations for Single-Strand Flexure Beams

$$\varepsilon_1 = \frac{f_{se}}{E_p} = \frac{175}{28,500} = 0.00614$$

$$P_e = f_{se} \times A_{ps} = 175 \times 0.153 = 26.775 kips$$

$$\varepsilon_2 = \frac{1}{E_c}\left[\frac{P_e}{A} + \frac{P_e \times e^2}{I}\right] = \frac{1}{4074}\left[\frac{26.775}{96} + \frac{26.775 \times 4^2}{1152}\right]$$

$$\varepsilon_2 = 0.00016$$

$$Assume: f_{ps} = 267.5 ksi$$

$$a = \frac{A_{ps} \times f_{ps}}{0.85 \times f_c^{'} \times b} = \frac{0.153 \times 267.5}{0.85 \times 5 \times 8} = 1.20$$

$$c = \frac{a}{\beta_1} = \frac{1.2}{0.8} = 1.50$$

$$\varepsilon_3 = \frac{d_p - c}{c} \times \varepsilon_c = \frac{10 - 1.5}{1.5} \times 0.003 = 0.017$$

$$\varepsilon_{ps} = 0.00614 + 0.00016 + 0.017 = 0.0233$$

From curve in PCI Handbook (2004)

$$f_{ps} = 270 - \frac{0.04}{\varepsilon_{ps} - 0.007} = 267.5 ksi$$

Equaled assumed value:

$$M_n = A_{ps} \times f_{ps} \times \left[d_p - \frac{a}{2}\right] = 0.153 \times 267.5 \times \left[10 - \frac{1.2}{2}\right] = 384.7 kip - in = 32.06 kip - ft$$

A.10 Prestress Loss Calculations for Flexural Beams

Single-strand beams: PCI Method

Elastic Shortening of Concrete (ES):

$$ES = K_{es} E_s \frac{f_{cir}}{E_{ci}}$$

K_{es}= 1.0 for pretensioned members

$$E_{ci} = 33w^{1.5}\sqrt{f_c'} = 33\times 110^{1.5}\times\sqrt{3500} = 2250ksi \text{ (ACI 318 2008)}$$

E_s= 28,500 ksi

$$f_{cir} = K_{cir} f_{cpi} - f_g$$

K_{cir}= 0.9 for pretensioned members

$$f_{cir} = 0.9\times\left[\frac{31}{96}+\frac{31\times 4^2}{1152}\right]-\frac{1.32\times 12\times 4}{1152} = 0.623ksi$$

$$ES = 1\times 28500\times\frac{0.623}{2250} = 7.89ksi$$

Creep of Concrete (CR):

$$CR = K_{cr}\frac{E_s}{E_c}\times[f_{cir} - f_{cds}]$$

K_{cr}= 1.6 for lightweight concrete

$$f_{cds} = 0ksi$$

$$CR = 1.6\times\left[\frac{28500}{2692}\right]\times(0.623-0) = 10.552ksi$$

Shrinkage of Concrete (SH):

$$SH = \left(8.2\times 10^{-6}\right)\times K_{sh}\times E_{ps}\times\left[1-0.06\times\frac{V}{S}\right]\times[100-RH]$$

K_{sh}= 1.0 for pretensioned members

V/S= 2.4

RH= 65%

$$SH = \left(8.2\times 10^{-6}\right)\times 1\times 28500\times[1-0.06\times 2.4]\times[100-65] = 7ksi$$

Relaxation of Tendons (RE):

$$RE = \left[K_{re} - J \times \left(SH + CR + ES \right) \right] \times C$$

$$K_{re} = 5.0$$

$$J = 0.04$$

$$C = 1.0$$

$$RE_L = \left[5 - 0.04 \times \left(7 + 10.55 + 7.89 \right) \right] \times 1 = 3.98 ksi$$

$$RE_i = f_{st} \left[\frac{\log 24t - \log 24t_1}{45} \right] \times \left[\frac{f_{st}}{f_{py}} - 0.55 \right] = 1.60 ksi$$

Total Losses:

$$f_{si} = f_{pj} - ES - RE_i = 202.5 - 7.89 - 1.6 = 193 ksi$$

$$f_{se} = f_{pj} - ES - CR - SH - RE_L = 202.5 - 7.89 - 10.55 - 7.0 - 3.98 = 173.03 ksi$$

$$f_{se@test} = 175 ksi$$

ACI 318 Calculations:

Transfer length (L_{tr}):

$$L_{tr} = \frac{f_{se}}{3} \times d_b = \frac{175}{3} \times 0.5 \approx 29 in.$$

Development length (L_{dev}):

$$L_{dev} = \frac{f_{se} \times d_b}{3} + \left[f_{ps} - f_{se} \right] \times d_b = \frac{175 \times 0.5}{3} + \left[266.8 - 175 \right] \times 0.5 \approx 75 in$$

Five-strand T-beams: PCI Method

Elastic Shortening of Concrete (ES):

$$ES = K_{es} E_s \frac{f_{cir}}{E_{ci}}$$

K_{es}= 1.0 for pretensioned members

$$E_{ci} = 33 w^{1.5} \sqrt{f_c'} = 33 \times 110^{1.5} \times \sqrt{3500} = 2250 ksi \text{ (ACI 318 2008)}$$

E_s= 28,500 ksi

$$f_{cir} = K_{cir} f_{cpi} - f_g$$

K_{cir}= 0.9 for pretensioned members

$$f_{cir} = 0.9 \times \left[\frac{155}{466} + \frac{155 \times 10.52^2}{17733} \right] - \frac{2.131 \times 12 \times 10.52}{17733} = 1.15 ksi$$

$$ES = 1 \times 28500 \times \frac{1.15}{2250} = 14.62 ksi$$

Creep of Concrete (CR):

$$CR = K_{cr} \frac{E_s}{E_c} \times [f_{cir} - f_{cds}]$$

K_{cr}= 1.6 for lightweight concrete

$$f_{cds} = 0 ksi$$

$$CR = 1.6 \times \left[\frac{28500}{2692} \right] \times (1.15 - 0) = 19.47 ksi$$

Shrinkage of Concrete (SH):

$$SH = \left(8.2 \times 10^{-6}\right) \times K_{sh} \times E_{ps} \times \left[1 - 0.06 \times \frac{V}{S} \right] \times [100 - RH]$$

K_{sh}= 1.0 for pretensioned members

V/S= 4.088

RH= 65%

$$SH = \left(8.2 \times 10^{-6}\right) \times 1 \times 28500 \times [1 - 0.06 \times 4.088] \times [100 - 65] = 6.173 ksi$$

Relaxation of Tendons (RE):

$$RE = \left[K_{re} - J \times \left(SH + CR + ES \right) \right] \times C$$

$$K_{re} = 5.0$$

$$J = 0.04$$

$$C = 1.0$$

$$RE_L = \left[5 - 0.04 \times \left(14.6 + 19.4 + 6.1 \right) \right] \times 1 = 3.39 ksi$$

$$RE_i = f_{st} \left[\frac{\log 24t - \log 24t_1}{45} \right] \times \left[\frac{f_{st}}{f_{py}} - 0.55 \right] = 1.60 ksi$$

Total Losses:

$$f_{si} = f_{pj} - ES - RE_i = 202.5 - 14.62 - 1.6 = 186.28 ksi$$

$$f_{se} = f_{pj} - ES - CR - SH - RE_L = 202.5 - 14.62 - 19.47 - 6.17 - 3.39 = 158 ksi$$

$$f_{se@test} = 170 ksi$$

ACI 318 Calculations:

Transfer length (L_{tr}):

$$L_{tr} = \frac{f_{se}}{3} \times d_b = \frac{170}{3} \times 0.5 \approx 28 in.$$

Development length (L_{dev}):

$$L_{dev} = \frac{f_{se} \times d_b}{3} + \left[f_{ps} - f_{se} \right] \times d_b = \frac{170 \times 0.5}{3} + \left[268.7 - 170 \right] \times 0.5 \approx 77 \frac{1}{2} in$$

A.11 Nominal Moment Calculations for T-Beam Specimens

$$\varepsilon_1 = \frac{f_{se}}{E_p} = \frac{170}{28,500} = 0.005965$$

$$P_e = f_{se} \times A_{ps} = 170 \times 0.153 \times 5 = 130.05 kips$$

$$\varepsilon_2 = \frac{1}{E_c}\left[\frac{P_e}{A} + \frac{P_e \times e^2}{I}\right] = \frac{1}{4074}\left[\frac{130.05}{466} + \frac{130.05 \times 10.52^2}{17733}\right]$$

$$\varepsilon_2 = 0.000268$$

$$Assume: f_{ps} = 268.7 ksi$$

$$a = \frac{A_{ps} \times f_{ps}}{0.85 \times f_c^{'} \times b} = \frac{0.153 \times 5 \times 268.7}{0.85 \times 5 \times 36} = 1.34$$

$$c = \frac{a}{\beta_1} = \frac{1.34}{0.8} = 1.68$$

$$\varepsilon_3 = \frac{d_p - c}{c} \times \varepsilon_c = \frac{10 - 1.68}{1.68} \times 0.003 = 0.0309$$

$$\varepsilon_{ps} = 0.005965 + 0.000268 + 0.0309 = 0.0371$$

From curve in PCI Handbook (2004)

$$f_{ps} = 270 - \frac{0.04}{\varepsilon_{ps} - 0.007} = 268.7 ksi$$

Equaled assumed value:

$$M_n = A_{ps} \times f_{ps} \times \left[d_p - \frac{a}{2}\right] = 0.153 \times 5 \times 268.7 \times \left[19 - \frac{1.34}{2}\right] = 3767 kip - in = 313.9 kip - ft$$